Nils Eivind Kamfjord

Mass and Energy Balances of the Silicon Process

- Improved Emission Standards

Thesis for the degree of Philosophiae Doctor

Trondheim, April 2012

Norwegian University of Science and Technology
Faculty of Natural Sciences and Technology
Department of Materials Science and Engineering

NTNU – Trondheim
Norwegian University of
Science and Technology

Preface

The work on this thesis was done from February 2009 until April 2012 within the FUME research programme. The primary objective of this programme is to develop in-depth competence in the area of "fugitive" emissions of materials (such as gas, fumes/particles) to the internal and external environment and energy (both low and high temperature) in the Norwegian ferroalloy industry.
FUME is a close cooperation programme between industrial partners and the Norwegian University of Science and Technology (NTNU) and is mainly funded by the Research Council of Norway and the Norwegian Ferro Alloys Research Association (FFF).

The basis for the work in this thesis is industrial measurements performed on full-scale operating silicon furnaces with all the challenges and surprises that field operations contain. The industrial part has also been the basis for pilot scale experiments and computer modelling of different emission situations.

Looking back at these campaigns and remembering everything from the happiest moments of success to the deepest valleys of despair the work would never have been possible without the clever minds of Svend Grådahl, Bendik Sægrov, Helge Midtdal and Ingeborg Solheim all from SINTEF Materials and Chemistry together with Lars Brøndbo from Norsk Elektro Optikk. Thank you all so much for some memorial moments.

I would also like to thank Elkem Salten with all its crew and especially plant manager Arve Ulriksen for opening the plant up and letting us have all required resources at our hands when needed.

In addition a lot of other people from FFF, SINTEF, NTNU and the industrial partners have been involved in discussions and activities that have helped me moving forward in my work but I will especially like to thank Dr Edin Myrhaug from Elkem Silicon for being a great help in model solving and in depth process discussions and off course my supervisor Professor Halvard Tveit from the Norwegian University of Science and Technology for all his help, inspiration and endurance throughout this project.

Finally I would like to especially thank my wife Vigdis and our children Johan and Astrid for the patience and understanding when having a husband and father not being there as much as you would have wanted. Without your support this work would never have been possible.

Trondheim April 2012

Nils Eivind Kamfjord

Summary

The main objective in this thesis has been to gain more knowledge about the different emissions that the silicon process emits both internally and externally in a silicon plant. Throughout the time period of the thesis several industrial measurement campaigns have been conducted to map and quantify the levels of emissions from the process. These campaigns have ranged from a full material balance over the silicon process to measurements of specific gaseous components and other emissions from selected process steps.

 The main work has consisted of:

- **Measurements of fugitive emissions inside a silicon plant.**

Based on a given quantitative assumption of the emission sources inside a silicon plant measurements of the fugitive emissions from the tapping and casting of silicon have been done. The measurements show the following:

   a. The tapping off gas system often fails to collect all the fumes from the tapping process. Whenever this happens these emissions tend to spread to the rest of the plant and thus end up as internal pollution elsewhere.
   b. The casting of metal generates fumes that rise and often leak from the roof of the building.

- **An energy and material balance over the entire silicon process from raw materials to end products.**

Samples of all in and outgoing material and gas streams to and from the furnace were collected. Data for 48 hours were collected from the production system and the full material and energy balance was calculated. The results of the two revealed:

   a. The major part of the elements show a yield close to 100 % and most of the deviating elements can be explained. In general the elements that enter the silicon process distribute themselves between the products according to their boiling point when leaving the furnace.
   b. The silicon process is a high energy consumption process and contains as much chemical energy as electrical energy when balanced. The result of this is an off gas with a high temperature that makes a silicon furnace well suited for energy recovery measures.

- **An energy and simplified material balance over the tapping process of silicon.**

A similar material balance as for the overall furnace has been conducted for the tapping area. The tapping material balance is however only based on the main elements going in and out of the area. The summary of the two are:

a. The material balance shows that the main portion of the gaseous content in the tapping area (air) is only being transported through the area and heated by the process. The elements contained in the metal are forced by the refining process to distribute themselves between the slag and metal phases.
b. As the energy situation in the tapping area is dominated by the energy contained in the metal, this study has instead focused on which of the different energy streams that contribute or demand energy from the ladle and refining processes. The study found that to close the energy balance substantial amounts of metal have to be oxidized to provide the energy.

- **A study of the emissions and formation mechanisms of NO in silicon production.**

Measurements of the NO formation in both the furnace and the tapping off gas have been done. In both areas the connection between the NO and SiO_2 fume formation is evident. For the tapping area the NO formation shows a strong correlation with the fume formation, while the NO formation at the furnace surface seems to be influenced by some other additional mechanisms. A description of the two different combustion environments is given and compared to the measurements. Other findings are

a. The NO formation per SiO_2 particle in the tapping area is almost constant and can be explained by the formation of particles heating up the surrounding air enough to produce NO via the Zeldovich mechanism.
b. The NO formation at the furnace surface is explained by the following three phases, being a function of the furnace process and the routines in adding new raw materials to the furnace:
   i. Primary NO formation phase
   ii. Transient phase
   iii. Secondary NO formation phase
c. Modelling the two combustion environments in a chemical reaction model with some simplifications show the same trends in results as the measurements.

- **Pilot scale experiments of the silicon process to study the influence of air inlet height on NO formation in the combustion zone above the furnace surface.**

Based on measurements and observations done on an industrial scale furnace several hypotheses regarding the NO formation and the air inlet to the furnace were established. A pilot scale experiment of the silicon process was conducted in a single phase 440 kVA furnace. The furnace was operated as close to industrial conditions as possible and the NO emissions were measured when changing the height of the air inlet to the furnace. The results from the pilot scale experiment were:

    a. Having the air inlet close to the charge surface produces more NO than moving it higher towards the off gas channel.

    b. Decreasing the amount of air into the combustion chamber increases the amount of NO produced.

    c. Based on the results there is reason to believe that the velocity fields inside the hood influence the NO formation significantly and that the NO formation might be influenced by the furnace design.

After the experiment the furnace was filled with epoxy and split down the middle giving valuable information in understanding the experimental results.

A simplified computational fluid dynamics model of the pilot furnace was also set up and simulation found that the experimental results could be explained by the velocity fields and high temperature zones inside the hood.

Nomenclature

Latin Symbol	Explanation
M_i	Molar weight of species i [gram/mol]
(g), (l), (s)	Species state, (gas), (liquid), (solid)
$\overline{X}$	Average of X
P_i	Pressure of species i [atm]
T_i	Temperature of i [°C]
k_{air}	Thermal conductivity air [W/m*K]
$\overline{h_c}$	Average convective heat transfer coefficient [W/m^2*K]
k_{if}	Forward reaction rate for reaction i [m^3/kmol*s]
K_{ib}	Backward rate for reaction i [m^3/kmol*s]
K_{eq}	Reaction equilibrium constant
R	Universal Gas constant
T	Temperature [K]
A_i	Frequency factor [cm$_3$/mol*s]
E_i	activation energy [cal/mol]
k_{fi}	Forward reaction rate for reaction i [cm^3/mol*K]
t	Time [s]
Kg	Weight in kilogram
N	particle concentration [#/cm^3]
c	collision sticking coefficient
C_o	number of silica molecules/cm^3
R_p	Particle radius
Q	Heat source term
k	Thermal conductivity
kA	Electricity, kilo Ampere
V	Electricity, Volt
Cp	Heat capacity [J/Kg*K]
k-ε	Turbulence, k is the mean turbulent kinetic energy and ε is the viscous dissipation rate
n	Sum notation, total number of occurrence

Greek Symbol	Explanation
ΣX	Sum of X_n
∇	Nabla, differential operator
$\dfrac{\partial T}{\partial t}$	Partial time derivative of T
ΔG_r	Gibbs free energy for reaction i[kJ/mol]
ΔH_r	Heat of reaction [kJ/mol]
χ_i	Concentration of i [ppm]
ρ	density
β_{air}	Expansion coefficient air [1/K]
ν_{air}	Kinematic viscosity air [m^2/s]

Abbreviations	Explanation
FEV_1	Forced Expiratory Volume in 1 second [litre]
ADN	Administrative norm of fume concentration[mg/m^3]
GWh	Energy notation, gigawatt hour
MW	Energy notation, megawatt
FixC	Content of carbon [%]
VM	Volatile Matter
MVA	Energy notation, Megavolt Ampere
kWh	Energy notation, kilowatt hour
Nm_3	Volume, Normal Cubic metre
XRF	An analytical technique, *x-ray fluorescence*
DegC	Temperature in degrees Centigrade [ºC]
Ar	Archimedes number, dimensionless, motion of fluids due to density differences
Gr	Grashofs number, dimensionless, proximate ratio of the buoyancy to viscous force acting on a fluid
Re	Reynolds number, dimensionless, ratio of inertial forces to viscous forces
Pr	Prandtl's number, dimensionless, ratio kinematic viscosity to thermal diffusivity.
$PM_{2.5}$	Particles less than 2.5 micrometres in diameter
VOC	Volatile Organic Compound

BAT	Best Available Technology
SEM	Scanning Electron Microscope
ppm	Concentration, part per million
R-Sq	Statistics, R-squared
R-Sq(adj)	Statistics, R-squared, adjusted
DF	Statistics, Degrees of freedom
SS	Statistics, Sum of Squares
MS	Statistics, Mean Square
F-value	Statistics, value of F-distribution
P-value	Statistics, Probability
SA	Surface area
CFD	Computational Fluid Dynamics
AC	Electricity, Alternating Current

Content

List of Figures

List of Tables

Chapter 1 Introduction

During the last few years there has been increased attention paid towards the work environment with respect to fumes and hazardous emissions. This is also the case in the smelter industry and has led to research programmes such as PROMILJØ (PROMILJØ) which aimed to gain a better understanding of the emissions from the processes.

The Norwegian government's demand for a better working environment is also increasing and the Norwegian smelter industry now faces limits related to the concentration of 10 mg fume/m^3 in air. Exceeding this fume concentration calls for respiratory protection for the workers (Norwegian Labour Inspection Authority 2009).

A recent medical study done by Johnsen (Johnsen 2009) on the working environment in Norwegian smelters concluded that the fume concentration is so high that is has a deteriorating effect on inline workers respiratory capacity. Some of the main findings from the study are:

- o Inline operators in the Si/FeSi plants are more exposed to fume than workers in the SiMn/FeMN/FeCr industry.
- o The reduction in the respiratory capacity measured in FEV_1/height[1] is connected to work operations and earlier exposure when comparing inline operators in the Si/FeSi plants with unexposed reference persons.
- o The reduced respiratory capacity is almost twice as high among the Si/FeSi operators compared to the operators in the SiMn/FeMn/FeCr plants.

All this leads to the conclusion that gaining a better understanding of fume emissions in the plants is necessary and as a consequence the research programme FUME has been established in order to create a continuum in the work done by PROMILJØ (FUME 2009).

The main objectives for the PROMILJØ project were to investigate the direct emissions from the furnace stack and tapping process. The FUME programme aims to continue this work, but to a greater extent and with a more detailed view on specific emissions and internal environment.

The R&D challenges in the FUME project are located in three main areas

- Materials emissions and reductions
- Energy emissions and reductions
- Measurements and tools

---

[1] Forced Expiratory Volume in 1 second

FUME aims to connect process understanding and process emissions as shown in Figure 1.1.
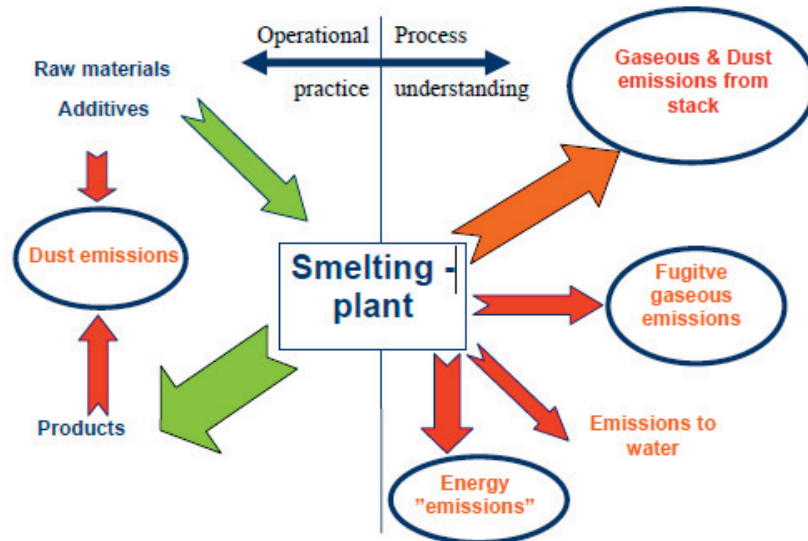
Figure 1.1: Schematic of the emissions from a ferroalloy plant (FUME 2009)

1.1 Outline of the thesis

This thesis has the objective of gaining a better understanding of the different energy and material emissions that occur during the production of silicon. Most of the experimental data acquired throughout this thesis have been collected in measurements done on an industry scale. The planning of these industrial measurement campaigns has been based on the experience from earlier PhD studies in related research programmes. This earlier knowledge about industrial measurements has been of considerable benefit to the present work and data collection.

With respect to gaseous emissions this thesis is especially focused on the NO emissions from the different process steps. The data are reported as NO but it is commonly assumed that all released NO will oxidize to NO_2 within a short period of time. The emission of NO could therefore just as well be reported as NO_2 if recalculated using the formula

$$NO_2\ emission\ [in\ grams] = \frac{M_{NO2} * NO\ emission\ [in\ grams]}{M_{NO}}$$

M denotes the molar weight of the species.

NO and NO_2 (the sum of them is commonly named NO_x) is considered a harmful gas because of its negative impact on the environment.

As mentioned the basis of much of the work reported in this thesis has been industrial measurement campaigns, but also pilot scale experiments and process modelling have been conducted to gain more knowledge about the emissions.

The work has consisted of:

- Measurements of fugitive emissions inside a silicon plant
- An energy and material balance over the entire silicon process from raw materials to end products
- An energy and simplified material balance over the tapping process of silicon
- A thorough study of the emissions and formation mechanisms of NO in silicon production
- Pilot scale experiments of the silicon process to study the influence of air inlet height on NO formation in the combustion zone above the furnace surface

This thesis describes and explains new knowledge in the connections between process performance variables and emissions from the silicon process. Through modelling the proposed connections and mechanisms have been validated on a principle scale. Much further work needs to be done to be able to explain the different connections and their interaction to the full extent.

1.2 Publications and reports

Several findings and connected work to this PhD have been published in cooperation with other authors and are summed up below.

- **Kamfjord N.E, Myrhaug E.M, Tveit H, Wittgens B**, "Energy balance of a 45 MW (ferro-) silicon submerged arc furnace"
INFACON XII, Helsinki Finland

- **Midtdal H.F, Kamfjord N.E**, "Undersøkelse av strømningsforhold knyttet til støvoppsamling i tappeområde, ELKEM Salten"
SINTEF Report nr. F14671

- **Næss M.K, Tranell G.M, Kamfjord N.E**, "FUGITIVE EMISSIONS RELATED TO OXIDATION OF LIQUID SILICON DURING LADLE REFINING"
TMS2011 Annual Meeting & Excibition, San Diego California, USA

- **Solheim I, Kamfjord N.E, Takla M**, "Pilot Scale Silicon Melting Experiment",
SINTEF Report nr. F21170

- **Solheim I, Kamfjord N.E, Takla M**, "Silisium smelteforsøk i 160 kW pilotovn",
SINTEF Report nr. F21171

- **Solheim I, Jensen R, Kamfjord N.E**, "EQUIPMENT FOR PILOT SCALE EXPERIMENTS OF NOX-EMISSIONS FROM THE SILICON PROCESS"
TMS 2012 Annual Meeting & Exhibition, Orlando Florida, USA

- **Kamfjord N.E, Tveit H, Solheim I**, "PILOT SCALE MEASUREMENTS OF NOX-EMISSIONS FROM SILICON PROCESS"
TMS 2012 Annual Meeting & Exhibition, Orlando Florida, USA

- **Kamfjord N.E, Tveit H, Næss M.K, Myrhaug E.H**, "MECHANISMS OF NO FORMATION DURING SIO COMBUSTION"
TMS 2012 Annual Meeting & Exhibition, Orlando Florida, USA

- **Næss M.K, Tranell G.M, Olsen J.E, Kamfjord N.E,** "MECHANISMS AND KINETICS OF LIQUID SILICON OXIDATION DURING INDUSTRIAL REFINING"
Oxidation of Metals DOI: 10.1007/s11085-012-9303-9

Chapter 2   The silicon process

2.1 The Silicon furnace

The main features of the silicon process is well described in the book "Production of High Silicon Alloys" written by Schei, Tuset et al. (Schei, Tuset et al. 1998) and this summary of the process is mainly drawn from this book.

A simple sketch of the (ferro) silicon process with energy recovery utilization is given in Figure 2.1.
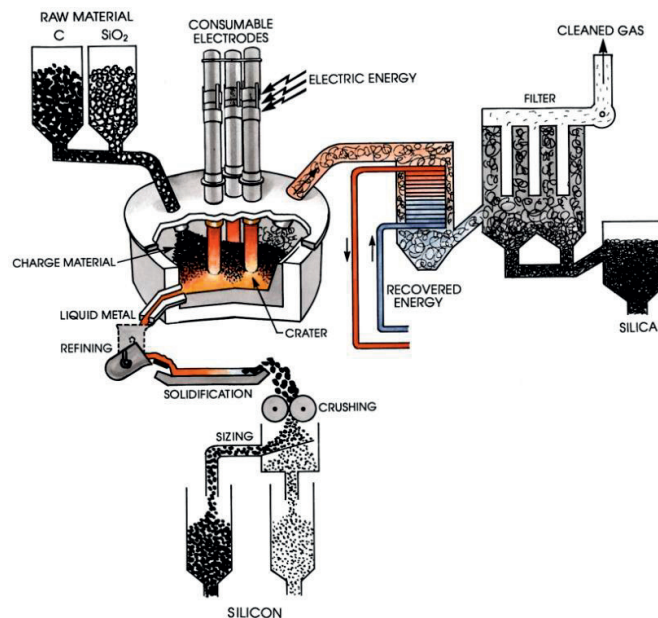
Figure 2.1: Principle sketch of the (Fe)Si process. From (Schei, Tuset et al. 1998)

The furnace consists of steel casing walls, covered on the inside by a refractory material capable of withstanding both high temperatures and chemical attacks. The bottom of the furnace is usually made of a carbon lining.

Raw materials are added to the furnace on the top, fed directly to the furnace surface by charge tubes, often placed symmetrically around the electrodes. The raw materials in silicon production can be divided into two main groups: silicon sources and carbon materials. Quartz or quartzites are the most commons sources of silicon while coke and coal are usually used as the carbon source. Because of raw material cost and availability there will be a lot of different raw material mixtures used from region to region in a global perspective.

The silicon process is a high energy process, requiring temperatures above 1800 °C to run properly. These temperatures are obtained by large amounts of electric energy, fed to the furnace through three electrodes deeply submerged in the charge mix.

The process itself is cyclical. The raw materials are consumed both on the way down and in the craters where the main silicon production occurs. This creates sinks in the furnace top which now have to be refilled with new raw materials. This cycle runs unattended most of the time, but sometimes the furnace operator has to manipulate the furnace surface to either gain a better sink in some places or to stop process gas escaping from the inner area of the furnace.

Above the furnace there is a hood collecting all the off gases from the process. The temperature of the off gas is controlled by the amount of excess air. The large amount of energy in the off gas may be recovered in heat exchangers. After being collected from the furnace top the off gas is filtered through bag house filters. The fume collected can be sold as a valuable product to the refractory industry, the oil industry, or as an additive in cement. The remaining gas components such as CO_2, SO_2 and NOx, etc are released to the air.

 Tapping of the furnace is done through tap holes located at the bottom of the furnace, tapping through one hole at a time. The furnace can have several tap holes, and as some furnaces rotate, the operators are given the opportunity to switch to another tap hole, leaving the old one for maintenance.

The metal is usually tapped into ladles where it may undergo some form of refining before casting. After casting and cooling, the metal is transported to crushing, screening and packing before it is shipped out to customers.

2.2 The chemistry of the Si process

The major difference between the ferrosilicon and the silicon process is that the ferrosilicon process adds an iron source to the raw material mixture. The presence of iron in the silicon process has several effects, such as lowering the silicon activity, making the chemical reactions run easier. For simplicity reasons the following theory is therefore given for silicon-related reactions only.

2.2.1 Compounds

The main components in the silicon process are the elements Si – C – O. Compounds that are stable in the temperature range of interest, 1400 – 2100 °C, are:

Solids: C, SiC

Liquids: Si, SiO_2

Gases: CO, CO_2, SiO and O_2

There are no commonly accepted ternary compounds in this system.

2.3 Overall chemical reactions

The overall main reaction for producing silicon can be given as

$$SiO_2(s) + 2C(s) = Si(l) + 2CO(g) \hspace{3cm} \textbf{2-1}$$

This equation is stoichiometrically correct. If less or more C is added the following reactions could occur:

$$SiO_2(s) + C(s) = SiO(g) + CO(g) \hspace{3cm} \textbf{2-2}$$
$$SiO_2(s) + 3C(s) = SiC(s) + 2CO(g) \hspace{3cm} \textbf{2-3}$$

The first one gives a high production of SiO gas flowing up from the crater zone, the latter one gives the undesirable product of SiC, which deposits on the furnace bottom and may cause severe operational problems if the reaction is left unattended for a long period of time.

Reaction (2.1) is a solid-solid reaction and seen from a kinetic perspective this would probably be slow. Motzfeldt (Motzfeldt 1961) did experiments heating a mixture of fine grain quartz together with C, observing that intermediate phases and reactions had to occur. Experiments by Motzfeldt and Steinmo (Motzfeldt and Steinmo 1972) also indicate that the reaction between SiO_2 and C is not a solid state reaction.

Looking at an industrial furnace some SiO gas will always escape through the furnace top and the combination of Reactions (2.1) and (2.2) then gives a good description of the overall furnace reaction:

$$SiO_2(s) + (1+y)C(s) = ySi(l) + (1-y)SiO(g) + (1+y)CO(g) \hspace{2cm} \textbf{2-4}$$
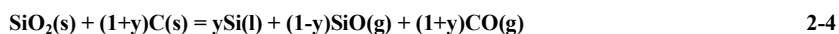
with y being the silicon recovery of the process, in other words the amount of silicon metal produced per mole SiO_2 added, $0 \leq y \leq 1$.

It is also common to give this equation with respect to the amount of carbon needed for the reduction of 1 mole of SiO_2:

$$SiO_2(s) + 2xC(s) = (2x-1)Si(l) + (2-2x)SiO(g) + 2xCO(g) \hspace{1.5cm} \textbf{2-5}$$
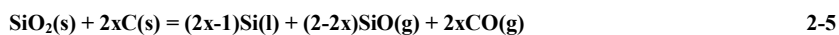
with x being the fixed carbon content of the charge mix, $0.5 \leq x \leq 1$

2.4 The different zones in a silicon furnace

Evaluating the silicon furnace from a process point of view the furnace can be simplified and divided into two main zones.

2.4.1 The outer structure of the furnace – the charge zone

The furnace surface and about 1.5 - 2 metres down, depending on the furnace size, can be considered something like a sinking fluid bed where process gas from the inner zones of the furnace counter flow with the fresh raw materials that are slowly sinking down. Depending on size distributions, the quartz or quartzite is more or less surrounded by the smaller carbon source particles as illustrated in Figure 2.2.
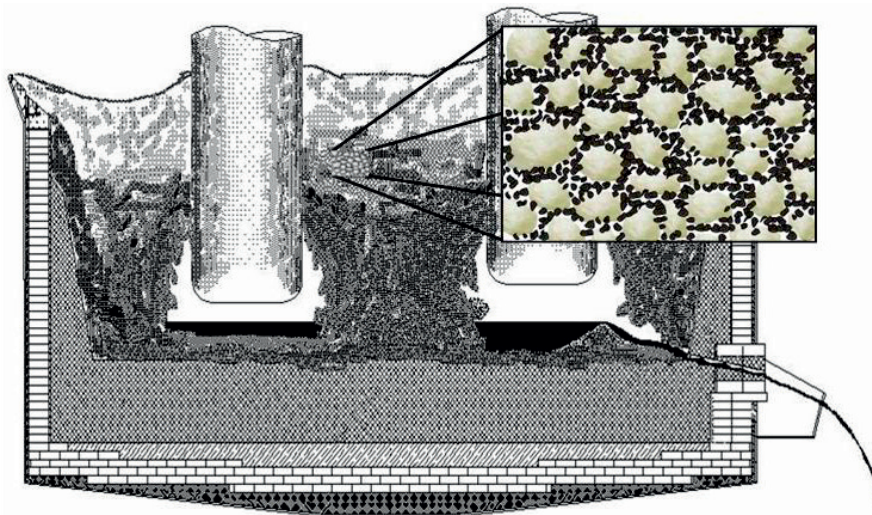
Figure 2.2: Cross section of silicon furnace

2.4.2 Reactions in the outer zone of the furnace

The process in the furnace craters produces mainly two gases, SiO and CO, which will flow upwards into the raw material mix. Most of the SiO gas will either react with C to form SiC or condense to Si + SiO_2, the latter reaction releasing heat which acts as a preheating of the new raw materials. Some of it will reach the furnace top, reacting with the O_2 in the air forming SiO_2, also named silica fume. The CO gas flows to the surface of the furnace and reacts with O_2 to form CO_2.

The main reactions in the outer zone of the furnace are:

1) Conversion of C to SiC through reaction with SiO

2) Recovery of SiO through either condensation or reaction with CO

3) Conversion of SiO(g) to SiO_2(g)

4) Conversion of CO(g) to CO_2 (g)

2.4.3 The inner structure of the furnace – the crater zone

In Figure 2.3 sketches of the area around the electrode tip, called the inner zone of the furnace. Underneath each electrode an electric arc burns between the electrode tip and the molten Si/SiC slurry creating an open spacing around the tip, called a crater. The crater is surrounded with SiC and other intermediate reaction products such as condensed Si and SiO_2.
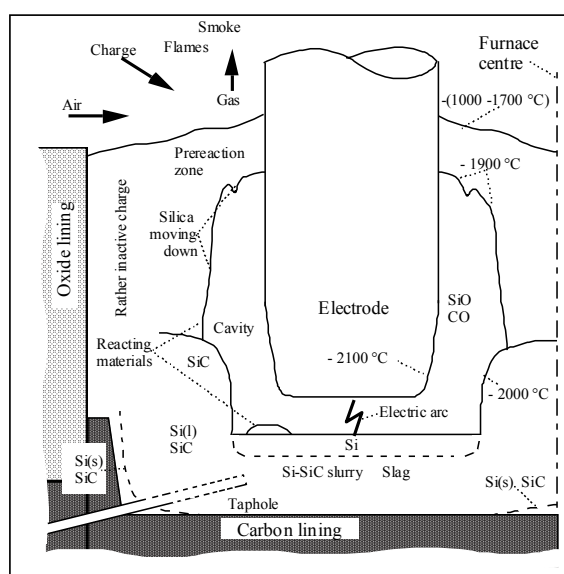
Figure 2.3: Inner structure of the furnace - the crater zone. From (Schei, Tuset et al. 1998)

Figure 2.3 also gives a good indication on the temperature in the different zones in the furnace.

The tapping channel, giving a direct connection to the molten silicon, is seen on the bottom left of Figure 2.3.

2.4.4 Reactions in the inner zone of the furnace

In the inner zone of the furnace the SiC from the outer zone reacts with SiO_2, forming free silicon, SiO(g) and CO(g) as the end products. If the stoichiometric balance is not correct the reaction will turn to producing either more SiO(g) or SiC(s), the latter causing severe operational problems if maintained over time.

9

Schei and Halvorsen (Schei and Halvorsen 1991) have given the following set of reactions for the inner zone:

$2SiO_2$ (s,l) + SiC(s) = 3SiO(g) + CO(g)	**2-6**
SiO_2 (s,l) + Si(l) = 2 SiO(g)	**2-7**
SiC(s) + SiO(g) = 2Si(l) + CO(g)	**2-8**

Multiplying Reaction (2.8) with a number z and adding it to Reaction (2.7) gives an expression for the overall reaction:

SiO_2 (s,l) + z SiC(s) = (2z-1)Si(l) + (2-z)SiO(g) + zCO(g)	**2-9**
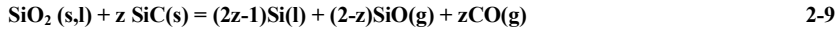
With z = ½ you get Reaction (2.6) and with z = 1 you get the reaction

SiO_2 (l) + SiC(s) = Si(l) + SiO(g) + CO(g)	**2-10**

Looking at Reactions (2.7) and (2.8) they connect through a gas phase, meaning that they both could be in a local equilibrium, but necessarily not the sum of them.

Figure 2.4 shows the equilibrium pressure for SiO over the condensed phases of the system which means that the lowest possible temperature where free silicon is produced is 1811 °C.
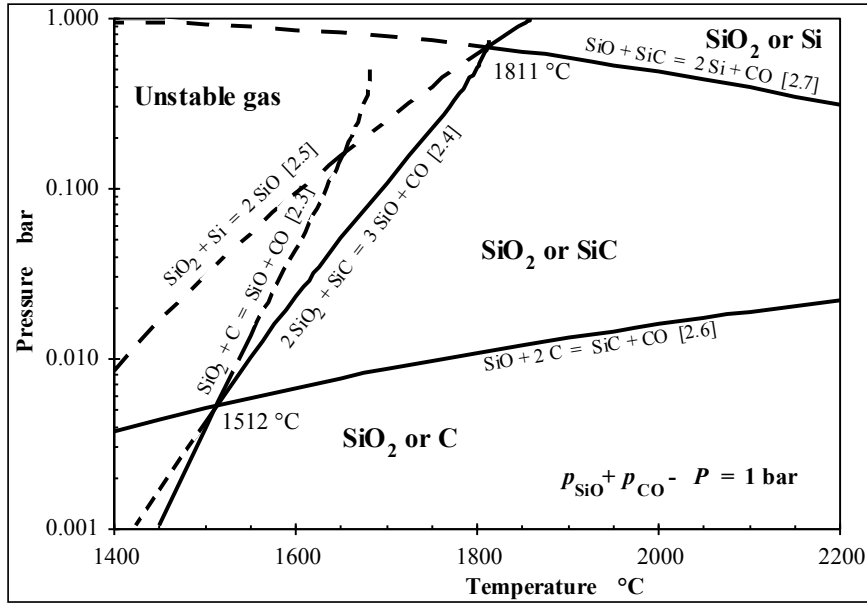
Figure 2.4: Equilibrium pressure of SiO over the condensed phases of the system. From (Schei, Tuset et al. 1998)

From the slope of the equilibrium curve for Reaction [2.7] in Figure 2.4 it is given that an increased temperature causes the reaction to proceed under a lower SiO pressure.

2.5 Silicon process models

Schei and Halvorsen (Schei and Halvorsen 1991) have described the silicon process in a stoichiometric model presented in Figure 2.5. In this model the outer zone is divided into two chambers, as suggested by Kolbeinsen (Kolbeinsen 1984), enabling the simulation of different reactivity on the C materials fed to the process. In addition this divided outer part of the model could easily simulate segregation in the raw material mix, creating an off balance between C and SiO_2 added.

Kolbeinsen initially suggested that the outer part of the model should be divided into four zones to simulate a real furnace better, having one zone per electrode and one for the centre of the furnace.
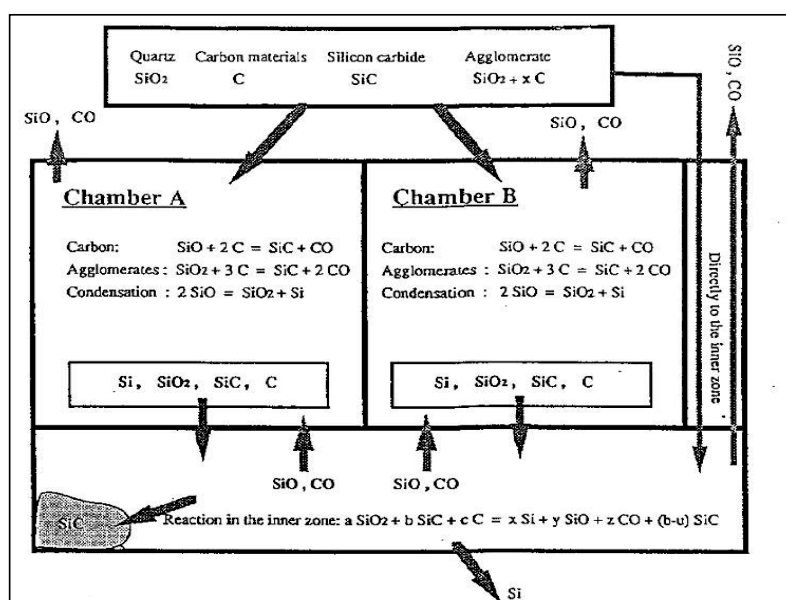
Figure 2.5: Stoichiometric model of the silicon process. From (Schei and Halvorsen 1991)

Schei, Tuset and Tveit (Schei, Tuset et al. 1998) also provided a thorough description of the different reaction schemes and the corresponding silicon recoveries. They have also taken the reactivity of the C into consideration, introducing a value r ($0 < r < 1$) as well as the total pressure conditions in the inner zone of the furnace, defined as a value "s" given as $s = P_{SiO}/(P_{SiO} + P_{CO})$.

11

For the reaction scheme giving 100 % silicon recovery they have calculated the heat capacity of the charge available for SiO condensation. The simple energy balance is given by:

Energy needed to heat new raw materials to 1800 K

  –   <u>Heat released into the zone (from SiO reactions and hot CO(g) from the crater)</u>

  =   Heat capacity available for condensation

Assuming that the condensation happens according to the reverse Reaction (1.7)

$$2SiO(g) = SiO_2(s,l) + Si(l) \tag{-1.7}$$

the calculations fall out rather easy, resulting in 0.16 moles of SiO(g) condensating per mole silicon produced.

The overall reaction scheme with 0.16 moles of SiO condensed per mole silicon produced and a gas composition in the crater zone equivalent to s = 0.537 is given in Figure 2.6 below.
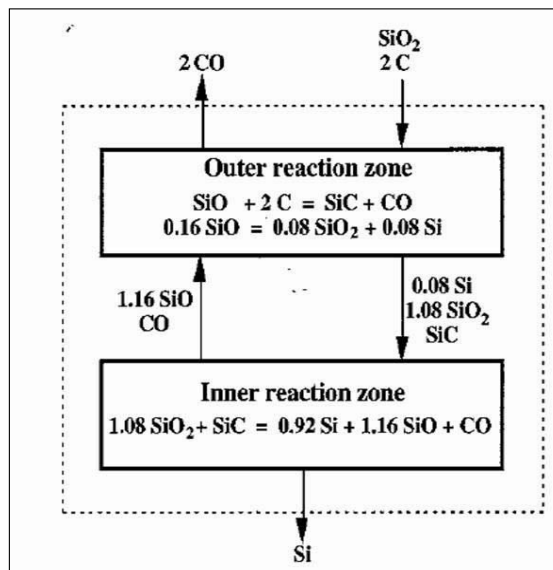
Figure 2.6: 100 % silicon yield reaction scheme. From (Schei, Tuset et al. 1998)

The silicon recovery becomes 100 % when adding the silicon condensed to the silicon produced in the inner reaction zone.

Chapter 3   Fugitive emissions at a silicon plant

Considering all the work operations involved in the silicon process there are several operations which could be identified as "polluters". Tveit, Myrhaug et al. (Tveit, Myrhaug et al. 2008) have identified several processes which influence the diffusive emissions and internal work environment. Figure 3.1 provides an overview of the silicon process with the different pollution sources they identified.
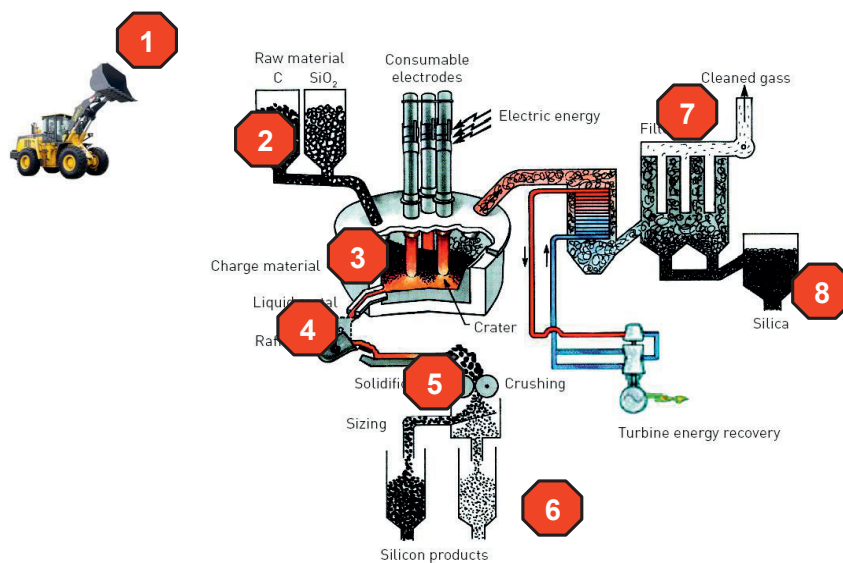
Figure 3.1: Sources for diffusive emissions from (Tveit, Myrhaug et al. 2008)

The different processes are:

1. Raw material handling from key to storage
2. Raw material transport from storage to furnace
3. Furnace processes
4. Tapping
5. Casting
6. Crushing, screening and packing
7. Off gas system
8. Product packing of collected fume from off gas

Tveit, Myrhaug et al. also tried to quantify the different contributions from each process with respect to the overall diffusive emissions and with respect to the internal pollution generated by the specific work process. Table 3-1 gives their estimate of the contribution in each area of the silicon plant.

Table 3-1: Overview of process emissions. From (Tveit, Myrhaug et al. 2008)

Work process	Share of diffusive emissions	Share of internal pollution	Description of emission
1: Raw material handling from key to storage	0 – 5 %	0 %	Fume generated by transportation, conveyer belts, etc
2: Raw material transport from storage to furnace	0 – 5 %	5 – 10 %	Fume generated by raw material mixing and internal transportation to furnace
3: Furnace processes	10 – 20 %	5 – 20 %	Smoke and fume escaping the off gas system and spreading inside the plant
4: Tapping	20 – 40 %	30 – 50 %	Smoke and fume from tapping process
5: Casting	20 – 40 %	15 – 25 %	Smoke and fume from liquid metal handling
6: Crushing, screening and packing	5 - 15 %	5 – 15 %	Metal fume from operations
7: Off gas system	5 – 10 %	0 – 5 %	Fume and smoke escaping channels, fans, etc
8: Product packing of collected fume from off gas	0 - 5 %	5 – 10 %	Fume into work environment from operations

It is clear from Table 3.1 that the two areas standing out most are "Tapping" and "Casting". Both these work processes involves the handling of liquid metal and are also processes where the operators are in close contact with the metal. Having identified these two as the worst internal polluters this simultaneously means that operators working with these two processes are the ones most exposed to fumes.

3.1 Measurements of the emissions inside a plant

On order to get an impression of the levels of fumes from the two main sources in Table 3.1, "Tapping" and "Casting", three measurements of fume emissions inside a silicon plant were set up.

One of the measurements was placed on the working floor in the tapping area, measuring the level of fumes in the air right above the main work position for the operators. The other two measurements aimed firstly to measure the emissions escaping the established off gas system at the tapping floor and secondly the emissions from the casting process, both emissions flowing freely out into the plant building.

To measure the emissions the fume concentration in air was measured using two DM4 Open Path Dust Monitor from NEO Monitors (NEO 2009). The DM4 Open Path Dust Monitor is based on a laser light principle, measuring the average dust concentration along an optical line of sight between a transmitter and a reflector. A sudden pointwise emission along that line would then be registered as an average increase in the fume level for the entire line in the DM4 results.

The two DM4 monitors were not fully calibrated before the measurements, but adjusted to measure between zero and 1 mg/Nm^3 in clean air, meaning that the measured increase in level could describe the magnitude of the emission and not necessary the exact value. Figure 3.6 illustrates the conditions that typically would give a measured value between zero and 1 mg/Nm^3.

Figure 3.2 show a sketch of the silicon plant with the three measuring paths drawn.
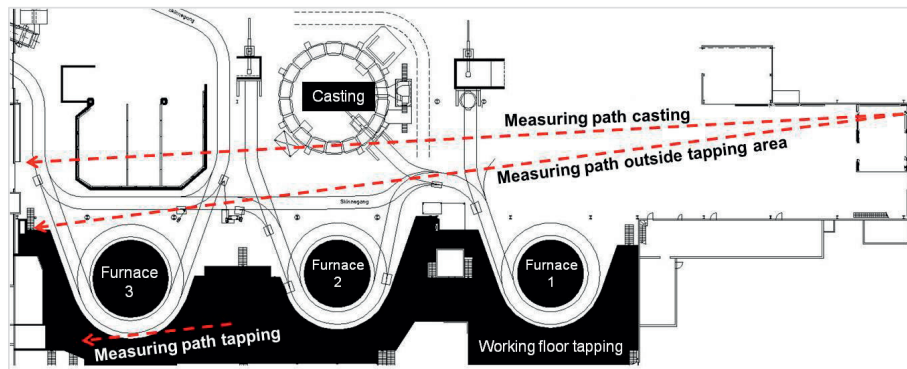
Figure 3.2: Sketch of a silicon plant with emission measuring paths

3.1.1 Measuring path tapping.

The target for the measurements on the tapping floor was to record any fumes not collected by the off gas suction system and therefore escaping out to the area where the tapping operators are working.

Placed between the furnace and the tapping operator there was a movable wagon containing several tools used in daily operation. The wagon was designed in such a way that it shielded the operators from the hot gases and flames coming from the tap hole. Observations revealed however that sometimes fumes could escape over this wagon entering the area in which the operator was placed while working. The measuring path was therefore located right inside the wagon but high enough to avoid interference with personnel or fork lifts that operated in the area, approximately 2.5 metres above the floor. The direction of the laser light was chosen so that it could capture as much of the area behind the movable wagon as possible.

Figure 3.3 shows the tapping area and chosen measuring path (dotted line). The wagon is on the left of the picture in Figure 3.3.

Figure 3.3: Measuring path in tapping area

The black circle in Figure 3.3 shows a leakage of fumes from the off gas system into the tapping area.

3.1.2 Measurement path outside the tapping area

Observations on site also found that some of the fumes spread out and drifted upwards and out to higher areas in the plant. Figure 3.4 shows a photo taken under conditions where a lot of fumes escape the off gas system and leaks up into higher levels of the plant (white circle).
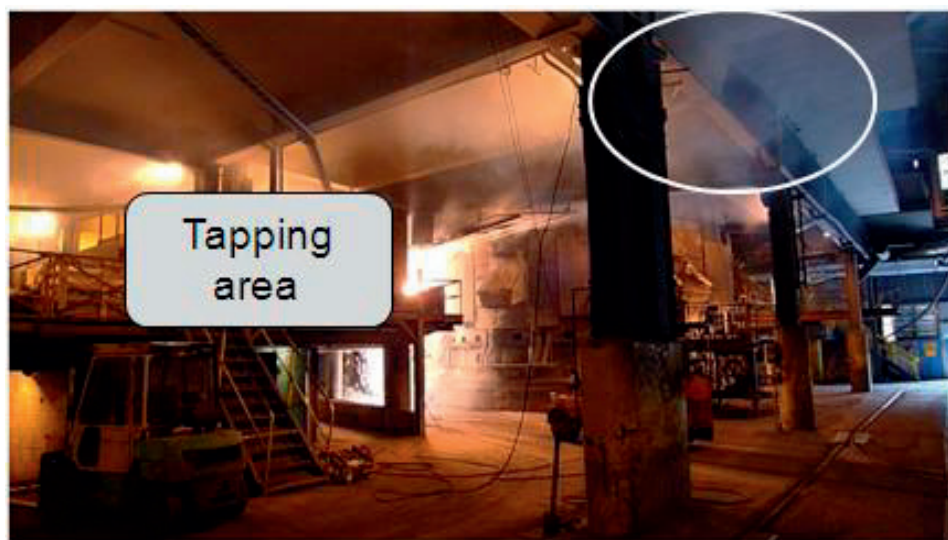
Figure 3.4: Leakage of fumes from the tapping area

To try to measure the amount of these escaping fumes a path was chosen according to Figure 3.2. This entailed placing the reflector in such a way that parts of the fumes leaking out and up would pass through the laser light.

3.1.3 Measurement path over casting

The last measuring path was chosen to measure the fumes that rise from the ladle during casting. During casting the ladle was placed in a tilting device while pouring the metal on to a casting carousel. Figure 3.5 illustrates the situation right before casting. The emission is fairly concentrated and rises more or less straight up from the ladle to the roof.

The reflector was in this case placed so that the laser light was send through the rising cloud of fumes from the ladle.

Figure 3.5: Fumes from ladle during casting

Figure 3.6 show the two measuring paths as seen from the transmitter.
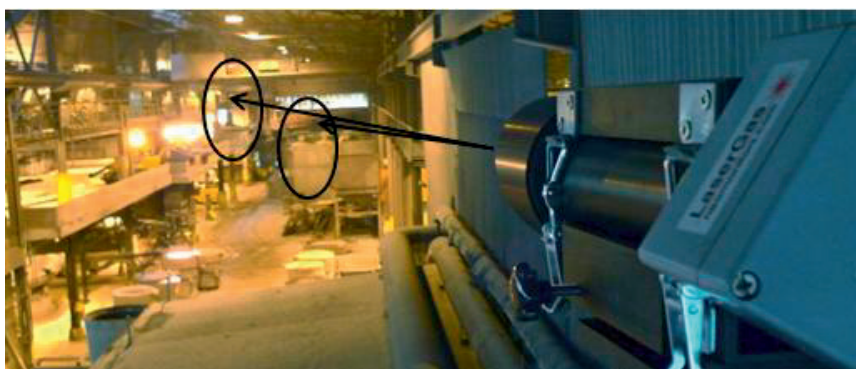
Figure 3.6: Measuring paths seen from the transmitter

The condition shown in Figure 3.6 also describes a situation without any leakage of fumes from the tapping and without any casting present. This situation would as earlier mentioned give a measured result between zero and 1 mg/Nm^3 fume.

3.2 Results of the measurements at the tapping floor

The measurements conducted at the tapping floor were done simultaneously with the measurements outside the tapping area. The two DM4 Open Path Dust Monitors were placed according the paths shown in Figure 3.2.

The measurements were conducted for 8 hours and the results are given in Figure 3.7 together with black triangles indicating the time when a new tapping cycle was started.
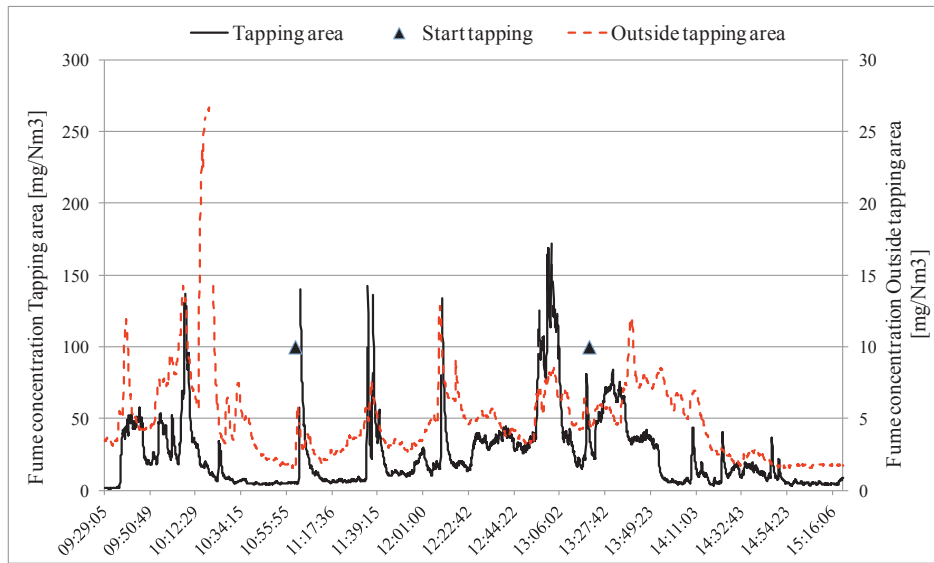
Figure 3.7: Fume concentration tapping area and outside

During these measurements the furnace was tapped continuously.

Note that according to Figure 3.7 there are several occasions where the off gas system seems to fail to collect all the fumes from the furnace and the fume level in the tapping area increases. There also seems to be a connection between the two measurements with the fume level outside the tapping area increasing after an initial increase in the fumes leaking out from the off gas system.

In addition to the DM4 Open Path Dust Monitors, two operators per shift, one in the tapping area and one on the stoking floor above, wear a *Casella Apex* Personal Sampling Pump for 48 hours, starting on the same day as the measurements were conducted and continuing on the following day.

The Casella Apex sampling pumps were analysed by MOLAB AS (MOLAB 2011) and the results from the eight parallel measurements are shown in Figure 3.8.
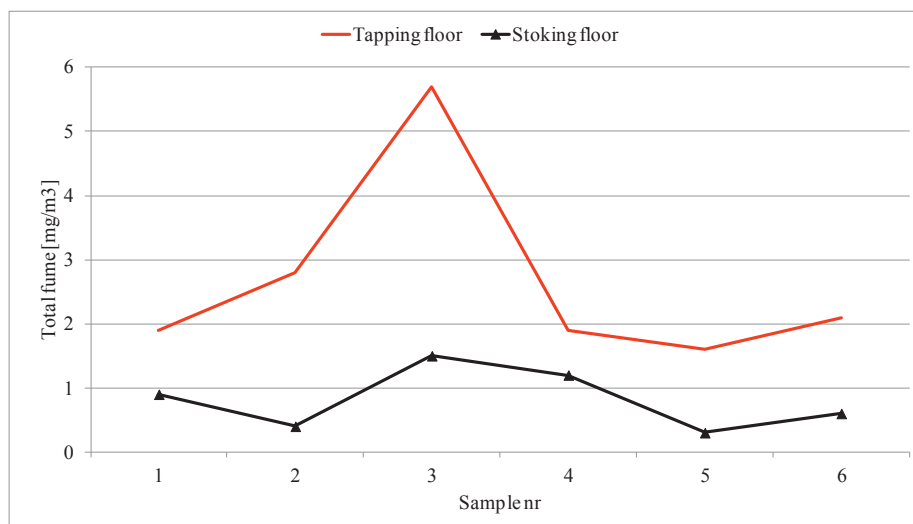
Figure 3.8: Casella Apex results

As seen in Figure 3.8 the two parallel measurements connect well, meaning that when the tapping operators experience an increased amount of fumes in their working environment these fumes spread to higher levels in the building, also influencing the work environment for the operators higher up.

3.3 Results from outside the tapping floor

The measurements outside the tapping floor were continued for several days to get an impression of the overall level of emissions over time. A typical 24 hour period is shown in Figure 3.9.
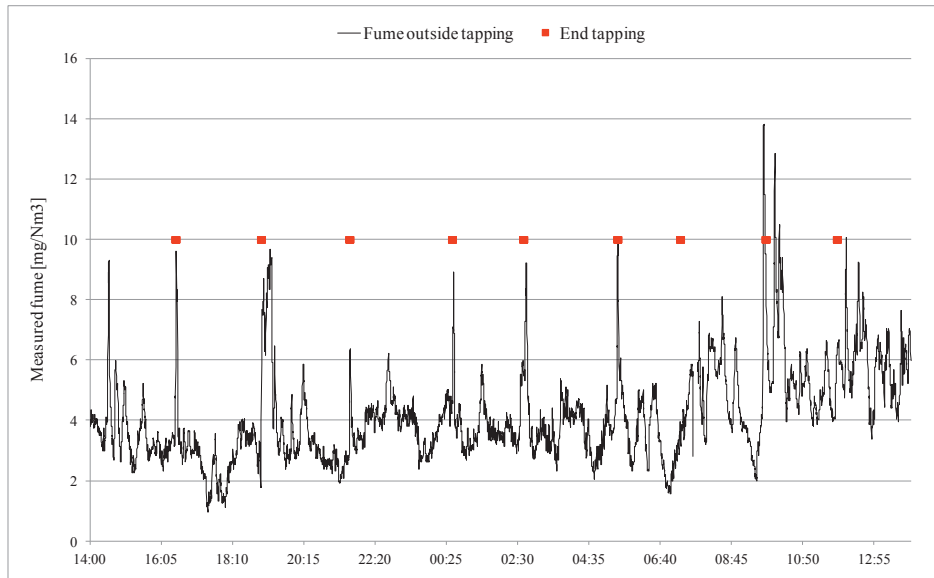
Figure 3.9: Measured fume outside the tapping area

The red markings in Figure 3.9 indicate the time of the end tapping, meaning that the ladle would be transported from the tapping area to casting. During this work operation the ladle passed the laser light at least once and in some cases stayed within the laser light for some time before going to casting. The peaks connected to the ladle passing's are assumed caused by the purge gas stirring the metal all the way up until casting is finished.

Comparing the base level of emission in Figure 3.9 and Figure 3.7 they are in the same range for longer periods of time, showing that the tapping area leaks fumes to the rest of the plant on a regular basis.

3.4 Results from casting

In the same way as for the measurements outside the tapping area the measurements over the casting machine were continued for several days. In contradiction to the measurement outside the tapping area, where the ladle passes the laser light during transportation, the measurements at the casting carousel show the situation when the ladle is placed in a fixed position inside the laser light for a longer period of time. Figure 3.10 presents the measurements for a whole 24 hour period at the casting carousel.
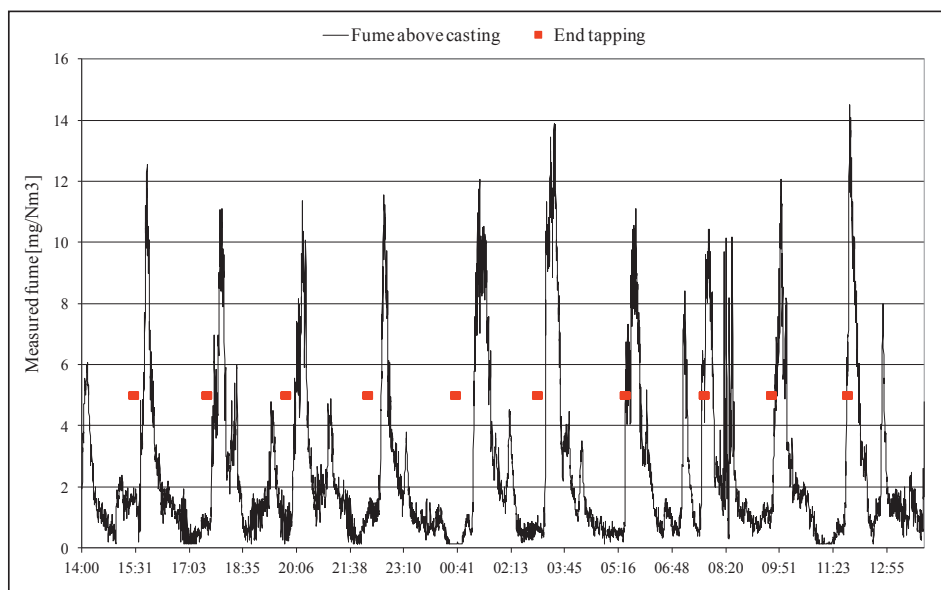
Figure 3.10: Measured fume above the casting machine

Once again the red markers indicate the time when the tapping cycle was finished. As expected the fume concentration increases some time after ended tapping, meaning that the ladle has arrived at its casting position. According to the plant the casting usually lasts for approximately 30 minutes and taking this information into consideration the level of fume is fairly constant during casting. It is also interesting to see that if comparing the maximum level of fumes in Figure 3.10 and Figure 3.9 the same values are observed, meaning that the fume emission from a ladle full of metal seems fairly stable.

3.5 Quantitative assumptions of the emissions

The laser light transmitted by the DM4 Open Path Dust Monitors embrace approximately a one metre wide column along the measurement path. It is now possible to estimate the fume emission that has passed through the laser light as long as the total measurement path and the length of the emission giving the increase are known.

Figure 3.11 provides a sketch over the measuring paths as seen in Figure 3.6 and the length of the emissions as measured on site.
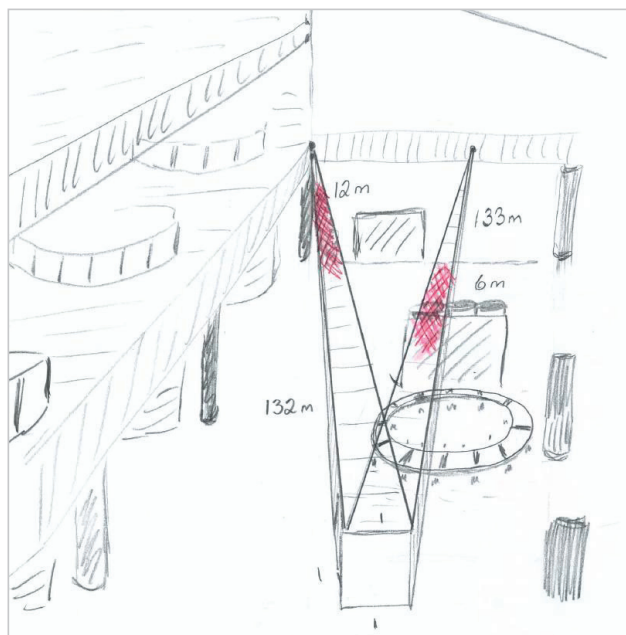
Figure 3.11: Sketch of measuring paths and emissions

The DM4 Open Path Dust Monitors report the emissions as if they were equally distributed along the whole measuring path, meaning that if you have a measuring path of 10 metres and a point release of 100 mg/Nm^3 on the first metre of the path (while the rest of the measuring path is emission free), the results reported by the DM4 Open Path Dust Monitors would be 10 mg/Nm3.

In other words if the DM4 measures over n cells the reported result from the device would follow the formula

$$\frac{1}{n}\sum_1^n X_n = \overline{X_{path}} = measured\ value \qquad\qquad \textbf{3-1}$$

Now assuming that the emission is equally spread inside the emission zone and that the cells not experiencing any increased emissions have a level of $X_1 = 1$ mg/Nm^3 the measurement becomes a sum of two sums:

$$measured\ value\ \overline{X} = \frac{1}{n}\left(\sum_1^{n\ cells\ with\ emission} X_n + \sum_1^{n\ cells\ without\ emission} X_1\right)$$ 3-2

By using this equation the level of emission for the cells inside the emission zone can be estimated.

3.5.1 Estimated level of emission outside tapping

Looking at Figure 3.11 the fumes escaping from the tapping area have a length of 12 metres and according to Figure 3.9, when looking at the time periods without the ladle passing, the level of fumes is in the area of 3-5 mg/Nm^3.

The total path length is 132 metres, meaning that n = 132, n cells with emissions = 12 and n cells without emission is 120.

Inserting these in Equation 3.2 you get: $\frac{1}{132}(12x + 120) = measured\ range$.

Solved for x being the single cell value in the emission zone, x becomes 23- 45 mg/Nm^3.

In other words the fume concentration in the air inside the emission zone was 23-45 mg/Nm^3.

3.5.2 Estimated level of emission during casting

For the casting measurements the emission zone was only 6 metres and the measured value during casting according to Figure 3.10 was on average around 11 mg/Nm^3. Using a total measuring path of 133 metres, inserting in Equation 3.2 and solving the results is 223.

This means that casting generates a fume concentration of 223 mg/Nm^3 in the air above the casting position.

These results reveal that the emissions from the ladle is in the order of five times higher than the leakage from the tapping area, meaning that having a situation with a lot of ladles with liquid metal transported around the plant outside any off gas suction equipment would represent a substantial contribution to the plants internal pollution.

3.6 Concluding remarks

The silicon process consists of several process steps each contributing to diffusive emissions or internal pollution. With respect to the latter the work processes inside the silicon plant has two; tapping and casting, which stand out as they are high polluters and at the same time work processes where the plant operators are close to the emissions. Descriptive studies of the emissions from these two could provide the understanding and knowledge needed to reduce and minimize them.

Measurements of the fume emissions to the operators' work environment on the tapping floor have been done simultaneously with measurements of any fumes leaking out of the area. The leakage is probably caused by an unsatisfactory tapping floor in terms of off gas suction. A connection between the two has been found and measurements done with operators wearing sampling equipment show that an increased fume concentration at the tapping floor spreads higher up in the building, polluting the floors above.

The fume concentration in the air has been measured over several days for the area right outside the tapping floor and during casting. The results show that whenever a ladle full of metal passes the measurement path the fume concentration is raised to almost the same level, independent of measured during transportation or casting. Most likely the fume emerging from the ladle is caused by the purge gas stirring the metal and as seen from the casting measurements they continue at the same level up until the casting is almost finished.

Based on several assumptions the fume concentration in the rising hot air outside the tapping floor and above the ladle during casting has been calculated. The results show that the rising fumes from the ladle are in order of magnitude five times higher than the leakage from the tapping floor. This means that the ladle containing liquid metal, being outside any off gas suction equipment, would itself be a major contributor to the internal pollution inside a silicon plant.

Chapter 4   Material and energy balances in the silicon process

The purpose for this chapter is to get an overview of how the different chemical elements and energy fed to the furnace though raw materials and electricity are distributed between the main outputs.

The material and energy balance is based on data collected from a 93 MVA silicon furnace at Elkem's plant in Salten over a period of 48 hours.

The overall emission situation for a silicon furnace can be described by the sketch in Figure 4.1.

Materials and energy

Electric energy   **Silica fumes to furnace stack**

Raw materials

Gaseous emissions to furnace stack

Silica fumes

Emissions of energy

Gaseous and energy emissions

Products
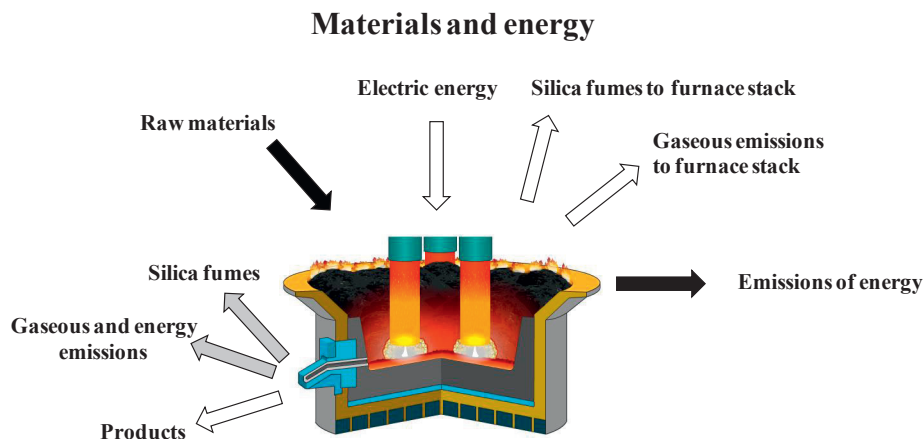
Figure 4.1: Overall emission situation for a silicon furnace

The main inputs to the silicon process are the raw materials and electric energy (shaded arrows) while the output is divided in to several categories, the main ones (white arrows) being:

- Products
- Silica fumes
- Off gas components

The energy output (black arrow) is mainly divided between the following:

- Off gas
- Products
- Cooling water
- Other losses

In addition the tapping process will have some emissions of fumes and gaseous species as well as some energy (grey arrows).

4.1 The material balance

To calculate the material balance for the furnace process operational data from the plant's own systems were collected. These data included

- Raw material consumption and additives to the process
- Energy consumption
- Production of
  - Metal, including
    - Liquid metal
    - Slag from furnace
  - Silica fumes, including
    - In grade fumes
    - Coarse particles sorted out through cyclones

In addition, the off gas volume and chemical analysis were measured.

Since the measurements were done over two full days, data for each day were collected and the average of the two was used as input to the balance.

4.1.1 Material sampling

Due to the available time frame prior to the two days of collecting output data the raw material samples for analysis had to be collected in several ways.

Table 4-1 gives a summary over the different materials and samples taken

Table 4-1: Material balance input and output

Input	Output
Coke	Metal day 1
Coal A	Metal day 2
Coal B	Slag day 1
Bio carbon A	Slag day 2
Bio carbon B	Silica fumes day 1
Additive	Silica fumes day 2
Quartz A	Coarse silica material day 1
Quartz B	Coarse silica material day 2
Quartz C	Off gas analysis
Quartz D	
Electrode paste	
Electrode casing	

4.1.2 Raw materials and additives

All raw materials at the plant were stored in individual silos enabling the possibility to manually sample a "cut of stream" of the wanted raw material. Because of the extensive numbers of raw materials the samples had to be collected over several days prior to the two days of collecting the furnace data. Ideally all the samples should have been collected approximately 8 hours before starting the furnace data collection. The chosen strategy still would embrace any variations in the raw materials since they were taken over a longer period.

Table 4-2 lists the amount of each raw material sampled. The total sample size is equal to approximately 0.1 % of the assumed consumption of that material during the two days of measurements.

Table 4-2: Raw material samples

	Day A	Day B	Day C	Day D	In total
Coke	20 litres	20 litres	20 litres	20 litres	80 litres
Coal A	10 litres	30 litres	20 litres	20 litres	80 litres
Coal B	10 litres	30 litres	20 litres	20 litres	80 litres
Bio carbon A		40 litres	20 litres	20 litres	80 litres
Bio carbon B		50 kg	50 kg		100 kg
Additive		10 litres			10 litres
Quartz A		80 kg			80 kg
Quartz B		60 kg	60 kg		120 kg
Quartz C		60 kg	60 kg		120 kg
Quartz D		60 kg	60 kg		120 kg
Electrode paste		10 litres			10 litres
Electrode casing					1 kg

4.1.3 Products from tapping

One sample from each ladle of metal was collected and in total 20 samples of metal were collected. The samples for each day were mixed and represent that day.

As the slag from the furnace varies, several samples were taken throughout each day and all samples for the same day were mixed.

4.1.4 Silica fume and coarse particles

The silica fume was sampled just before being send to the fume storage silos, collecting 2 litres of fumes every hour over a period of approximately 8 hours each day. The samples for each day were mixed into one sample.

The coarser particles in the off gas stream were separated from the fumes at an earlier stage. They were sampled in the same matter as the silica fume

4.2 Sample preparation

All samples were dried, crushed and prepared for analysis according to guidelines given by Lab Nett, Norway (http://www.labnett.com/). See Appendix A.

4.3 Analysis of the samples

To analyse the different samples several laboratories were chosen based on an expectation of core competence in analysing that specific material or element.

The following laboratories were used:

Table 4-3: Overview of laboratories

Laboratory	Elements
Lab Nett, Norway	Analysis of heavy metals in raw materials and products
Elkem Silicon Materials, Norway	Analysis of the silica fumes and main components in raw materials and products
MOLAB, Norway	Analysis of heavy metals in the off gas
Own analysis	Gaseous components like CO, CO_2, SO_2, NO and NO_2 measured with a TESTO 350XL

4.4 Results

Considering the results, there are some elements with analysis for only one of the material flows and these elements are excluded from the reported results. There are also some elements where the reported level of content is below the detection limit and this is compensated by adding 50 % of the detection limit to the element. By doing this any uncertainties in the analysis should be accounted for.

In addition the measurement of the off gas volume was believed to be somewhat inaccurate so the total amount of off gas from the furnace is balanced to have a 100 % yield in nitrogen.

The element yields for all elements with a closed material balance are given in Figure 4.2.
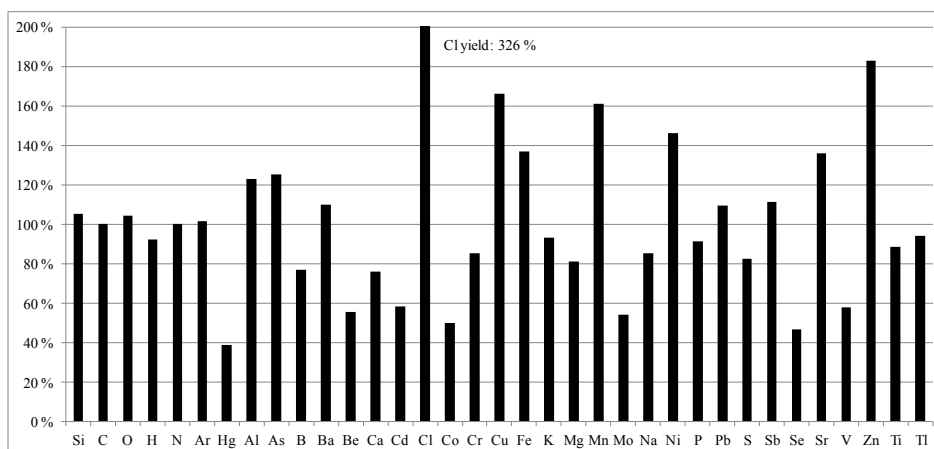
Figure 4.2: Element yield for all elements with a closed material balance

4.4.1 Elements with high yields

As seen in Figure 4.2 there are several elements with high yields, but Cl and Zn are clearly much higher than the rest.

The high yield in both elements is caused by high off gas analysis and low product analysis.

- Chlorine

Chlorine is found as hydrochloric acid (HCl) in the off gas and a closer look at the dataset shows that the variations synchronize with the level of moisture in the off gas. During the sample preparation of the raw materials they are all dried since the analysis is done on a dry basis. Given the low boiling point of HCl (110 ºC) it is plausible to believe that the HCl is evaporated during sample preparation and therefore results in a lower raw material content of HCl than in reality. In the furnace however the HCl would evaporate together with the water ending up in the off gas, but since the calculation of the raw material contribution is based on the dry analysis adjusted for moisture content the level of HCl from the raw materials would be too low.

- Zinc

For zinc the high content in the off gas could be explained by the use of a tapping tool giving zinc in the off gas from the tapping area, but not in the metal. The off gas analysis is influenced by the use of this tools on day two. Calculations adjusting for these tools would give a yield of approximately 135%.

30

The other elements with a high yield, Cu, Fe, Al, Mn and Ni, could all be explained by assuming that they follow the metal phase because of high boiling points. It is plausible that the process could either accumulate or drain more metal than the raw materials fed to the process would call for. This accumulation or extra drainage could occur over several days and a high yield could be explained by the furnace releasing more metal during our measurements.

The last element with a high yield is arsenic (As). Looking into the detailed element balance the high yield is caused by a high analysis in the silica fume. The main source of arsenic is one of the coals going into the process so it is reasonable that the low boiling point (603 ºC) causes the arsenic to evaporate and end up in the silica fumes.

4.4.2 Elements with low yields

Figure 4.2 also show several elements with a very low yield. These can then again be divided into two categories:

- Elements with low yield and high boiling point: Be (2472 ºC), Co (2928 ºC), Mo (4639 ºC) and V (3409 ºC).

  The low yield is caused by a low content in the product phases. Because of the high boiling point it could be assumed that these elements would end up in the metal or slag phase. Common for them all is the general low content in both input and output.

- Elements with low yield and low boiling point: Hg (357 ºC), Cd (767 ºC) and Se (685 ºC).

  For selenium the off gas analysis is missing. Taking into consideration the boiling point much of the selenium is probably lost to the gas phase.

  Looking at the analysis most of the elements with a low yield are reported to have a content below the detection limit, meaning they are given half the detection limit as a value. The low yield could indicate that this way of assigning them a value underestimates the real content.

4.5 The distribution of elements between metal, silica fume and off gas

Based on the element yields from Figure 4.2 it is straight forward to plot the distribution of the different elements.

Figure 4.3 shows where the different elements were found in addition to the boiling point for each element, given by the black line.
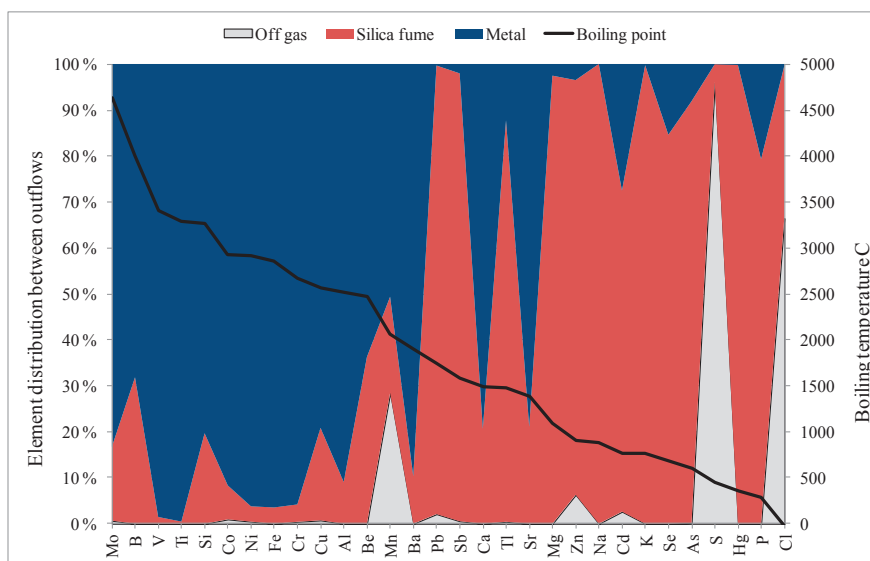
Figure 4.3: Element distribution and boiling point of element

To calculate the values shown in Figure 4.3 the sub group of "Slag" is included in the "Metal" group and the sub group of "Coarse particles" included in the "Silica fume" group. The contribution from these two sub groups are weighted based on the amounts of each sub group compared to the main group.

Myrhaug (Myrhaug 2003) did a similar investigation for a silicon furnace in 2003 and his results are shown in Figure 4.4.
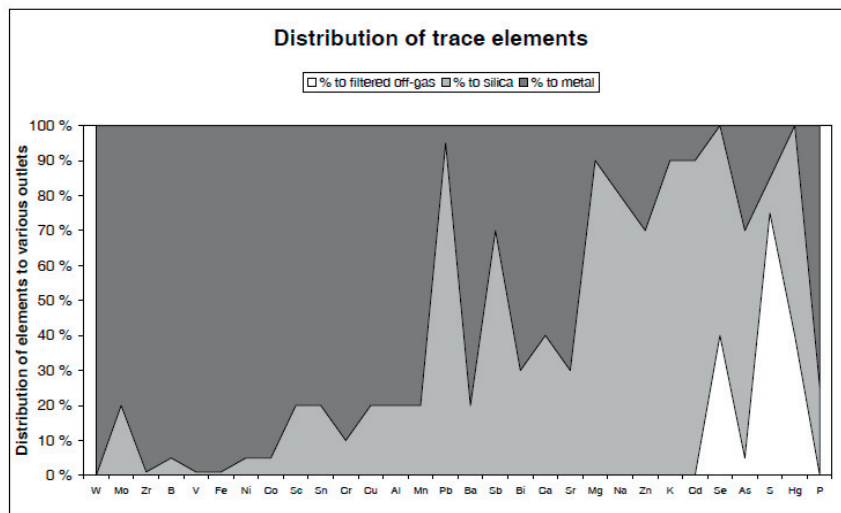
Figure 4.4: Myrhaugs distribution of elements (Myrhaug 2003)

Comparing the two boiling point figures they have in general similar results, but some elements deviate in the two models. Table 4-4 presents a more detailed comparison between the two results.

Table 4-4: Comparison of distributions

Element	Kamfjord 2012			Myrhaug 2003		
	% to Metal	% to Silica fume	% to Off gas	% to Metal	% to Silica	% to Filtered off-gas
Cl	0	33	67	No Analysis		
P	21	79	0	75	25	0
Hg	0	100	0	0	60	40
S	0	4	96	15	10	75
As	8	92	0	30	65	5
Se	15	85	0	0	60	40
Cd	28	70	3	10	90	0
K	0	100	0	10	90	0
Zn	4	90	6	30	70	0
Na	0	100	0	20	80	0
Mg	3	97	0	10	90	0
Sr	79	21	0	70	30	0
Tl	12	87	0	No Analysis		
Ca	79	21	0	60	40	0
Bi	No Analysis			70	30	0
Sb	2	97	1	30	70	0
Ba	90	10	0	80	20	0
Pb	0	98	2	5	95	0
Mn	51	21	28	80	20	0
Al	91	9	0	80	20	0
Be	64	36	0	No Analysis		
Cu	79	20	1	80	20	0
Cr	96	4	0	90	10	0
Sn	No Analysis			80	20	0
Sc	No Analysis			80	20	0
Co	92	7	1	95	5	0
Ni	96	3	0	95	5	0
Fe	96	4	0	99	1	0
V	99	1	0	99	1	0
B	68	32	0	95	5	0
Zr	No Analysis			99	1	0
Mo	83	16	1	80	20	0
W	No Analysis			100	0	0
Si	80	20	0	No Analysis		
Ti	100	0	0	No Analysis		
Green elements have close results						
Yellow elements show similar main features						
Red elements show major differences in the distributions						

For the elements showing the largest deviations in the models there are two main features:

- Large difference in metal/fume distribution: P, As and Sb
- Large difference in metal/off gas distribution: Mn, S and Se

Going back to Figure 4.3 and knowing from Chapter 2 that the temperatures inside the lower reaction zone of the furnace must be at least 1811 ºC to have a proper silicon process running the element distribution looks reasonable.

However there are some elements with a distribution that has a different behaviour than expected, taking the boiling point into consideration.

- Ca and Sr both show high values in the "Slag" analysis, influencing the distribution towards a higher "Metal" content.
- The two elements Pb and Sb should expectedly end up in the off gas, but the analysis reveals that they end up in the silica fume instead. A plausible explanation could be that these elements condensate on the fume particles on the way to the bag house filter.
- Hg could be expected to end up in the "Off gas" but as the analysis shows it probably either condensates on the silica fume or form some chemical component connecting to the fume particles. The measured amount of Hg exiting the process is very low and the distribution could be influenced by this.
- For P the off gas analysis is missing, introducing an error in the calculations.
- The last element is Cl, expected to end up solely in the off gas. However the analyses show that some Cl is found in the fumes.

Myrhaug argued in his explanation that several of the deviations in the model could be caused by the fact that some elements form oxides, sulphides or other chemical compounds changing the boiling point considerable compared to the element in its pure state. Since both models only consider input vs output of pure elements this explanation could easily be considered reasonable for this study as well.

4.6 Energy balance of a 93 MVA (ferro-) silicon submerged arc furnace

According to the "International Energy Outlook" for 2009 by the EIA (Energy Information Administration 2009) the total marketed energy consumption in the world will grow by 44 % from 2006 to 2030. This growth is predicted to occur first in non-OECD countries. Even though there is an expected increase in the use of renewable energy, coal and natural gas are still assumed to fuel nearly two thirds of the world's electric generation in 2030.
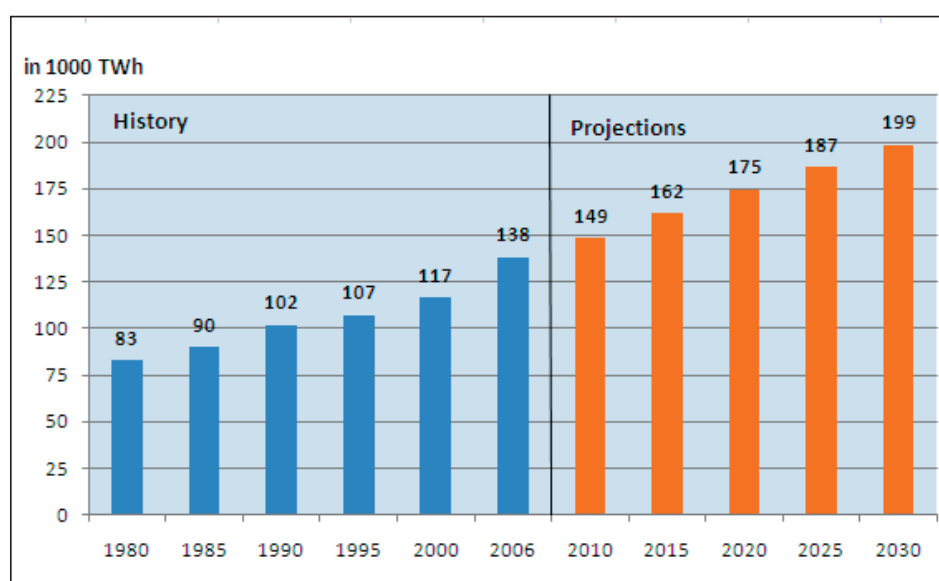
Figure 4.5: World energy consumption as estimated by EIA

This increase in energy demand will probably stimulate even more research on and realization of energy production based on renewable energy, but the utilization of the existing potential in high and low quality energy will become an important part of future energy production.

The global resources of fossil fuels are limited and therefore production of clean or CO2-free energy might have an important financial benefit for the user. In addition the consequences of new energy production replacing energy produced from coal or natural gas will benefit the environment.

Looking at the ferroalloy industry there are two main potential sources for energy recovery, an off gas with a high temperature that is suitable for electric energy production and the considerable amounts of cooling water that represent potential thermal energy

A study done by Norsk Industri in 2002 (Kjelforeningen-Norsk Energi and Institutt for energiteknikk 2002) summed the consumption of electric energy in the Norwegian ferroalloy industry (including silicon metal) to approximately 7700 GWh/year, excluding energy in reduction materials. From this the potential suitable for energy recovery is calculated to be in the area of 1310 GWh/year, or approximately 17 % of the total electric energy consumption.

A new study presented by ENOVA in 2009 concludes that the thermal energy potential in the Norwegian ferroalloy industry is 4795 GWh per year, divided into 74 % in off-gas, 3 % in steam and 23 % in hot water (ENOVA 2009).
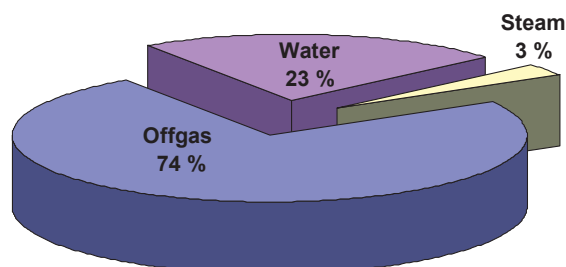
Figure 4.6: Distribution of energy in the Norwegian ferroalloy industry (ENOVA 2009)

Utilizing these energy potentials in energy recycling could according to their calculations decrease CO_2 emissions by approximately 460 000 tonnes/year if it replaces natural gas or by 1 010 000 tonnes/year if it replaced coal.

4.6.1 Energy streams in the (ferro-)silicon process

As Chapter 2 indicated the silicon process is dependent on a stable temperature above 1811 ºC in the inner reaction zones to run properly. The high temperature is mainly a product of the electric arcs burning underneath each electrode. In addition the carbon materials added to the furnace have to be considered as an energy source because of the energy bonded in both carbon and volatile components.

Even though the raw materials to produce silicon metal are few the use of different carbon sources probably vary from region to region, most likely caused by a combination of availability, experiences and cost per tonne. The energy contribution to the furnace from the carbon materials will therefore vary from furnace to furnace dependent of the choice of carbon sources.

The outlet of energy from the process will also vary depending on installed technology at the furnace, but the overall energy streams in and out of the furnace would be as follows:

In:

- Electric energy, energy in carbon and volatile matters in the carbon materials

Out:

- Energy in off gas, energy bonded in products, energy lost to cooling water, electrical losses and other losses like energy lost out through the furnace lining, etc.

4.6.2 Improvements in measuring energy captured in cooling water

The investigation after an accident at an Elkem silicon plant in 2006 concluded that one of the root causes of the accident was cooling water leaking into the furnace over a period of time, in the end causing a violent explosion (Tveit, Garcia et al. 2008). This led to the action that a lot of silicon furnaces in Norway installed a surveillance system for the cooling water flow, focusing on getting a total overview of the equipment located closest to the furnace centre.

The furnace from which these energy data was collected had a system from Endress & Hauser (Endress & Hauser 2009) installed , measuring inline flow and temperature. This new and improved energy data was utilized in the energy balance.

4.6.3 The energy balance for the furnace

To present the energy balance for the furnace a Sankey diagram is drawn which presents the distribution of the different energy streams in and out. Figure 4.7 shows the situation for the furnace as operated during the measurements. The detailed numbers are given referred to a furnace with an output of 10 MW in electrical effect.
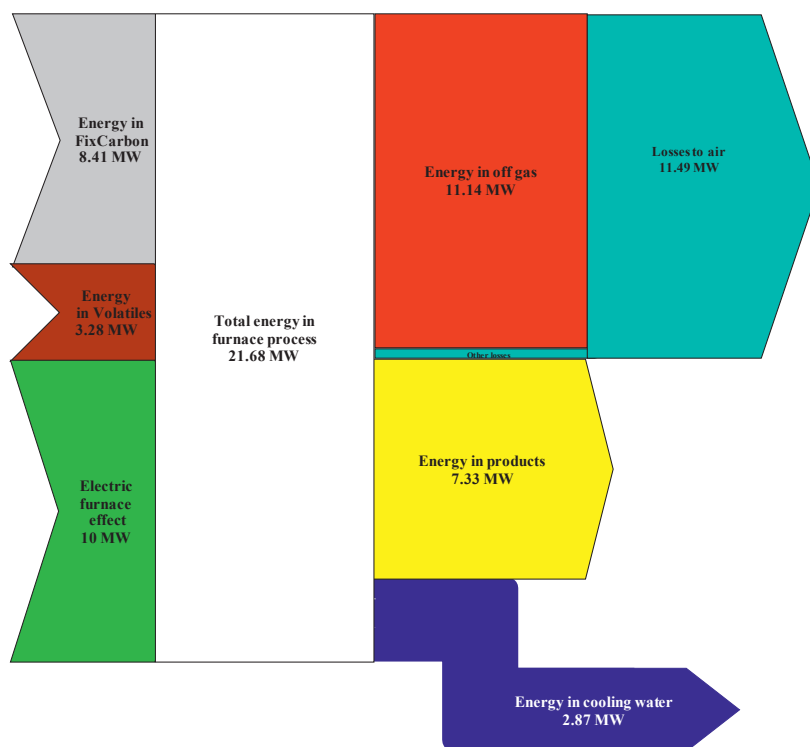
Figure 4.7: The Sankey diagram for the silicon furnace

Note that the energy content in raw materials actually exceeds the electric energy input and that the amount of energy captured in the cooling water system is approximately 28 % of the electric input. With no energy recovery system installed, all the energy in the off gas is released to air by allowing cold outside air to enter at the furnace top. The energy released represents approximately 115 % of the input electric furnace effect.

The details for the Sankey diagram are presented in Table 4-5.

Table 4-5: Sankey diagram details for furnace without energy recovery

	Today's situation [in MW]
Electrical furnace effect	10.00
Energy in FixCarbon	8.41
Energy in volatiles	3.28
Total energy in furnace process	21.68
Energy in products	7.33
Energy in cooling water	2.87
Other losses	0.35
Energy in off gas	11.14
Released to air	11.49

It is interesting to see how the energy streams change if the same furnace had an energy recovery system installed. Using numbers reported by Almås, Delbeck et al. (Almås, Delbeck et al. 2002) new energy streams can be calculated as shown in Figure 4.8.
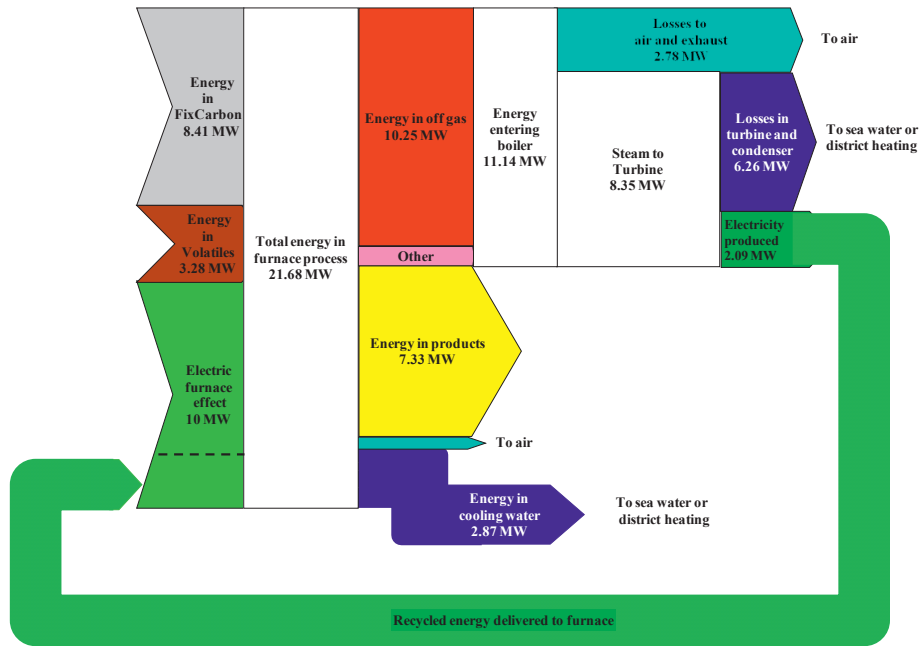
Figure 4.8: Sankey diagram for furnace with energy recovery installed

The Sankey diagram in Figure 4.8 returns the recovered energy back to the furnace, but an option could be to deliver this energy to external users.

Approximately 20 % of the input electric effect could be recovered, but installing an energy recovery system also adds an additional source of thermal energy, namely the cooling water from the turbine and generator. This new thermal energy source together with the already described furnace cooling water adds up to 91.3 % of the input electric effect.

To increase the energy recovery the most important parameters are:

- Furnace effect
  - Since the energy in the off gas is proportional to the furnace effect an increased furnace size may have a relative lower loss of energy per unit size
- Volatile matters in the raw materials.
  - Increased usage of coal and wood-chips gives higher energy in the off gas compared to the use of coke and charcoal as the carbon source

- Off gas temperature
  - A higher off gas temperature will lower the off gas volume and energy in the off gas after the boiler and allows higher steam temperature and pressure that improves the efficiency of the boiler and turbine system
- Access to cooling water
  - Good access to cold cooling water will allow a lower condenser pressure, this is also important to the energy recovery process

Table 4-6 gives the detailed numbers for the Sankey diagram with energy recovery.

Table 4-6: Sankey diagram details for furnace with energy recovery

		With energy recovery installed [numbers in MW]
Input to furnace	**Electrical furnace effect**	10.0
	Energy in FixCarbon	8.41
	Energy in volatiles	3.28
Total energy in furnace process		21.68
Output from furnace	**Energy in products**	7.33
	Energy in cooling water	2.87
	Other	0.35
	Energy in off gas	10.3
	From steam surfaces	0.89
Energy entering boiler		11.1
	Losses to air and exhaust	2.78
Energy in steam to turbine		8.35
	Losses in turbine and generator	6.26
Electricity produced		2.09

However, the recovery of electric energy will require a partial redesign of the furnace exhaust gas handling system. The financial implications of this will not be discussed here. An alternative system where primarily hot water is produced could also be of interest, assuming there are available customers for the hot water.

4.6.4 Energy changes and variation in the system

Due to the fluctuating nature of the furnace process there will be considerable variation in the energy flows when looking at the data on a shorter time frame. To try to illustrate this variation the energy balance over a period of 48 hours is calculated, letting the average of 8 hour data represent one period. For convenience all numbers are related to the electrical furnace effect, letting the effect represent 100 %.

The variation in input and output energy is given in Figures 4.9 and 4.10.
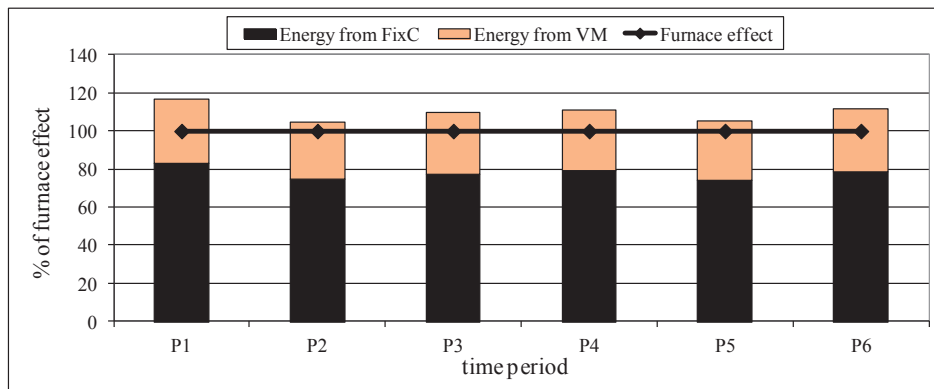
Figure 4.9: Input flows of energy to the furnace[2]
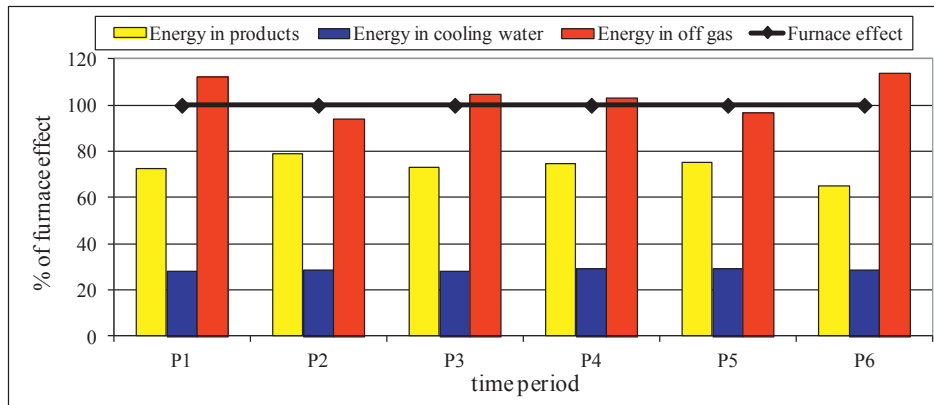
Figure 4.10: Output flows of energy from the furnace

Based on the input of electric effect it is clear that a considerable amount of the variation is explained by variation in either the charging of new raw materials or tapping of metal.

---

[2] The variation in electric furnace effect over the given time periods is +/- 0.45 MW.

4.7 Concluding remarks

In this chapter the material and energy balances for a 93 MVA silicon furnace have been calculated based on industrial measurements of consumption/production and material analysis done by certified laboratories.

4.7.1 The material balance

A material balance over a vast amount of chemical elements entering the silicon furnace has been made, based on sampling and analysis of all material streams going in and out of the furnace. Most elements show a yield close to 100 %, but some elements have either too high or too low values compared to what should be expected. Most of these deviations could be explained by either process variations or work operations done towards the furnace.

The material balance also shows that most of the elements entering the silicon furnace distribute themselves according to their boiling points. Comparing our results with an earlier model done by Myrhaug most elements have the same behaviour with respect to where they end up. Some elements differ from the expected behaviour but there are possibilities that these could bond with other elements and in such a way change their boiling point.

4.7.2 The energy balance

The energy balance for the furnace shows considerable opportunities for energy recovery projects. Both hot off gas and large amounts of hot cooling water are available and the installation of a steam-based energy recovery system would give an extra source for thermal energy through "new" hot cooling water from the turbine and generator.

Installing an efficient energy recovery system on the furnace studied could give a total of 11.3 MW energy recovered, either in the form of electricity or thermal energy. In comparison this energy would represent an emission in the order of 76 000 tonnes CO_2 if produced by a coal fired energy plant (Kjelforeningen-Norsk Energi and Institutt for energiteknikk 2002). Table 4-7 sums up the different energy possibilities in the two cases.

Table 4-7: Summary of thermal and electric energy potentials per 10 MW electric input effect

	Available thermal energy [MW]	Available recovered electric energy [MW]	Potential CO_2 emission savings [tonnes/year]
Today's situation	2.87	-	
With energy recovery installed	9.2	2.1	76 220

Chapter 5   Material and energy balance in the tapping process

One of the most critical processes during silicon production is the tapping of metal. To maintain a high production yield and a stable operation the furnaces need to be drained of metal on a regular basis. According to the back reaction of silicon with quartz, failing to do this could increase the production of gaseous species inside the crater zone:

$$SiO_2(l) +\ Si\ (l) =\ 2\ SiO(g) \qquad\qquad\qquad\qquad \textbf{5-1}$$

Reaction (5.1) runs to the right for temperatures above 1850 ºC and is highly endothermic consuming 6 kWh of energy and producing 1.6 Nm^3 of SiO gas per kg silicon converted. Once the extra SiO gas is produced it would either flow upwards in the charge or escape out through the tap hole. Some of it will condense to Si and $SiO_2(l)$ but in many cases it will flow to the furnace surface and oxidize to SiO_2 silica fumes. During this oxidation a vast amount of energy is released in addition to the fumes.

After looking at the overall energy and material balance for the silicon furnace in Chapter 4 it is interesting to narrow down the area of interest and look at the tapping process only. This chapter therefore considers the material flows as well as the energy balance in and out of the tapping area.

Figure 5.1 gives a principle sketch of the furnace, runner and tap hole, off gas channel and work platform in the tapping area. The red square in Figure 5.1 indicates the limits of the mass and energy balance areas.
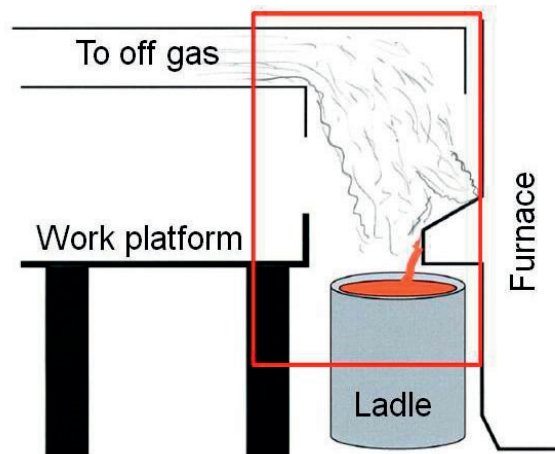
Figure 5.1: Area of scope for the material and energy balance

5.1 Main flows and work processes

In determining the different flows in the area all substances entering the area were defined as ingoing and the ladle sent to casting together with the hot off gases were defined as the outgoing flow.

Table 5-1 gives an overview over the ingoing and outgoing flows as well as the measured temperatures of that specific flow.

Table 5-1: Main flows in and out of selected area

Ingoing	Outgoing
Metal from the furnace (1617 ºC)	Refined metal (1464 ºC)
Additives to the refining of metal (25 ºC)	Slag from refining (1464 ºC)
Additives to adjust metal temperature (25 ºC)	Skulls[3] frozen in ladle (1464 ºC)
Gas through ladle for refining (5 ºC)	Fumes in off gas (57 ºC)
Furnace gas from tap hole (1600 ºC)	Hot gases into off gas system (57 ºC)
Cold air into off gas system (14 ºC)	

As seen in Table 5-1 there are more material streams going into the area than out of it. This is caused by the need for additives and purge gas to refine the metal and other additives used to adjust the temperature of the metal before it is send to casting.

The chemistry and details of the refining process is outside the scope of this work, but it consists of exchange reactions between the metal and slag phases contained in the ladle. A more thorough description of the refining process can be found in Schei, Tuset et al. (Schei, Tuset et al. 1998).

5.2 Measurements and assumptions

The material and energy balances were based on measurements from three tapping cycles. Two of the cycles were conducted using a specially adapted hood over the tap hole, named a Doghouse, to ensure that all the fumes from the tapping process were collected. The details of the principles behind the set up are described in Kadkhodabeigi, Tveit et al. (Kadkhodabeigi, Tveit et al. 2010).

The weights of tapped metal, finished refined metal, additives and slag formed was collected from the production reporting system in the plant.

Samples of the metal and additives were delivered to the plant's laboratory and analysed on an ARL ADVANT'XP Sequential XRF.

---

[3] Skulls describes the mixture of metal and slag that freeze inside the ladle during tapping

The slag samples were analysed at the Department of Chemistry, Norwegian University of Science and Technology, Norway using High Resolution Inductively Coupled Plasma Mass Spectrometry (HR-ICP-MS). Samples were dissolved in HF and HNO_3.

The amounts of purge gases were varied somewhat during tapping, but for the element balance an average value is assumed to be valid during the whole tapping.

Samples of the fumes in the off gas were taken and the fume was analysed by atomic absorption spectroscopy and combustion analysis with a LECO TCH600. The gaseous content in the off gas was analysed with a TESTO 350 XL and the volume flow measured with a pitot pipe.

Two material flows need to be balanced based on other measurements, namely the amount of cold air flowing into the off gas system and the amount of furnace gas coming out of the tap hole.

To balance the inflow of cold air the argon analysis in the off gas is used and the amount of cold air into the system adjusted to gain a 100 % yield in argon.

For the furnace gas it is assumed that the gas mixture inside the furnace consists of SiO and CO gas only, and that the composition is given by the two relations described in Schei, Tuset et al. (Schei, Tuset et al. 1998):

$$P_{tot} = P_{SiO} + P_{CO} = 1 \; atm \text{ and } s = \frac{P_{SiO}}{P_{SiO} + P_{CO}} = 0.5$$

From this it follows that the amount of moles of the two are equal.

To find the amount of gas flowing out from the furnace the element carbon is balanced, assuming that the main source for the extra carbon measured in the off gas is the CO coming from the furnace gas.

By doing this a second source of SiO combusting to silica fumes is added as well as an energy source since the combustion of SiO to SiO_2 fumes is highly exothermic.

5.3 The element balance and distribution

Compared to the element balance for the whole furnace the tapping area balance has less elements because of the available analysis. The full heavy metal analysis programme used in calculating the furnace balance was not done for the tapping samples, only the main elements going in and out of the area.

The element yield for the main elements entering and leaving the tapping area is given in Figure 5.2.
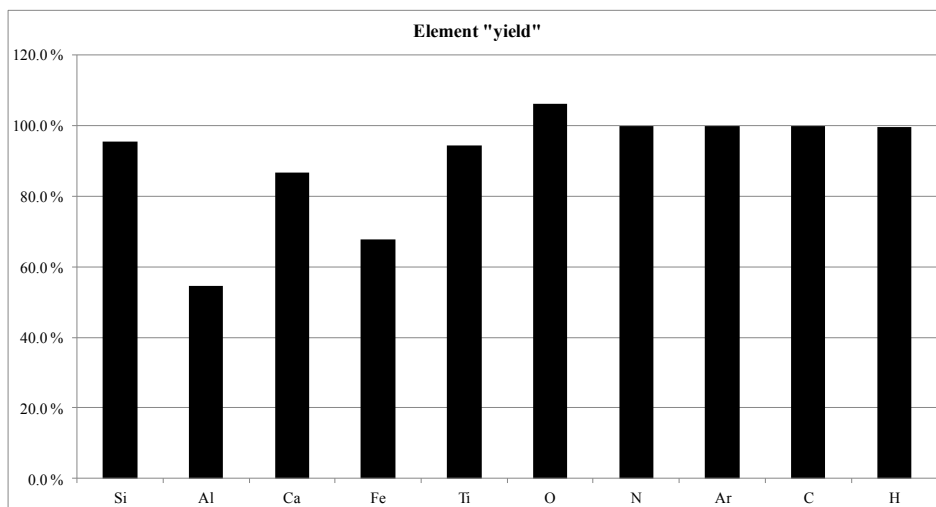
Figure 5.2: Element "yield" for the tapping area

As Figure 5.2 show most of the elements have a yield close to 100 % except the elements Al, Ca, Fe and O.

Aluminium and calcium both transfer from the liquid metal to the slag through the refining process.

The slag is a non consistent mixture of metal and oxides from the refining process. Getting a significant sample of the slag was difficult and it is therefore reasonably to believe that the uncertainty in the slag sample causes the low yield of these two elements. To illustrate the difference in two samples Table 5-2 shows the slag analysis taken during the full furnace mass balance in 2009 and the slag analysis from the tapping balance in 2010.

Table 5-2: Slag analysis comparison

	% Si	% Al	% Ca	% Fe	% Ti
Slag 2010	53.27	2.597	1.124	0.4455	0.02354
Slag 2009	86.35	3.950	3.320	5.050	0.02535

In both cases the alloy produced and the refining procedures was similar.

In Figure 5.2 the oxygen yield is above 100% even though the amount of ingoing air is balanced based on the amount of argon. The second largest contributor to oxygen in the outgoing material streams is the oxygen contained in the slag, supporting the idea that the values of Al, Ca and O are skewed in the slag.

For the element iron the yield is higher than 100 %, meaning that the ingoing amount of iron is too low. This extra iron missing in the ingoing material streams could be from oxygen lances used to ease the metal flow from the furnace. The lances are made of iron coated with a thin ceramic layer.

In addition to the element yields, a distribution chart over the tapping area was made. This gives the distribution of the elements in the origin streams and how they distribute themselves between the outgoing streams. Figure 5.3 shows the weight percentage distribution of each element, calculated based on the total sum of that element in all ingoing and outgoing streams, respectively.

This way if calculating the distribution is chosen to account for the elements not showing a yield close to 100 %. As an example, of all the aluminium entering the tapping area, 98 % is brought in with the metal but only 31% of the aluminium leaves the area following the refined metal. For carbon, the gas from the furnace contributes to 47 %, while 91 % of the carbon leaving the area goes into the off gas.

Summing up the main features of Figure 5.3 the main stream of gaseous components just passes through the tapping area without any major changes except being heated up. Further will the refining process, as expected, move the aluminium and calcium from the metal to the slag and skulls, while elements like iron and titanium stay in the metal phase.
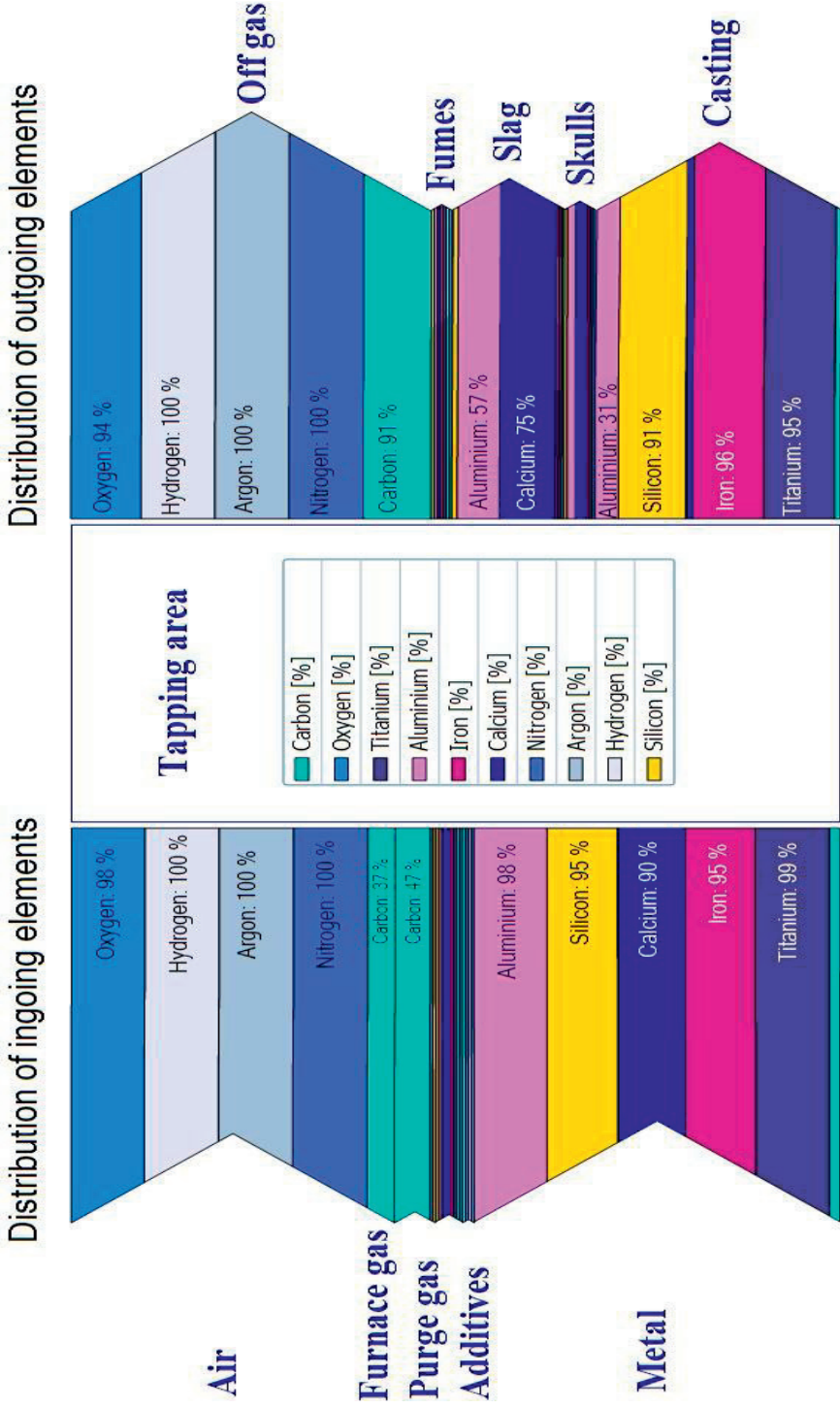
Figure 5.3: Element distribution given in weight percent for each element

5.4 The energy balance for the tapping area

In the furnace energy balance described in Chapter 4 two main contributors of energy dominated: the electric load and the carbon raw materials. Looking at the tapping area the energy picture is somewhat different since most of the energy coming into the area is bonded in the stream of liquid metal from the furnace. During tapping some of it is lost through radiation and other processes in the ladle, but the main part follows the metal to casting. During casting the metal will lose its energy due to cooling against the casting machine and radiation to the surroundings. Figure 5.4 illustrates the situation during the casting of silicon.

Figure 5.4: Casting of silicon

As seen the radiation from the casting process is substantial and would easily heat up the surrounding constructions. Continuous temperature measurements during casting at the wall to the left in Figure 5.4 shows that the wall temperature exceeds 400 ºC in several places (Takla 2009).

5.4.1 The energy streams in the tapping process

Since the main portion of the energy is bonded in the liquid metal any energy distribution diagram (Sankey) showing energy contents would be dominated by the inflow and outflow of metal.

Instead the present work looked at the different material streams and the energy added or released from each stream during a tapping cycle.

Since each cycle runs more or less similarly each time, the average numbers for the two tapping cycles with the Doghouse installed were used.

Common for both tapping cycles are the main work operations involved, which includes setting the purge gas to get stirring in the metal, adding of flux materials for the refining process and the addition of the temperature adjusting additives before the ladle is send to casting. Figure 5.5 shows the material streams in and out of the tapping area during a typical tapping cycle.
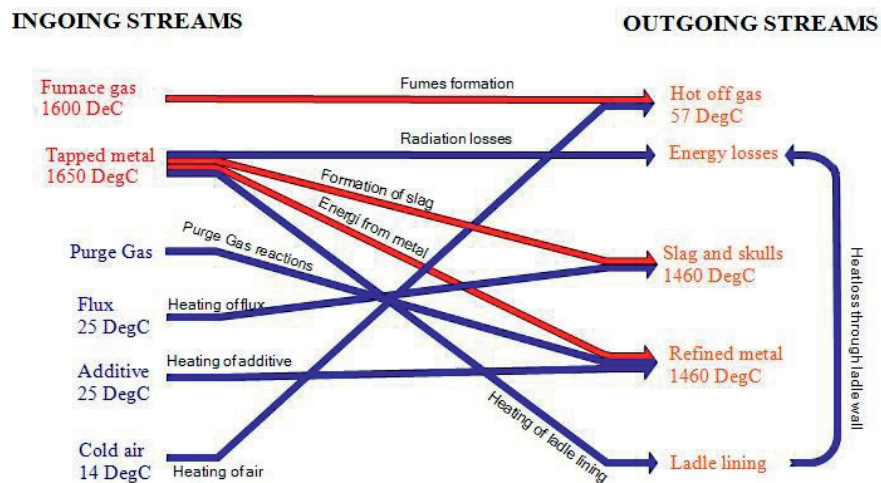
Figure 5.5: The energy streams in the tapping area

The red arrows indicate a process releasing heat into the area and the blue arrows show processes that demand energy. There are three arrows showing energy sources, containing four reactions/mechanisms feeding energy into the system. All other processes or flows demand energy

5.4.2 The energy balance

Presenting the energy details for all the streams in Figure 5.5 in a Sankey diagram results in Figure 5.6.

Energy contributors

Formation of fumes (1%): 11 kW

Oxidation of metal (79%): 986 kW

Slag reactions (3%): 38 kW

Energi from metal (17%): 214 kW

Tapping area

Energy consumers

Air (13%): 160 kW

Heat loss through ladle wall (1%): 15 kW

Radiation (27.5%): 344 kW

Ladle lining (37%): 459 kW

Heating Flux (0.5%): 8 kW

Additives (15%): 184 kW

Purge gas (6%): 79 kW
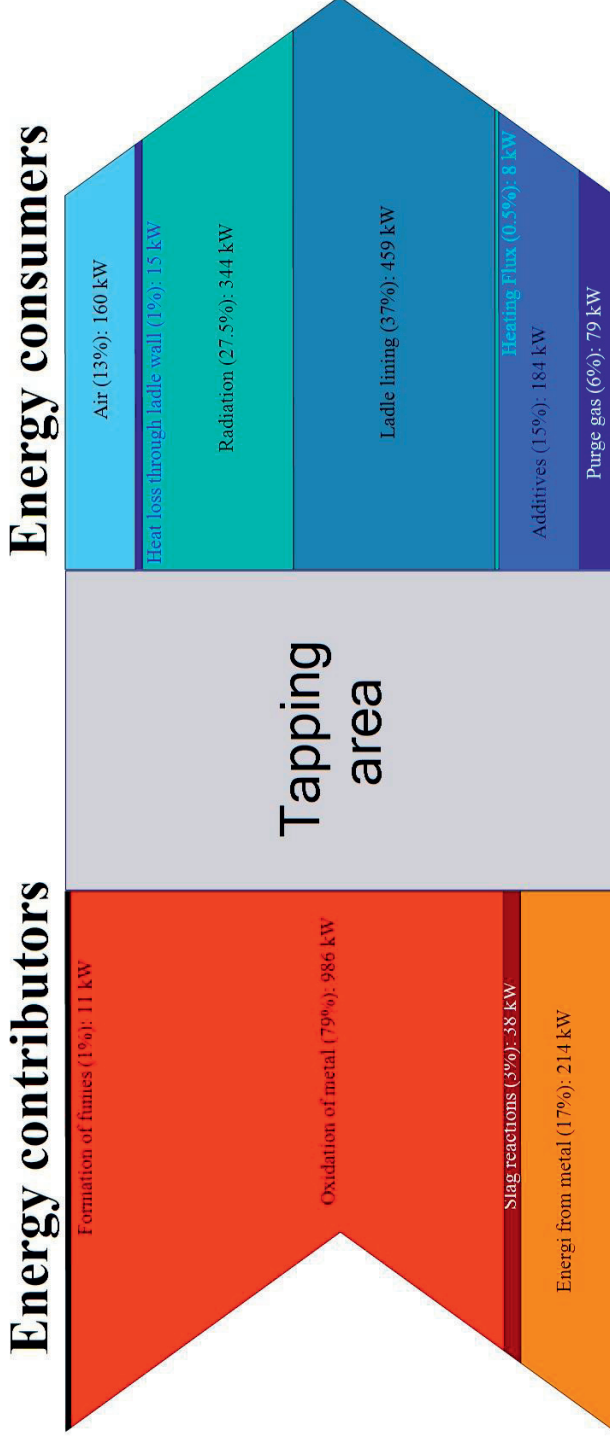
Figure 5.6: Energy balance for the tapping area

As Figure 5.6 show the main energy contributor during tapping is the oxidation of liquid silicon while losses through radiation and heating of the ladle lining dominate the energy consuming processes.

The calculation behind Figure 5.6 is based on the following assumptions:

- The crater gas leaving the furnace reacts to silica fume at 1600 ºC, feeding the area with both surplus reaction energy and hot fumes being cooled from 1600 ºC to 57 ºC.
- The exchange reaction for Al, Ca, Fe and Ti with SiO_2(l) all occurs at 1650 ºC.
- The amount of "Refined metal" is cooled from 1650 ºC to 1460 ºC.
- The purge gas (PG) consisting of air and oxygen is heated to T_{Tapped} and all the oxygen reacts to SiO_2 while the N_2 leaves through the metal surface.
- The flux is heated from 25 ºC to $T_{Refined\ metal}$ and goes into the slag.
- The additives are heated from 25 ºC to $T_{Refined\ metal}$ and enters the metal.
- The air is heated from 14 ºC to 57 ºC.
- Energy losses
  - Heating of the ladle lining.
  - Radiation and convection at the outer ladle wall.
  - Radiation from the metal at the ladle top.
- To close the energy balance some oxidation of metal to SiO_2(l) is needed.

The heat losses to radiation, convection, ladle lining and slag processes need some explanation.

5.4.2.1 Radiation and convective losses from ladle wall

The outer ladle wall temperature was measured with a FLUKE Thermo camera, showing a temperature of 100 ºC.

A question would be if the heat loss from the ladle walls happens through natural or forced convection. A simple way of checking this is by calculating the Archimedes number, describing the strength between free and forced convection through the relation between the Grashofs number and the square of the Reynolds number:

$$Ar = \frac{Gr}{Re^2}, having\ Ar \gg 1 = free\ convection\ and\ Ar \ll 1 = forced\ convection$$

Since the area around the ladle in our case is relatively closed the air velocity is assumed to be 1 m/s. Using the following properties for air: k_f = 0.028 W/m*K, β = $3.0*10^{-3}$ K^{-1}, v = $1.9*10^{-5}$ m^2/s, giving a Prandtl's number of Pr = 0.71, Grashofs number becomes Gr = $1.22*10^{11}$. Solving for the Archimedes number gives Ar = 6.515, meaning that free convection dominates.

To calculate the heat loss from the ladle walls an estimate of the average convective heat transfer coefficient, $\overline{h_c}$ is needed. Solving the Nusselt number, $Nu = \frac{h_c*l}{k_{air}}$ for h with the ladle height l = 2.6 metres gives an expression for $\overline{h_c}$. To find the Nusselt number the simplification that as long as $10^9 < Gr * Pr < 10^{13}$ Nu is given by

$Nu = 0.021(Gr * Pr)^{0.40}$ is used (Bakken 1993).

Rearranging the expression for Nu and solving for $\overline{h_c}$ the average heat transfer coefficient for the ladle walls is $\overline{h_c}$ = 5.37 W/m^2*K.

The ladle wall is made of ordinary steel so using an emissivity of 0.8 together with the calculated $\overline{h_c}$ both the radiation losses and the convective cooling of the ladle walls can be calculated. As the $T_{Sorroundings}$ the measured air temperature was used.

5.4.2.2 Radiation from liquid metal at ladle top

In order to calculate the radiation loss at the furnace top it was decided to simplify the real tapping situation. Since both the metal inside the ladle and the metal flow from the furnace will emit energy through radiation the real tapping situation is complicated to calculate. To represent the overall radiation loss from the metal the radiation loss from the top of the ladle was calculated, assuming it to be filled with metal of temperature T_{Tapped} .

Assuming that the radiation is uniform over the whole top surface the radiation loss was calculated using a hemispherical total emissivity of 0.20 for liquid silicon (Takasuka, Tokizaki et al. 1997) and the two temperatures T_{Tapped} and air temperature.

5.4.2.3 Energy bonded in ladle lining

The ladle lining is made of a refractory material consisting mainly of Al_2O_3 and with a low heat capacity. Since the time of tapping was short in these trials (average of 40 minutes per ladle) it was assumed that the temperature increase was only in the area of 200 ºC.

5.4.2.4 Formation of slag components

Looking at the amount of Al, Ca, Fe and Ti that assumingly reacts with SiO_2 in an exchange reaction the need for SiO_2 is approximately 44 kg. Given that all the oxygen that is brought to the melt through the purge gas forms $SiO_2(l)$ this gives 38 kg and it seems that these two sizes match fairly well.

The slag analysis however shows that the end slag contains over 550 kg of SiO_2 so there has to be some other source of SiO_2 as well. Considering the stirring of the metal from the nitrogen in the purge gas it is likely that some SiO_2 could form on the metal surface exposed to air and dragged down in the melt. To close the energy balance more energy is needed and letting approximately 0.8 % of the tapped silicon react to SiO_2 gives enough energy to close the balance.

Even with this extra SiO_2 close to 430 kg SiO_2 is needed to fulfil the slag analysis and it can only be assumed that the source for this missing SiO_2 is the furnace, since the furnace craters assumingly contains unreacted melted quartz.

5.5 Energy released during oxygen lancing

One of the most common work operations in the tapping area is oxygen lancing to enhance the metal flow out of the furnace. The consequences of this work operation towards emissions of gaseous species will be treated in Chapter 6 so this section focuses only on the energy released during lancing.

Figure 5.7 shows data from one of the tapping cycles where the Doghouse was installed. Each peak in temperature is connected to the use of an oxygen lance.
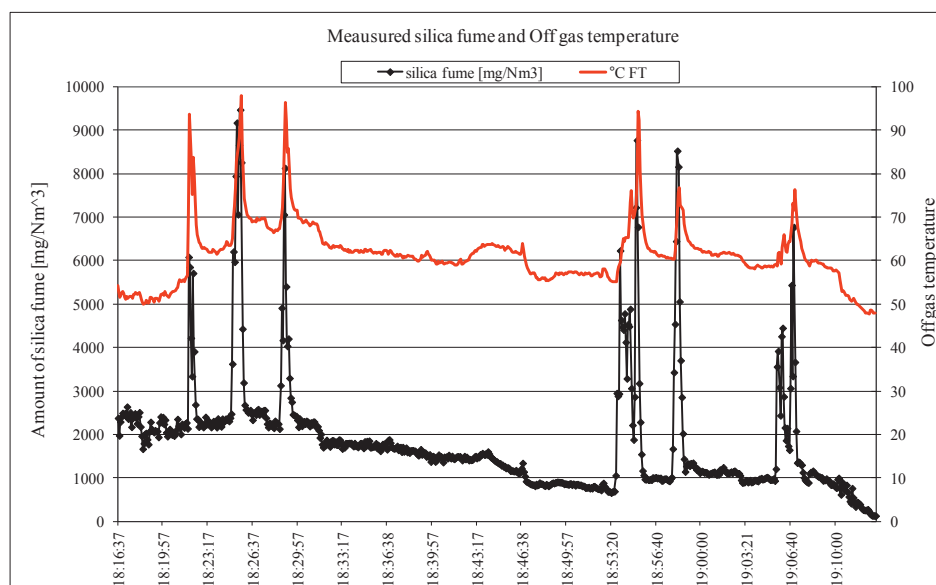
Figure 5.7: Temperature raise during oxygen lancing

As seen in Figure 5.7 the use of the lance also increases the emission of silica fume which is assumed to be caused by one of the following two mechanisms:

- Oxidation of metal to silica fumes
- Increased flow of SiO gas from the inside of the furnace.

Both mechanisms above are exothermic and will release energy to the off gas.

Looking at the highest four of the peaks, the temperature increase in the off gas is in the order of 95 ºC. It is interesting to see how the temperature rise in the off gas correlates with the energy released from either of the two assumed reaction mechanisms.

The balanced amount of ingoing air for this specific tapping cycle was 398 Nm^3/minute at an air temperature of 14 ºC. Figure 5.7 illustrates that the average lancing time was one minute and that the air was heated to about 95 ºC.

The fume concentration rises by approximately 7000 mg/Nm^3 during lancing. Using this, assuming that the fume formed consists mainly of SiO_2 the lancing operation then generates approximately 46 mol of SiO_2 per minute.

According to HSC 7.14 (Roine, Lamberg et al. 2011) the heat of the reaction for the two mechanisms above is fairly stable in the temperature range of 1500 – 2000 ºC and it was decided to base the calculations on 1600 ºC. Table 5-3 shows a comparison of the energy needed to heat the ingoing air to the measured temperature and the energy released from the two reaction mechanisms when forming the measured amount of silica fume.

Table 5-3: Energy during oxygen lancing

Energy needed for heating air	Energy released in Si(l) + O2(g) = SiO2	Energy released in SiO(g)+1/2O2(g)=SiO2
626 kW	731 kW	603 kW

As Table 5-3 shows the energy amounts are within the same range, something that could be expected since no other large energy source is active towards the off gas. Some uncertainty could be introduced from heat transferred to the off gas via radiation against the off gas inlet and surrounding constructions.

Compared with the energy released during the periods without lancing, given in Table 5-4, the amount of energy released during lancing is several times higher.

Table 5-4: Energy during non lancing periods

Level of fume formed	Energy released in Si(l) + O2(g) = SiO2	Energy released in SiO(g)+1/2O2(g)=SiO2
1000 mg/Nm^3	104 kW	86 kW
2000 mg/Nm^3	209 kW	172 kW

From this it could be concluded that if the lancing operation is performed over long time periods during tapping, substantial amounts of energy have to be transported away from the tapping area.

In addition, since the heated air increases in volume because of the temperature change one might end up with a capacity problem with respect to off gas suction.

Using the measured air temperature as our initial condition the volumetric increase in off gas volume, based in ideal conditions, goes from 13 % at 50 ºC to 28 % at 95 ºC. In other words there is a need to remove almost 30 % more off gas during lancing.

5.6 Concluding remarks

Through an element material balance of the tapping, it was found that most of the entering elements have a yield close to 100 % when leaving. As one of several processes taking place during tapping the refining process consists of several chemical reactions, introducing a complexity in establishing an accurate element balance because of the variations in the slag produced. A comparison of two slag samples shows very different chemical analysis, and it is considered that the uncertainty in the slag analysis is the explanation for the elements not having a yield close to 100%.

Looking at how the ingoing elements are distributed between the outgoing streams, it appears that most of the gaseous components flow straight through the area, only being heated, while the refining process moves some elements from the metal to the slag as expected.

An energy balance over the tapping area has been made, looking at the energy contributors and consumers in the area. Since the metal flow from the furnace would be so dominating in an ordinary energy distribution diagram the investigation rather has been pointed at what processes/material streams that needs to be heated or cooled to have a closed energy balance.

The investigation shows that oxidation of liquid metal to SiO_2 has to be considered to close the energy balance. On the energy consuming side the radiation losses and heating of the ladle lining are dominating.

The connection between oxygen lancing and the energy content in the off gas has been investigated. The results show that the use of an oxygen lance increases both the off gas temperature and the fume formation.

There is good agreement when comparing the energy needed to heat the ingoing air to the measured temperature with the energy released from two possible fume-forming mechanisms.

Using an oxygen lance increases the energy content in the off gas multiple times which again increases the off gas temperature. Increased temperature leads to increased volume and in a worst case scenario with oxygen lancing over a long time period the off gas suction efficiency could be affected. Such a scenario would of course depend on the chosen design and fan capacity in the off gas system.

Chapter 6   Formation of NO in industrial silicon production

6.1 Background

According to the Norwegian Climate and Pollution Agency, Norwegian silicon producers are responsible for several of the highest onshore pointwise emissions of NOx in Norway (KLIF 2010).

This chapter considers the connection between the silicon process and NOx through NO formation theory, industrial measurements of emissions and theoretical modelling of NO forming mechanisms.

NOx is the common notion for the two gases nitric oxide (NO) and nitrogen dioxide (NO_2) formed during the combustion of fuels. All fuels, such as gasoline, diesel, biodiesel, propane, coal, and ethanol, emit NOx when burned.

In Europe the main sources for NO_x emissions are the onshore and offshore transport industries, power generations based on fossil fuels, agriculture and other industries (EEA 2009).

NOx is considered to be an environmentally harmful gas because of its impact on air pollution. NO would easily oxidize to NO_2 and NO_2 would further, in the presence of hydrocarbons and ultraviolet light, react to tropospheric ozone and nitriate aerosols. The latter being a source for ambient air particulate matter, $PM_{2.5}$ (WHO 2003).

Other known environmental concerns regarding NOx are the formation of acid rain when combined with oxides of sulphur (SO_x), deterioration of water quality through eutrophication (leading to oxygen depletion) and global warming through formation and accumulation of N_2O in the atmosphere.(Bireswar and Amitava 2008)

Exposure to NOx has known health risks, both with respect to long-term and short-term exposure (WHO 2005).

Long-term exposure: there are indications that long-term exposure could give an increase in bronchitic symptoms of asthmatic children and reduced lung function growth.

Short-term exposure: a 1-hour exposure to NO_2 concentrations above 500 μg/m^3 gives an acute health reaction among asthmatics.

These consequences of NOx emissions have led to the need for international attention and cooperation in reducing emission levels. The United Nations Economic

Commission for Europe has through its "*Convention on Long-range Transboundary Air Pollution*" focused on emissions reduction and through its latest protocol "*The 1999 Gothenburg Protocol to Abate Acidification, Eutrophication and Ground-level Ozone*" set emission ceilings for 2010 for four pollutants: sulphur, NOx, VOCs and ammonia. Included in the protocol is tight emission limits for specific emissions, forcing and promoting the use of Best Available Technology (BAT) to reach the emission targets.

Estimates of the effect of a fulfilled emission reduction show a substantial reduction in areas with excess acidification and eutrophication as well as reducing the number of days with excessive ozone levels with 50 % (UNECE 1999).

6.2 NO_x formation mechanisms in combustion processes

NO_x formation in combustion processes are described by three major formation mechanisms: thermal NO_x, fuel NO_x and prompt NO_x (De Nevers 2000). Fuel NO_x is formed from the nitrogen contained in the fuel itself and prompt NO_x is oxides formed quickly through the interaction between oxygen and nitrogen with active hydrocarbon species present.

The mechanism for formation of thermal NO_x was first described by Zeldovich (Zeldovich 1946) stating that at high temperatures the oxygen and nitrogen in the air would react to form NO via reactive radicals such as O and N. Zeldovich also stated that the mechanisms forming NO are highly dependent on the temperature reached in the O_2/N_2 mixture. The temperature dependency for all three mechanisms can be seen in Figure 6.1 below.
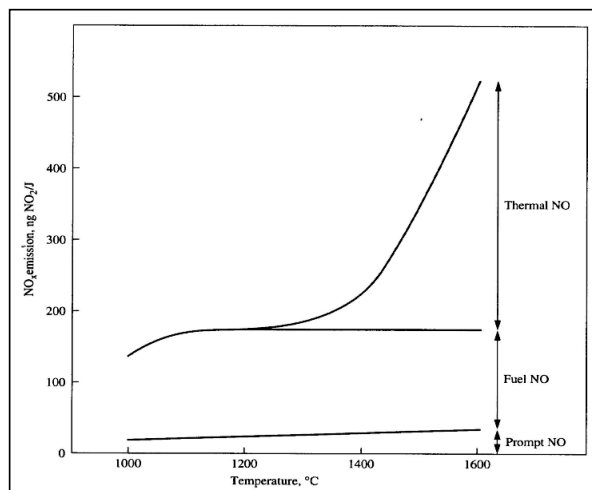
Figure 6.1: Temperature dependency in NOx formation mechanisms. From (De Nevers 2000)

6.2.1 The Zeldovich mechanism

The thermal or ***Zeldovich mechanism*** consists of two chain reactions involving reactive radicals.

$$O + N_2 \underset{k_{1r}}{\overset{k_{1f}}{\leftrightarrow}} NO + N \qquad\qquad \textbf{6-1}$$

$$N + O_2 \underset{k_{2r}}{\overset{k_{2f}}{\leftrightarrow}} NO + O \qquad\qquad \textbf{6-2}$$
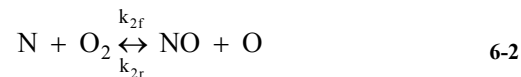
which can be extended with an additional equation, giving us the ***extended Zeldovich mechanism***.

$$N + OH \underset{k_{3r}}{\overset{k_{3f}}{\leftrightarrow}} NO + H \qquad\qquad \textbf{6-3}$$
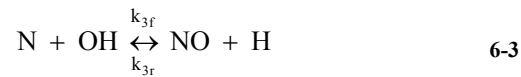
Zeldovich suggested that since these reactions usually are much slower than the fuel combustion processes they have a pure thermal dependency. The strong thermal dependency is shown in the reaction rate coefficients given by Turns (Turns 2000):

Table 6-1: Reaction rate coefficients in [m^3/kmol*s] for Reactions (6-1), (6-2) and (6-3) (Turns 2000)

Forward rate	Backward rate
$k_{1f} = 1,8 \cdot 10^{11} \exp(-38370/T)$	$k_{1b} = 3,8 \cdot 10^{10} \exp(-425/T)$
$k_{2f} = 1,8 \cdot 10^{7} \exp(-4680/T)$	$K_{2b} = 3,8 \cdot 10^{6} \exp(-20820/T)$
$k_{3f} = 7,1 \cdot 10^{10} \exp(-450/T)$	$K_{3b} = 1,7 \cdot 10^{11} \exp(-24560/T)$

6.2.1.1 Equations describing the formation of NO

The formation of NO is well described in literature and for this work the equations and assumptions given by Turns (Turns 2000) are choosen.

In calculations of NO formation it is usually assumed that the NO concentration is low compared to the equilibrium concentration and thereby neglecting the reverse reactions. Since Reactions (6-2) and (6-3) are much faster than (6-1) the steady state approximation [N_{ss}] given as dN/dt = 0 is assumed. The NO reaction scheme is also slow compared to reactions involving O and O2 and in Turn's deductions the reaction

$$O_2 \overset{K_{eq}}{\leftrightarrow} 2O \qquad\qquad \textbf{6-4}$$
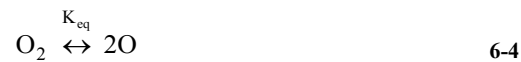
is assumed to be at equilibrium, thereby defining the concentration of O radicals at the temperature of interest.

Reactions (6-1) and (6-2) give the expressions for dNO/dt and dN/dt and together with $[N_{ss}]$ and the equilibrium expression for Reaction (6-4) the expression for the formation of NO can be deduced, given as

$$\frac{dNO}{dt} = 2k_{1f}\left(\frac{K_{eq}P}{RT}\right)^{1/2} [N_2][O_2]^{1/2} \qquad\qquad \textbf{6-5}$$

where k_{1f} is given in Table 6.1 in $[m^3/kmol*s]$, K_{eq} is the equilibrium constant for the reaction $O_2 \leftrightarrow 2O$ at the given temperature, T given in Kelvin, P is pressure and R is the ideal gas constant.

If considering a very small time step Equation 6-5 could be used to find an expression for the NO formation as a function of time only. With the concentration of O radicals given by the equilibrium, assuming that $[N_2]$ and $[O_2]$ does not change over the time span of interest, integrating Equation 6-5 from $NO_{(t=0)} = 0$ to $NO_{(t=t)} = NO(t)$ gives the following expression for the NO formation as a function of time, given in $[kmol/m^3]$:

$$NO(t) = 2k_{1f}\left(\frac{K_{eq}P}{RT}\right)^{1/2} [N_2][O_2]^{1/2}\, t \qquad\qquad \textbf{6-6}$$

6.3 NO formation in Silicon Production

As seen in Chapter 2 a silicon furnace is a complex system of solid and gas material flows moving up and down through the furnace shaft. An ideal model of a silicon process with 100 % silicon yield is shown in Figure 6.2
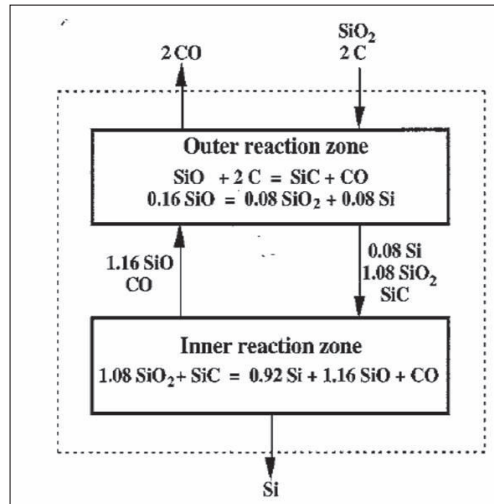
Figure 6.2: Process model with 100 % silicon yield from (Schei, Tuset et al. 1998)

Figure 6.3 shows a cross section of the furnace with 2 of the 3 electrodes together with the material/gas flow patterns.
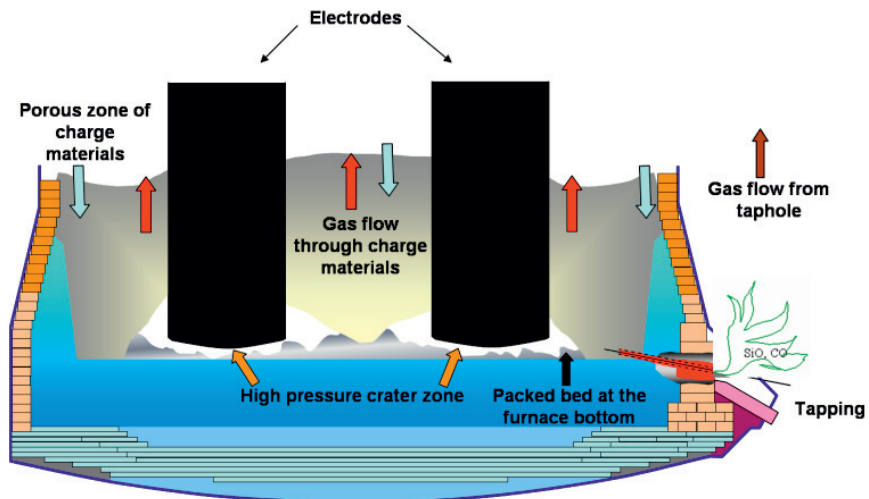
Figure 6.3: Cross section of a silicon furnace from (Kadkhodabeigi, Tveit et al. 2010)

6.3.1 Combustion at the furnace surface

The gases from the crater would mainly rise up through the furnace and combust on the furnace surface. Figure 6.4 shows the surface in a silicon furnace during normal operation.

Figure 6.4: Silicon furnace surface

In addition to the combustion of SiO and CO gas from the crater the furnace surface environment also contains chemical reactions involving any constituents added with the raw materials, such as combustion of volatile matters and evaporation of any moisture.

This means that any nitrogen added to the furnace via the raw materials could form both fuel NOx and prompt NOx at the furnace surface since there are hydrocarbon components in the volatile matters.

Earlier investigations involving full-scale experiments on several FeSi/Si furnaces show a strong correlation between fume and NO formation (Johansen, Tveit et al. 1998). They stated that the correlation could be explained by the fume forming SiO combustion releasing energy and giving locally high temperatures, thereby assuming that the formation of NO is dominated by the thermal mechanism. Grådahl, Johansen et al. (Grådahl, Johansen et al. 2007) later found the same correlation and showed that the NOx formation could be influenced by changing the stoking/charging pattern done towards the furnace.

6.3.2 Combustion at the tapping

During tapping there is a connection between the crater and the tap hole which in some cases gives combustion of crater gases right outside the tapping channel. Figure 6.5 shows the situation when the gas from the furnace crater meets air and combusts just above the runner.

Figure 6.5: Tapping of silicon

Whenever this situation occur vast amounts of energy from the combustion will be released to the surroundings.

In addition there is also several work operations done in the tapping channel during tapping, all aiming to maintain a high metal flow out of the furnace. All these work operations could increase the flow of crater gases from the inner zone as well as lead to oxidation of silicon.

The gases combusting outside the tap hole would experience a totally different environment than the ones combusting on the furnace surface. The surrounding air or any effect from the tools used is the only addition to the combusting process, creating an ideal arena for investigating any correlations between SiO combustion, work processes and NO formation.

6.3.3 The combustion of SiO

As mentioned earlier measurements done by Johansen, Tveit et al. (Johansen, Tveit et al. 1998) showed a strong correlation between fume and NO formation assumed to be dominated by the thermal mechanisms. In addition they also measured the furnace surface temperature using two thermocouples, one placed close to the surface/inside the charge and one placed above the charge. The measured temperatures ranged from 800 ºC to 1400 ºC inside the charge and from 1000 ºC to over 1500 ºC above the charge. They also measured the temperature inside the freshly charged raw materials finding it to drop from 800 ºC to 400 ºC and then have a surprisingly slow increase in temperature, as time evolved.

A study done in 2000 by Grådahl, Johansen et al. (Grådahl, Johansen et al. 2000) measured the furnace surface temperature on two different furnaces using a thermo camera. The temperatures varied from 860 ºC to 1290 ºC in one case and 680 ºC to 1290 ºC in the other.

6.3.3.1 The O radical and combustion of SiO

In Turns deduction of the NO forming expression, given in Equation 6-5, the equilibrium between O_2 and $2O$ is used in to determine the level of O radicals at the temperature of interest. Investigating the $O_2 \leftrightarrow 2O$ equilibrium using HSC (Roine, Lamberg et al. 2011) for the temperature range of $1133 - 1563$ K ΔG_r is positive throughout the entire temperature range. This means that another source most likely is determining the level of O.

Knowing that both the tapping area and the furnace surface area are fed with SiO gas from the furnace crater zone a look at SiO combustion mechanisms will be of interest in the search for an O radical source.

Combustion of silanes (SiH_4) involves SiO combustion and Britten, Tong et al. (Britten, Tong et al. 1990) used this in their numerical model of the kinetics in a SiH_4 / O_2 mixture. Chagger, Hainsworth et al. (Chagger, Hainsworth et al. 1996) investigated the formation of silica fume from hexamethyldisiloxane (HMDS) oxidation in a CH_4-N_2/air atmosphere using the same set of reactions for SiO combustion.

They both base their SiO combustion reactions on an investigation done by Jachimowski and McLain (Jachimowski and McLain 1983) estimating the reaction rates for SiO_2 forming reactions to fit a reaction scheme involving silane combustion with H_2 in a shock tube. Jachimowski and McLains three reactions involving SiO is given in Table 6-2.

Table 6-2: SiO reactions and rate coefficients. From Jachimowski and McLain (Jachimowski and McLain 1983)

Reaction	Rate coefficient, k
$SiO + O + M \rightarrow SiO_2 + M$	$2.5*10^{15} \exp(-4370/RT)$
$SiO + OH \rightarrow SiO_2 + H$	$4.0*10^{12} \exp(-5700/RT)$
$SiO + O2 \rightarrow SiO_2 + O$	$1.0*10^{13} \exp(-6500/RT)$

Where the rate coefficient is defined as $k_{fi} = A_i \exp(-E_i/RT)$ in $[cm^3/mol*s]$. The activation energy E_i is given in [cal/mol], R is the gas constant equal to 1.987 [cal/mole*K] and T is the temperature given in Kelvin. M is a third body molecule.

Even though Jachimowski and McLain found a good agreement between their reaction mechanisms and the overall results of the silane/H_2 combustion they underlined that the individual rates needs to be confirmed through experimental verification.

Both Chagger, Hainsworth et al. and Britten, Tong, et al. came to the same conclusion with respect to overall experimental results compared to chosen reaction model involving the reaction rates described by Jachimowski and McLain.

Balram, Anderson et al. (Balram, Andersson et al. 2011) introduced a new SiO combustion mechanisms based on molecular simulations and compared it to the combustion mechanisms initially given by Jachimowski and McLain. The results for a single cell Perfectly Stirred Reactor (PSR) on NOx formation and temperature, having SiO combust in a CO/H_2/N_2 atmosphere, showed very little difference between the two mechanisms.

Even with the weaknesses Jachimowski and McLain described for their own reaction mechanism it is assumed to be satisfactory for representing the SiO combustion in this thesis. This is supported by experiments and modelling cases like the ones done by Chagger, Hainsworth et al. and Britten, Tong et al. both showing satisfactory equal results between the model and the experiment. Establishing this, the third reaction in Table 6-2 represents a source for O radicals.

6.4 Measurements of NO in the furnace off gas

As a part of the material and energy balance described in Chapter 4 several measurements of the off gas from the silicon furnace were done. One of the purposes for the off gas measurements was to investigate how the formation of NO varies with time. The off gas temperature, chemical analysis and gas velocity in the off gas channel were measured at a location with laminar flow behaviour situated between the furnace and bag house filter.

The NO was measured with a Testo 350 XL from Testo (TESTO). For the amount of silica fume in the off gas data from the plant's own measurements were used.

The plant measures the amount of silica fumes in two ways. The fume concentration in the off gas channel is measured based on a principle where light is send through the channel and the percentage of light lost is measured. In addition the weight of the fume is registered when the fume has passed through the filter bags and is send to storage silos.

Since the fume concentration in the channel is measured instantly it is suitable in measurements towards correlations and variations in the off gas.

The results for NO and silica fume are presented in Figure 6.6 below, the silica fume being reported as a light percentage lost.
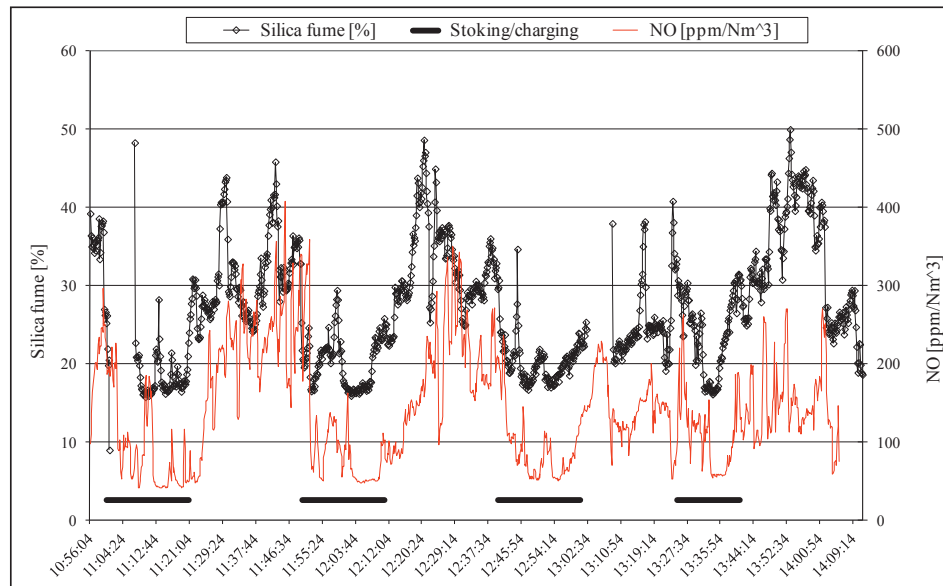
Figure 6.6: Off gas content of NO and silica fumes from the silicon furnace

As seen from Figure 6.6 the NO formation cycles together with the fume formation. The thick black lines at the bottom of Figure 6.6 indicate the time intervals where the furnace was stoked and charged with new raw materials. The large variation in the amount of silica fume from the furnace is due to process variations. The main reasons are:

- Variation in condensation of SiO gas from the crater. After adding new materials the condensation at the new cold raw materials are high.
- Accumulation of SiO gas due to a minor pressure build up in the furnace. This variation has been measured and the effect is small.
- Void build up due to raw material conversion. Sometimes the void collapses and releases process gas.
- Constant off gas suction. Increased process gas gives less cold air sucked into the furnace and the concentration of fumes increase.

The overall effect of this variation in fume concentration may be seen as a major variation in off gas temperature.

6.4.1 NO formation as a function of silica fume weight

Because of the time lag between the furnace and the fume weighing system, using the fume weight signal as a direct NO leading indicator is unsuitable. Instead accumulated values for the silica fume weight over 30 minutes can be collected.

Using the plant's already installed NO measurements for the same 30 minutes to calculate the amount of NO formed the influence from the fume formation towards NO formation can be shown. Figure 6.7 shows the NO formation per kilogram fume for three different silicon furnaces.
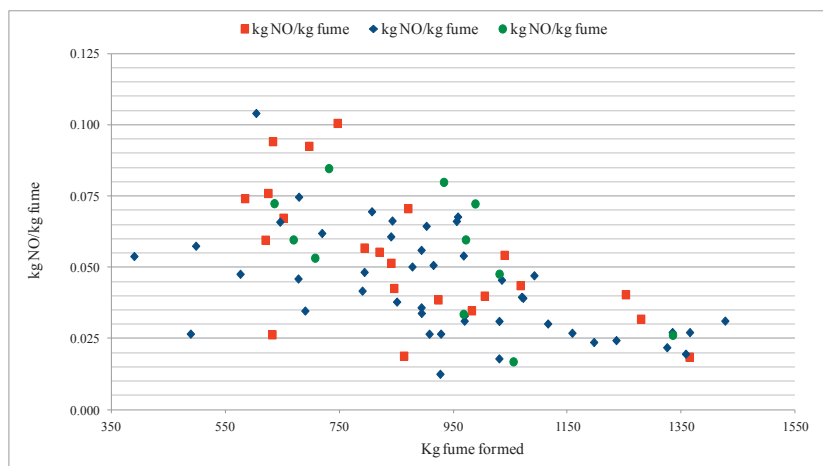
Figure 6.7: Relative NO formation for three different silicon furnaces

Looking at Figure 6.7 it is interesting to note that the relative NO formation is sinking when the amount of fume formed increases. A flat horizontal connection between the two would suggest that the amount of NO formed is a function of fume formation only, instead there seems to be some other mechanisms influencing on the NO formation together with the silica fume.

The results in Figure 6.7 can be influenced by several uncertainties, such as the fume weight, the off gas amount and any measurement errors in the NO measurements.

6.4.1.1 Measurement setup and uncertainties

The NO in these data sets was measured with a LaserGas II SP from NEO Monitors (NEO 2009) with a detection limit on 10 ppm, see Appendix E. The plant's industrial setup of the LaserGas II SP is shown in Figure 6.8. The measurement principle is based on a laser beam send through the off gas stream and registered in a receiver on the opposite side.

The off gas volume is calculated based on the gas velocity and temperature at the same location in the off gas channel.

The weight of the silica fume is registered in such a way that after being collected in the bag house filter the fumes are mechanically transported to a pneumatic sender, collecting 150 kg of fumes before sending the fumes to a storage silo. The uncertainties in the plants silica fume weights are unknown, but the accuracy of the weighing cells are 1.5 kg, equal to 0,5 % of the total weight per sending and the yearly weight control the last two years have shown no deviations when testing against know weights (Elkem 2009).

Figure 6.8: Industrial setup for NO measurements at the plant

6.4.2 NO formation as a function of energy released

Based on the same data the connection between the formation of NO and silica fume can be expressed in a different matter, assuming that the combustion of furnace gases feeds the air with sufficient energy to have the Zeldovich reactions occur.

The amount of NO formed is compared to the amount of silica fume formed from a heat of formation perspective by calculating the theoretical energy needed to form the measured amount of NO and dividing it with the theoretical energy released when the measured amounts of silica fume is formed.

Dividing the fume weights into groups of hundreds and looking at the average value for the energy bonded in NO formation within each fume group results in a plot as in Figure 6.9.
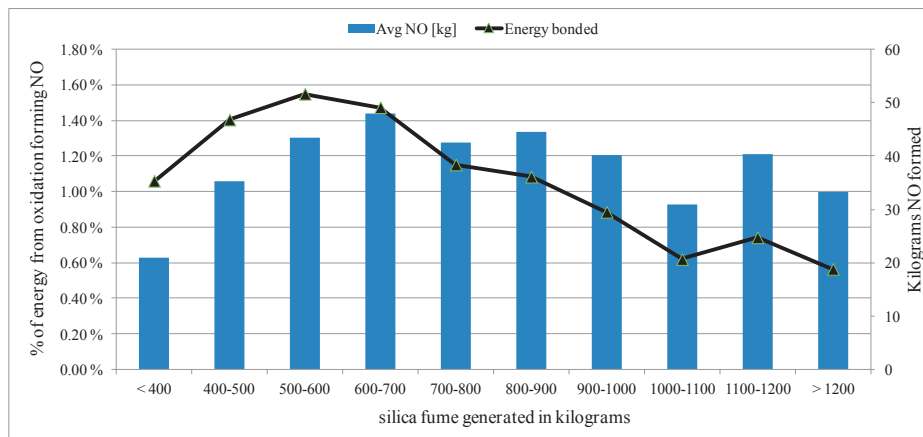
Figure 6.9: Share of released energy bonded in NO formation

Figure 6.9 also shows the average amount of kilograms NO formed within each group. It is interesting to note that there seems to be an area in fume formation generating more NO per kilograms of silica fume. The decreasing amount of energy bonded when the fume formation increases supports the observations seen in Figure 6.6 and Figure 6.7, that the NO formation is most likely controlled by several simultaneously occurring mechanisms.

6.5 Measurements of NO in the tapping off gas

To maintain a high yield on the silicon process it is necessary to keep the silicon furnace drained of metal as much as possible. The metal is drained from the furnace through tap holes located at the lower part of the furnace and tapping is done through one hole at a time. Tapping of silicon metal is usually done either continuously or discontinuously. The latter meaning that the furnace is opened, drained for metal and then closed again.

6.5.1 Measurement set up

The measurements were done at a 69 MVA silicon furnace running at a furnace effect close to full capacity. At the time of the measurements the furnace produced an alloy containing 96 % or more of silicon.

The main measurements were done in cooperation with a test of a new equipment, named a "Doghouse", for collecting all gases escaping from the tap hole thoroughly described by Kadkhodabeigi (Kadkhodabeigi 2011).

The off gas system of this tapping area consist of 5 individual hoods placed side by side over the tapping area, in that way following the furnace perimeter. The channel from each hood is then connected together through a manifold and the joint off gas from the tapping area is send to a bag house filter. Each hood is installed with butterfly valves which gives the possibility to close and open the suction from of each hood.
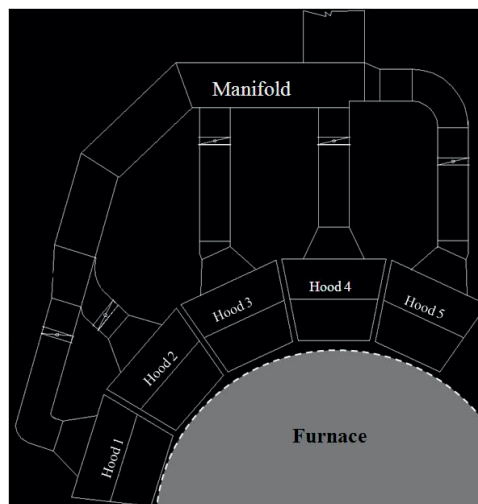
Figure 6.10: Arrangement of the off gas hoods in the tapping area

The Doghouse was installed on top of the runner and connected to Hood no. 2 in Figure 6.10 in such a way that when closing all other channels the suction was concentrated down the Doghouse.

Figure 6.11 shows the tapping situation with the Doghouse mounted on top of the runner.

Figure 6.11: Tapping with "DogHouse" installed

As seen in Figure 6.11 most of the fumes are sucked into the Doghouse, but some fumes rise straight up and enter the same channel as the Doghouse is connected to. Visual observations done during the tapping with the Doghouse estimated that over 95 % of the fumes entered the Doghouse and corresponding off gas channel.

To measure the fume generation a LaserDust MP from NEO Monitors AS was installed in the off gas channel, see Figure 6.12. At the same location the chemical off gas analysis were conducted using a TESTO 350XL.

Figure 6.12: Measurement setup of the NEO LaserDust

The fume measurement equipment, the LaserDust MP, is based on a laser transmission principle. A laser beam is send through the off gas channel and the reminding signal is registered at a receiver in the opposite side. The measured transmittance signal corresponds to the amount of fume in the measuring path, see Appendix C.

The uncertainty in the NEO Laserdust MP measurements can be compared to the uncertainty in an isokinetic measurement. Investigations done by TÜV Rheinland on gas with a known fume concentration and size distribution conclude that the Laserdust MP has good the repeatability and linearity. The accuracy for some fume types is shown to be good even without being calibrated for that specific fume (NEO 2011).

To analyse the gaseous content of NO in the off gas a Testo 350XL Portable Combustion Analyzer was used.

Figure 6.13: The TESTO 350 XL Portable Combustion Analyzer

The TESTO 350XL had an electrochemical measuring cell for NO with a resolution of 0.1 ppm and an accuracy of < 5 ppm in the area of [0,100] ppm, 5% of measured value in the area [100,2000] ppm and 10% of measured value between 2001-3000 ppm (TESTO), see Appendix B for more details.

The off gas velocity was measured at a location with fully developed laminar flow using a KIMO AMI 300 (KIMO Instruments 2011). See Appendix F for more details.

6.5.1.1 Duration of measurements

The main measurements were taken over a whole day, first 2.5 hours of tapping without the Doghouse installed and then two tapping cycles of approximately 1 hour each with the Doghouse installed to ensure that all the fumes/gases from the tapping was collected. In addition several 1-day measurements were done both before and after the main campaign to ensure that the main measurements were representative of normal furnace operation.

6.5.2 Measurements at the initial stage – opening the tap hole

The sequence of opening the tap hole usually starts with the use of an oxygen lance to burn away the carbon paste used to clog the tapping channel. During this sequence a lot of fumes are generated and the situation could be best visualized by the photo in Figure 6.14.

Figure 6.14: Fumes during initial oxygen lancing

To the left in Figure 6.14 is the furnace and runner while the top right corner shows the outlet to the off gas channel. The sparks are most likely carbon paste particles burning that were ignited by the oxygen.

Measurements of the fume and NO concentration in the off gas during this initial operation show a lack of NO formation, but some formation of CO gas, see Figure 6.15. Note that because of the processing time in the TESTO 350XL the NO measurements are adjusted for a time lag of 30 seconds. The most likely explanation to the missing NO formation is that the combustion of the carbon materials inside the tap hole do not generate enough energy to start the formation of thermal NO. After some lancing a small metal flow will develop and combustion of metal starts as well as combustion of carbon materials. This is illustrated by the small amounts of NO formed during the second and third fume peaks in Figure 6.15.

Table 6-3 shows a semi-quantitative analysis of the fumes formed during the initial stage of tapping. The samples were sprinkled on a carbon tape and examined using a scanning electron microscope (SEM). As the analysis show the fume contains some silicon that could be bonded as SiO_2 but the content of iron and other elements is considerable larger than for the pure fume samples presented later in this chapter.

Table 6-3: Analysis of the fume in initial stage given in weight percentage

Element	O	Si	Ca	Fe	Al	C
Analysis	43.2	26.9	2.97	24.5	2.75	1.42

The analysis of the fumes supports that there is very little oxidation of silicon or SiO gas in the initial stage of opening the tap hole. The high content of iron in the fume is most likely from the oxidation of the oxygen lance since these are mainly made of iron.
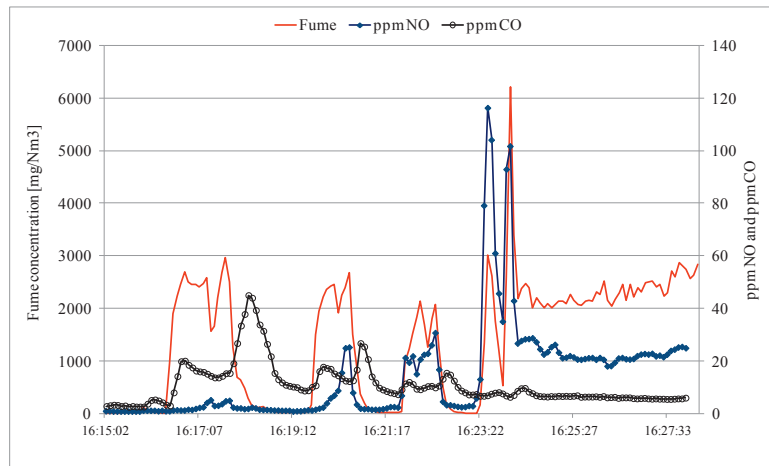
Figure 6.15: Off gas analysis and fume concentration during initial opening sequence

6.5.3 Measurements during tapping

The time chart in Figure 6.16 on the next page shows the NO and silica fume content in the off gas during the beginning of a silicon metal tapping. The dark purple line shows the accumulated metal weight in the ladle as the tapping progresses. Note that because of the processing time in the TESTO 350XL the NO measurements are adjusted for a time lag of 30 seconds.

The figure shows that the formation of NO seems to correlate well with the amount of fume generated.

Figure 6.16 presents three interesting cases in the NO formation:

a) High fume – low NO

b) High fume – high NO (peaks)

c) Low fume – high NO
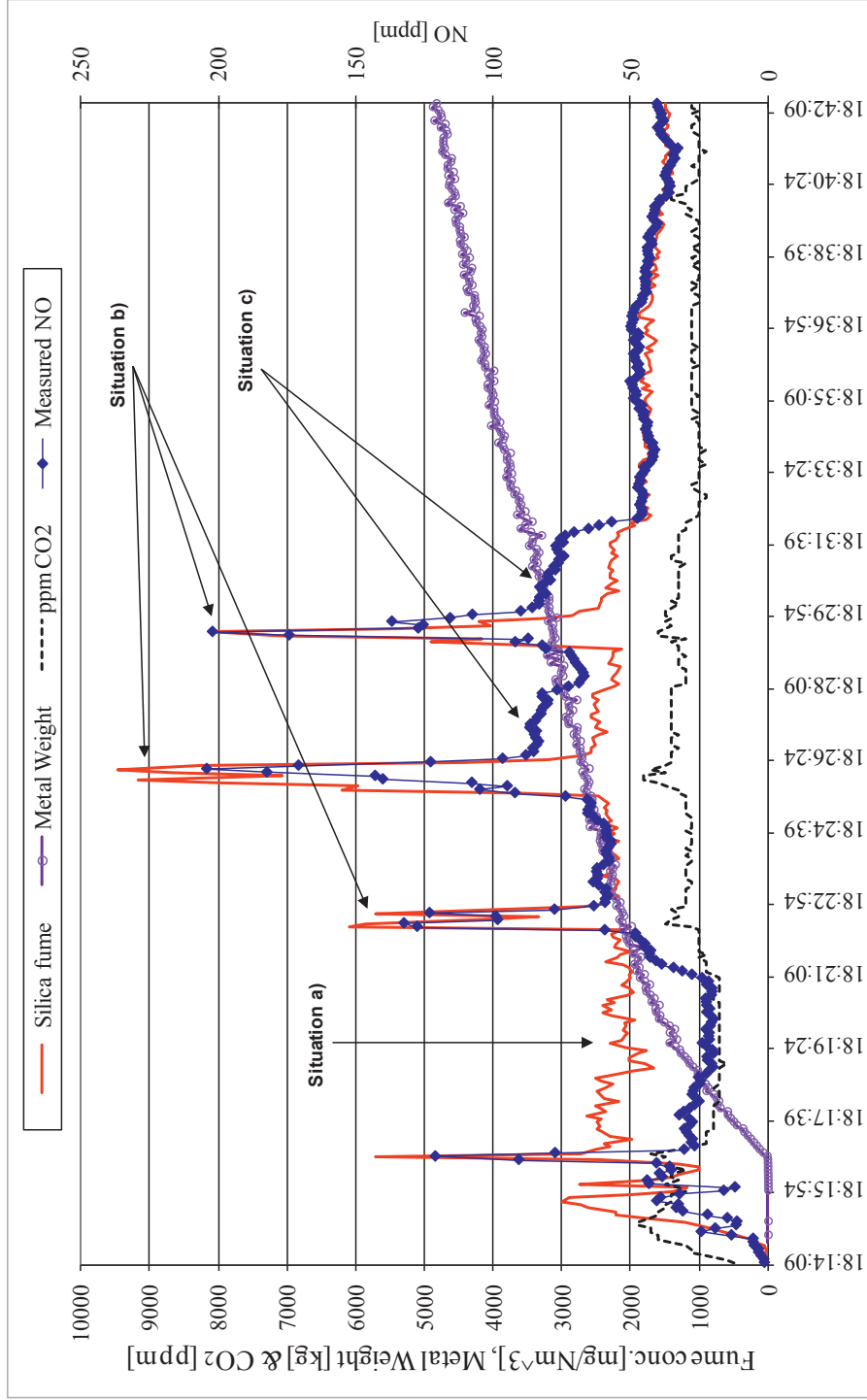
Figure 6.16: Measurement results of NO formation, silica fume and metal flow during tapping of silicon

6.5.3.1 Situation a) High fume – low NO

At the beginning of the tapping there is a period of high fumes but low NO formation, time 18:17-18:19. In silicon production it is normal to clog the tap hole for a time period and then open it to drain the furnace for metal. This cycle is repeated and this practice is often referred to as "discontinuously tapping". During the time period when the tap hole is closed the metal level inside the furnace will rise and when opening the tap hole the flow rate of metal out of the furnace will be high. This high flow of metal creates large amounts of fume when the hot metal hits the empty ladle, but the NO generation is low during this period.

6.5.3.2 Situation b) High fume – high NO (peaks)

Each observed peak is connected to the use of an oxygen lance. The oxygen lance is used to open up the tapping channel to increase the metal flow out of the furnace. These time periods are of special interest since they generate high amounts of fume and NO simultaneously.

6.5.3.3 Situation c) Low fume – high NO

After each peak there is a time period where the NO formation is higher than before the peak and decreasing to a "normal" level in about two-three minutes. At the same time the fume formation is at the same level as before the peak, but looking at Figure 5.7 there is an increase in the temperature that is not connected to the fume formation.

A possible explanation for the increased NO formation after the peak could be described by two mechanisms:

- The SiO combustion releases large amounts of energy by extreme radiation in such a way that the entire off gas system surfaces are heated to a higher temperature. These surfaces are covered with a layer of fume having a low heat capacity and conductivity. Because of this the surface temperature might exceed the NO forming temperature. The temperature conditions inside the Doghouse is modelled by Kadkhodabeigi (Kadkhodabeigi 2011) and show that the flame temperature can reach 3200 Kelvin. The heated surfaces may hence continue to produce NO during two to three minutes after the SiO combustion has ended.
- Secondly the much slower CO combustion could heat up some air above the NO forming temperature, giving this extra contribution in NO. Looking at the measured value of CO_2 in Figure 6.16 it is clear that the two situations with low fume – high NO have a higher value of CO_2.

A consequence of the first assumption above is that not only primary formation of NO due to SiO combustion is important, but that surfaces heated by this combustion acts as a additional source for NO. Overall process design that avoids such heated surfaces may reduce NO emissions.

6.5.4 NO formation as a function of silica fume weight in tapping

Looking back at Figure 6.7 the amount of NO formed per kilogram of silica fume in the furnace off gas was calculated. Looking at the measurements done towards tapping and plotting a whole tapping cycle, the results is a plot like Figure 6.17.
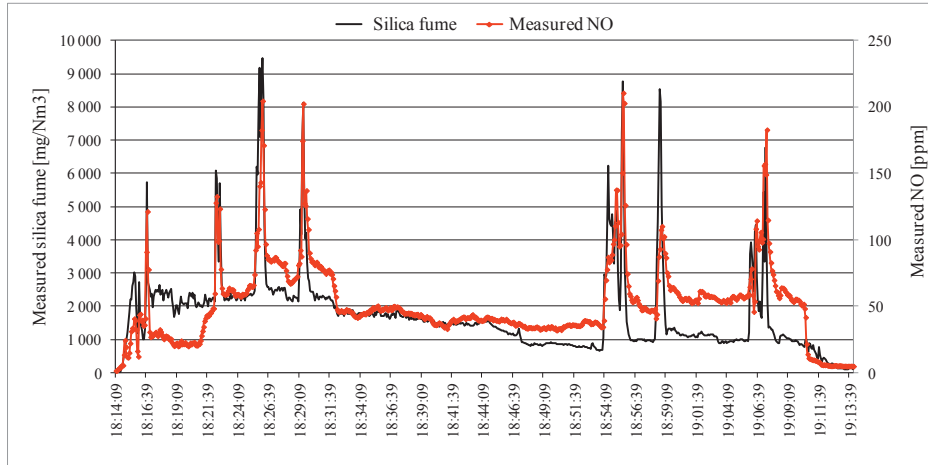
Figure 6.17: Measured NO and silica fume in silicon tapping

As indicated from the different situations during tapping described in Figure 6.16 the peaks in fume and NO are all connected to the use of an oxygen lance. It is interesting to see how the NO formation as a function of the silica fume formation behaves during the oxygen lancing situation. Figure 6.18 shows the relative formation of NO as a function of fume formed for the situations where the oxygen lance is used.
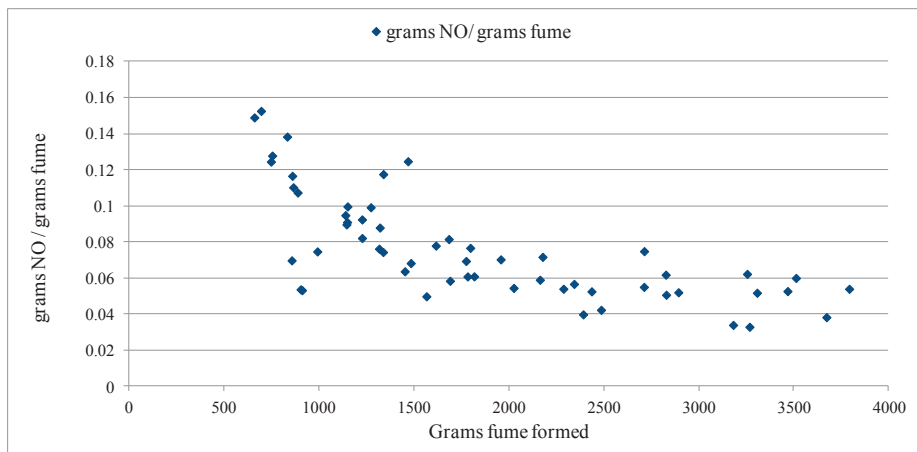
Figure 6.18: Relative NO formation as a function of fume formed

Compared to Figure 6.7 the behaviour of the NO formation as a function of fumes formed in the tapping off gas, is similar to the behaviour in the furnace off gas.

6.5.5 Measurements of NO at end tapping

In light of the metal temperature being as high as 1650 ºC it is interesting to see if the purge gas going through the melt could form NO.

Since the purge gas consists of both air and oxygen and the metal is hot enough to initiate the Zeldovich chain reaction there could possibly be places either inside or just above the melt where the needed radicals are formed.

Most likely all the oxygen entering the melt would react to SiO_2 because of the high Si activity, but the question is whether the heated N_2 leaving the melt could initiate some kind of NO formation just above the silicon melt.

Figure 6.19 and Figure 6.20 show two measurements of NO in the off gas done at the end of the tapping cycle. At the time "End tapping", marked with a black arrow, the tap hole is closed and the ladle is set to rest underneath the off gas suction. After closing the tap hole the only process occurring towards the ladle is purge gas going through the melt. In each case the ladle was held in this position for approximately 5-10 minutes to measure the level of NO. Figure 6.19 shows the results of a tapping done without the Doghouse installed on the runner while Figure 6.20 presents the results when the Doghouse was installed.

In both measurements the level of NO falls to approximately 0-5 ppm after closing the tap hole and stays at a very low level as time goes by.
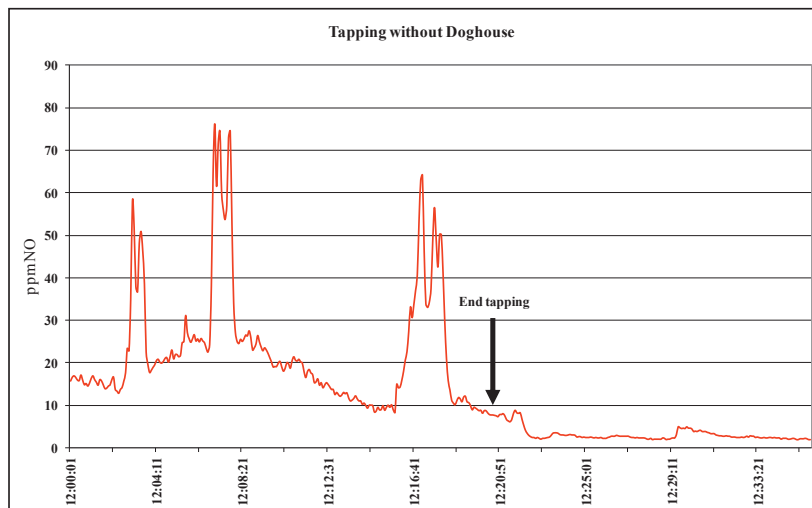
Figure 6.19: NO measurements during purging without Doghouse
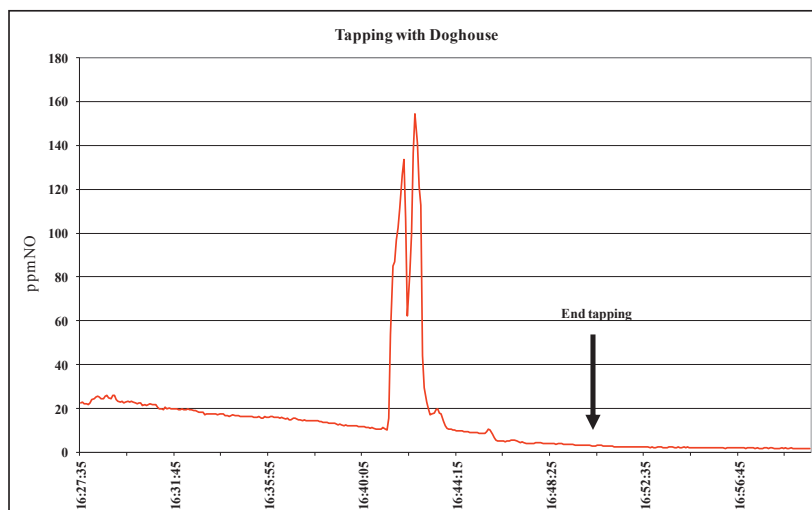
Figure 6.20: NO measurements during purging with Doghouse

According to the specification datasheet for the TESTO 350 XL the accuracy at low levels of NO, from zero to 99 ppm, is below 5ppm. The response time is 30 seconds with a resolution of 1 ppm.

Based on this and the results in Figure 6.19 and Figure 6.20 it is therefore assumed that the amount of NO formed during purging is of minor importance compared to the levels measured during tapping and when work operations are conducted towards the tap hole.

6.5.6 Comparison of measurements in furnace and tapping off gas

Plotting the data in Figure 6.7 and Figure 6.18 in the same diagram using a logarithmic x-scale gives Figure 6.21. The average value of both series is indicated with a line in each series. Notice that the specific NO formation is somewhat higher in the Tapping area than above the furnace surface.
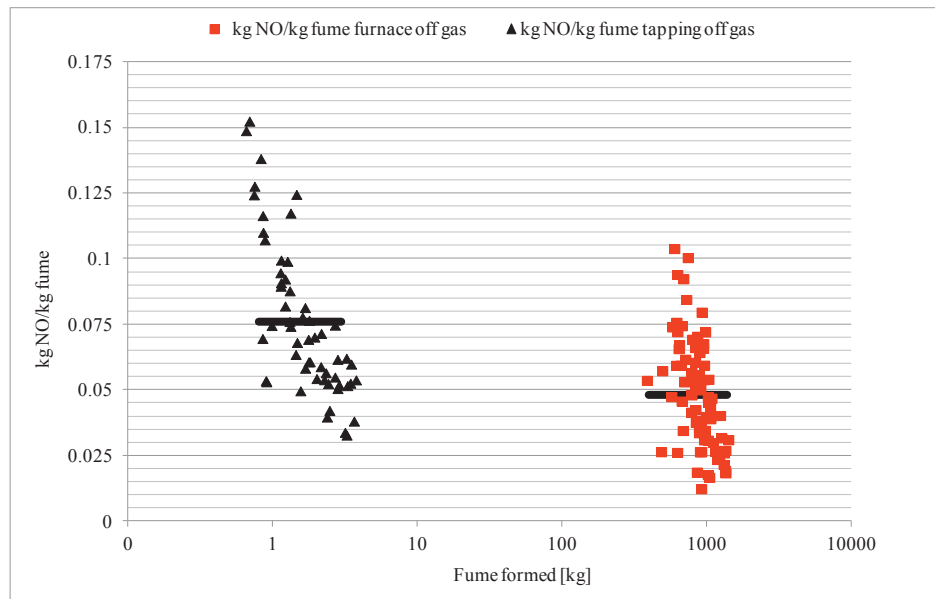
Figure 6.21: NO formation as a function of fume formation in tapping and furnace off gas

It is likely that the measurements done towards the tapping off gas has a higher accuracy with respect to both the NO measurements and the off gas volume based on more certain measurement conditions.

A possible explanation could first of all be that the oxygen lancing produces a more concentrated energy sphere when the fumes forms, in that way heating more air that undergoes the Zeldovich reactions.

Secondly the SiO combusting on the furnace surface would happen in a process gas environment, containing both CO and other gases from the volatiles in the charge materials. In that respect there could be "a competition" for oxygen during the process gas combustion.

Third the velocity fields in the tapping area is low compared to on the furnace surface, having a velocity field sweeping over the surface dependent on the off gas design. This forced flow of air into the process gas combustion zone could have a quenching effect on the combustion.

6.5.7 Correlation between measured NO and silica fume when lancing during tapping

Based on the seemingly good connection between the fume and NO formation during oxygen lancing only these time periods are selected. A scatter plot of the NO formation as a function of the corresponding silica fume formation is shown in Figure 6.22.
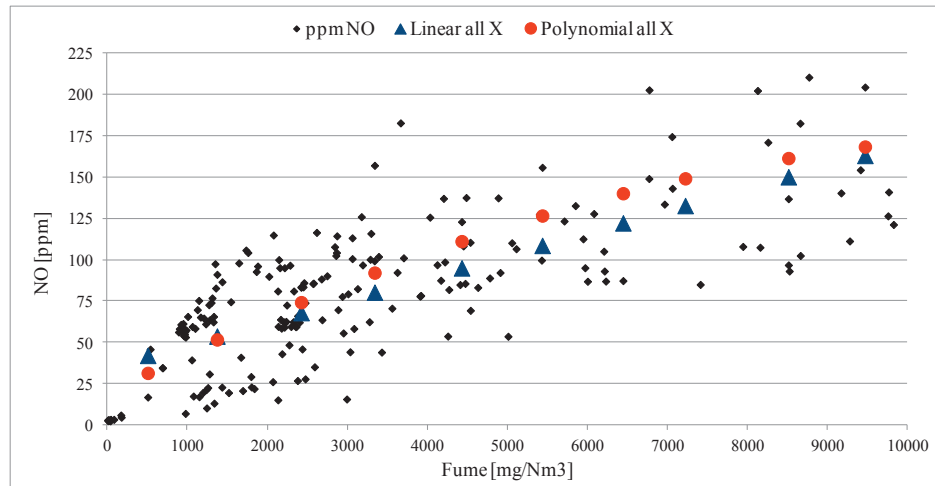
Figure 6.22: Scatter plot of NO with regression models

Figure 6.22 also contain two regression models, one linear and one polynomial, made with Minitab® Statistical Software (Minitab® 2007) based on the same data.

6.5.7.1 Regression model

Regression analysis is most often used in analysing data where the predictor is set to a constant value and the different responses analyzed. In this case the predictor is the fume, being more a stochastic value, in other words the fume value could not be set to a determined level and the response in NO formation measured. Nevertheless the Minitab models are evaluated.

The two regression models in Figure 6.22 are given by the following equations:

Linear: $y = 35.2 + 0.0135x$

Polynomial: $y = 18.9 + 0.02526x - 0.000001x^2$

Both equations could be expressed on the form $y = a + bx\ (+cx^2)$ where the constant "a" would describe the level of NO formed during the time when no fumes are formed, the "b" and "c" describes the connection between the fume generation and NO.

The variance and r-squared values for the two models are

Linear model: S = 29.3979   R-Sq = 56.1%   R-Sq(adj) = 55.8%

Polynomial model: S = 28.1481   R-Sq = 59.9%   R-Sq(adj) = 59.5%

To sum up the statistical details Table 6-4 gives the analysis of variation for both models.

Table 6-4: Analysis of variance for the regression models

Linear model					
Source	**DF**	**SS**	**MS**	**F**	**P**
Regression	1	216218	216218	250.18	0.000
Error	196	169390	864		
Total	197	385608			
Polynomial model					
Source	**DF**	**SS**	**MS**	**F**	**P**
Regression	2	231106	115553	145.84	0.000
Error	195	154502	792		
Total	197	385608			

6.5.7.2 Model validity

To investigate the two models ability to predict the NO formation on any dataset the models are used to predicted levels of NO formation on some of the other off gas measurements done at the same silicon furnace. The measured and modelled results are showed in Figure 6.23.
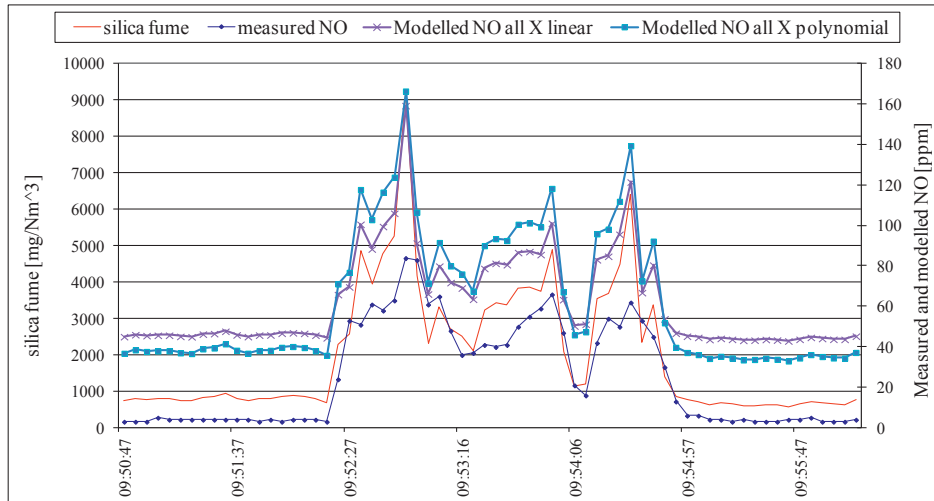
Figure 6.23: Predicted NO levels on different dataset together with actual measurements[4]

As seen in Figure 6.23 the baseline of the predicted NO levels are too high compared to the measurements. This is most probably because the NO and fume measurements in Figure 6.23 are done at a time when the Doghouse was not installed, giving a high amount of false air and dilution of the off gas. However the two models predict the changes and dynamics very well and the relative increase in the models results and the measurements are in the same range.

Based on Figure 6.23 the best model describing the NO variations seems to be the linear model given by the equation

$$NO_{ppm} = 35.2 + 0.0135 * fume_{mg/Nm^3}$$

---

[4] The NO measurements are adjusted for the time lag that the TESTO used to analyse the gas.

It is interesting to see how the chosen model predicts the level of NO on the entire dataset of the tapping with the Doghouse installed.

Processing the complete data set shows that the model predict NO well up to a level of approximately 150 ppm. At higher levels of NO the model fails, but as seen in Figure 6.25 the measured peak values of NO still seems to follow the formation of SiO_2.
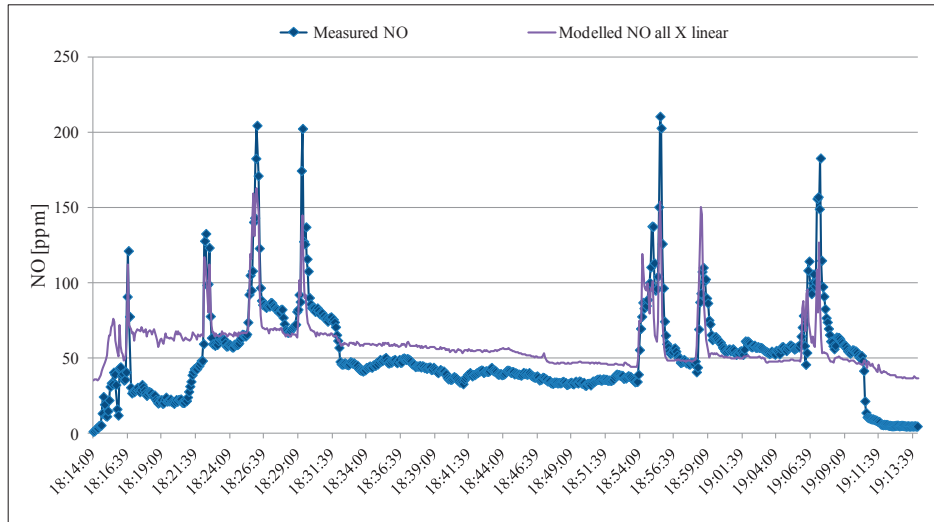
Figure 6.24: Measured and modelled NO for the entire data set
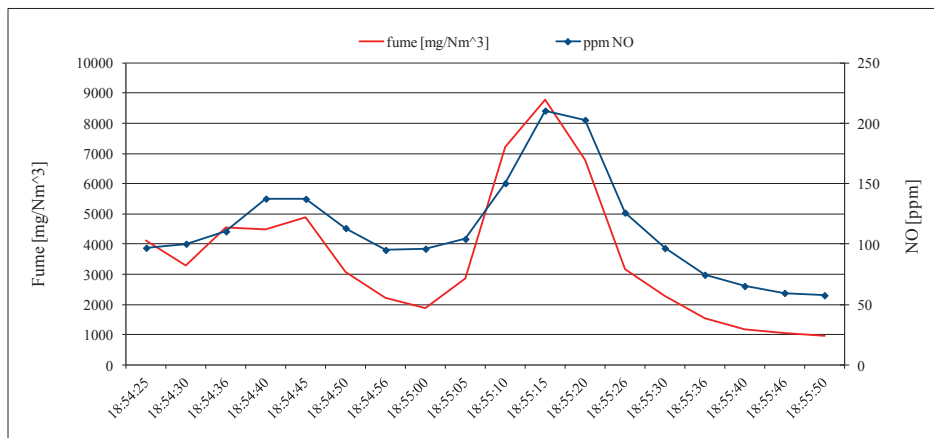
Figure 6.25: Measured peak values for NO and fume

Even though the regression model fails to predict the level of NO at high fume levels Figure 6.25 still illustrates that the connection between NO formed and fume formed are strong.

84

6.6 Mechanisms of NO formation during SiO combustion

Looking again at the peaks in Figure 6.16 from the previous section, these were all connected to the use of an oxygen lance that eases the metal flow out of the furnace.

The increased fume formation during this work operation is caused by one of two mechanisms:

- oxygen lancing opens up the tapping channel, releasing SiO gas from the crater which combusts in contact with oxygen to SiO_2 (fume)

- oxygen from the lance causes liquid metal to combust to SiO_2 (fume).

Both oxygen lancing (opening the tapping channel) and combustion of crater gases outside the furnace produces SiO_2 fumes, release large amounts of energy to the surroundings.

6.6.1 Fume properties

6.6.1.1 Chemical analysis of the silica fume sampled during tapping

Chemical analysis of the fume was done to ensure that the silica fume measured during tapping contains mainly SiO_2 and not other elements from the carbon materials in the runner or tap hole. The fume was analysed by atomic absorption spectroscopy and combustion analysis with a LECO TCH600, the results are given in Table 6-5.

Table 6-5: Chemical analysis of the silica fume sampled during tapping

Element	Si	Fe	Ca	Al	Ti	C	O	Other
Analysis	46.4	0.310	0.130	0.330	<0.0500	0.190	52.3	0.340

Assuming that the elements Fe, Ca and Al are present as oxides in the fume and that the rest of the oxygen is bounded in the SiO2 gives a SiO2 content of 97.16 wt% in the fume.

6.6.1.2 Particle size distribution for the fume

In addition to the chemical analysis of the fumes the size distribution of the particles was investigated. The fumes were examined using a scanning electron microscope (SEM) and from the SEM images the particle size distribution and mean particle diameter were estimated by measuring and counting ~1000 particles in several images. The silica particles were perfect spheres with a size distribution of 0.001-3 μm, with 70-90 % of the particles being < 0.05 μm (Næss, Tranell et al. 2012). The size distributions are given in Figure 6.26.
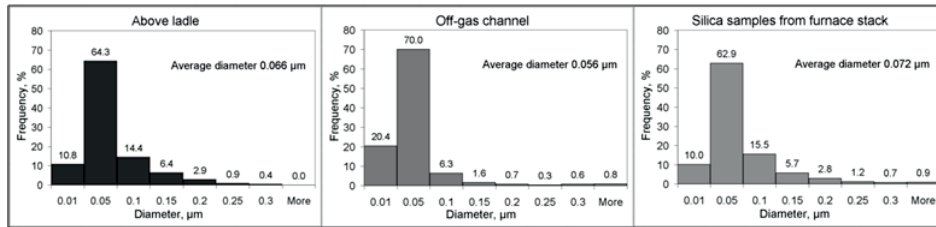
Figure 6.26: Measured size distributions on actual MS collected during the measurement campaigns. (Næss, Tranell et al. 2012)

Figure 6.26 shows the results for three categories of fume, from close to the tap hole (named "Above ladle"), fume from the off gas channel (named "Off-gas channel") and a third sample taken from the furnace off gas. The similarities between fumes from the furnace off gas and from the tapping off gas are interesting and indicate that the formation mechanisms for the different fumes could be similar.

6.6.2 Stoichiometric combustion of the SiO/CO gas – the NO formation hypothesis

A possible explanation for the observed correlation between the formation of fume and NO is to assume that the energy released from the combustion heats up the air surrounding the particles, which then forms NO through the Zeldovich mechanism.

To look further into this a three-step reaction chain forming both fume and NO is imagined, as shown in Figure 6.27. Combining Ulrich's particle growth theory (Ulrich 1971) with an additional chemical reaction forming NO it is assumed that SiO_2 is initially formed as a gas which in turn condenses to small droplets. These droplets collide and as time progresses and the temperature drops solid particles are formed.
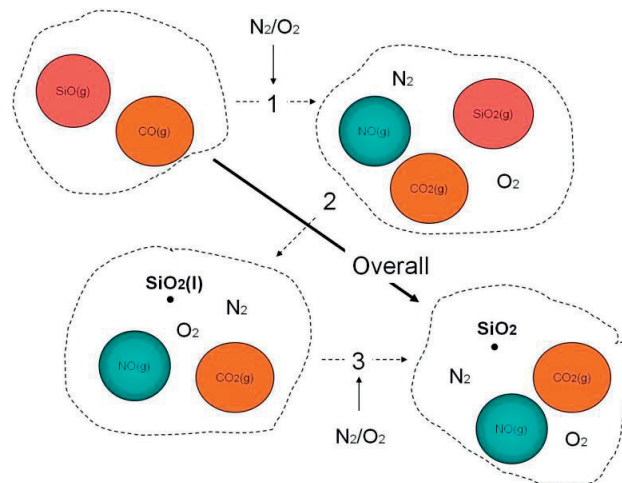
Figure 6.27: Reaction model for fume and NO

Step one: SiO and CO gas from the furnace (or SiO from the oxidation of metal) reacting with O_2 to form SiO_2 and CO_2 gas. Already at this stage it is assumed that the energy released is sufficient for NO formation.

Step two: The SiO_2 gas condenses to liquid droplets which collide into larger and larger droplets as described by Ulrich. The condensation into droplets is a highly exothermic reaction.

Step three: As the temperature drops the collisions between droplets will no longer result in new particles and the growth is suspended. The off gas is now fume particles and a gas mixture consisting of NO, CO_2 and excess N_2/O_2.

Using HSC (Roine, Lamberg et al. 2007) to calculate the heat of reaction for the reactions involved, assuming that the NO is formed through the Zeldovich mechanisms, Table 6-6 display that the combustion process releases energy all the way up until the SiO_2 condenses.

Given the amount of SiO_2 formed compared to the amount of NO formed, the overall energy released from the reaction chain is substantial.

Table 6-6: Thermodynamic data for the reaction scheme forming NO and SiO_2 at 1600 °C. Calculated with HSC (Roine, Lamberg et al. 2007)

Reaction step	Reactions	ΔH_r @ 1600 °C [kJ/mol]	ΔG_r @ 1600 °C [kJ/mol]
Step one	$SiO(g) + \frac{1}{2} O_2(g) = SiO_2(g)$	-211.976	-65.239
	$CO(g) + \frac{1}{2} O_2(g) = CO_2(g)$	-278.351	-120.531
	$O(g) + N_2(g) = NO(g) + N(g)$	315.194	291.415
	$N(g) + O_2(g) = NO(g) + O(g)$	-134.097	-157.997
	$N_2(g) + O_2(g) = 2NO(g)$	181.097	133.418
Step two	$SiO_2(g) = SiO_2(l)$	-560.236	-256.440
Step three	$SiO_2(l) = SiO_2$	-7.873	-0.8896

6.6.2.1 The NO formation time based on stoichiometric combustion of the furnace gases escaping out through the tap hole

Based on the reaction chain in Figure 6.27 and the measurements in the tapping off gas described earlier a combustion model in HSC Sim is set up (Roine, Lamberg et al. 2010) assuming that the gas mixture coming from the silicon furnace consists of equal amounts of SiO and CO (Schei, Tuset et al. 1998). The model is designed to feed the reactions with sufficient amounts of air to have stoichiometric combustion and NO formation as measured. The furnace gas enters at 1600 °C and in the end the hot gas mixture is diluted with cold air.

Looking at Figure 6.28 the second step produces a "cloud" of SiO_2 fume and a gas mixture consisting of CO_2, NO and N_2.
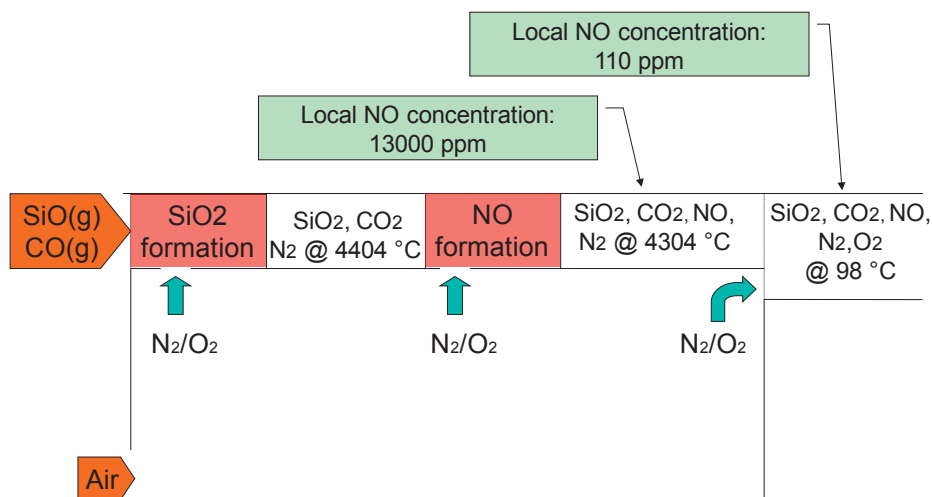
Figure 6.28: Combustion model and calculated results

Table 6-7 gives a detailed summary of the gas composition when the second step of Figure 6.28 is completed, calculated with HSC Sim.

Table 6-7: Gas "cloud" components calculated by HSC Sim

	INPUT	OUTPUT
Temperature in °C	**25.00**	**4304**
Gas phase in kg/h		
SiO(g)	77.40	0.00
CO(g)	49.25	0.00
N_2(g)	191.42	189.85
O_2(g)	58.01	0.00
CO_2(g)	0.00	77.39
NO(g)	0.00	3.36
Solid phase in kg/h		
SiO_2	0.00	105.49

Based on the "cloud" gas content shown in Table 6-7 the NO content is calculated to 12946 ppm.

To calculate the formation time of the NO Equation (6-6) is solved with the assumptions made in Section 6.2.1.1 and rearranged to a to ppm basis. Using the achieved temperature from the model and a pressure of one atmosphere[5] the solution for time t is:

$$t = \frac{\chi_{NO}[ppm] * P}{NO(t) * R * T}$$

6-7

Solving Equation 6-7 with the results from the HSC SIM model gives a formation time for the NO cloud equal to 0.0411 seconds. The summary of the HSC SIM model results are given in Table 6-8.

Table 6-8: HSC SIM model results

Calculated level of NO in "cloud"	Temperature in "cloud"	Formation time for NO
12946 ppm	4577 Kelvin	0.0411 Seconds

6.6.3 Growth time for the measured fume particles

The measured off gas particle concentration together with the growth theory for SiO_2 particles described by Ulrich enables the calculation of the growth time to be made for the given mean particle size.

Ulrich gave the following equation for particle growth in a cloud of uniform particles, given that the Knudsen number[6] is greater than 10 and that the initial nuclei are already formed:

$$N = (6.8 \cdot 10^{-12} * c * T^{\frac{1}{2}} * C_0^{\frac{1}{6}} * t)^{-6/5} \left[{}^{\#}\!/_{cm^3} \right]$$

6-8

N is the particle concentration, c is the number of successful collisions given by a sticking coefficient and C_0 defines the number of silica molecules/cm^3.

Using the equation for the specific surface area, SA = 3/(ρR), where ρ is the particle density and R is the particle radius, Ulrich also deduced an equation for the SA as a function of the above parameters, given as

$$SA = 1.81 \cdot 10^8 * (T^{\frac{1}{2}} * c * C_0 * t)^{-2/5} \left[{}^{m^2}\!/_g \right]$$

6-9

---

[5] T given in Kelvin, R given in [atm*m^3/kmol*K] and assuming O_2 and N_2 concentrations are constant equal to that in air

[6] The **Knudsen number** (**Kn**) being a dimensionless number defined as the ratio between the mean free path (distance travelled between collisions) and the particle diameter.

Solving both equations for C_0 and combining them gives us an expression for the particle growth time:

$$t = \frac{SA^{1/2}}{\left(1.81 \cdot 10^8 * T\right)^{1/2} * B^{6/5} * C * N}$$ 6-10

B is the first part of Equation. (6.8) equal to $6.8 \cdot 10^{-12}$ [$m^3/s*T^{1/2}$] as given by Ulrich and N is the particle concentration in the end gas mixture.

Choosing some peak values in fume concentration the growth time for the SiO_2 particles can be calculated, assuming a diameter of 55 nm, density equal to 2200 kg/m^3 and at the temperature equal to the "cloud" temperature. The results are shown in Table 6-9.

Table 6-9: Growth times of particles and calculated NO formation per particle. Sticking coefficient = 0.3

Fume concentrations [mg/Nm³]	Measured NO [ppm]	Calculated growth time of particles [sec]
4400	110	0.0283
6000	133	0.0207
8700	210	0.0143

Comparing the formation time of NO in Table 6-8 to the growth time of the SiO_2 fume particles it is clear that they are in the same order of magnitude.

Since the fume properties are known the amount of NO formed per particle can be calculated. Table 6-10 shows the calculated results for the three values chosen.

Table 6-10: Calculated specific NO formation per fume particle

Fume concentrations [mg/Nm³]	Measured NO [ppm]	Moles of NO formed per fume particle
4400	110	2.14E-019
6000	133	1.90E-019
8700	210	2.07E-019

Table 6-10 shows the NO formation per fume particle is almost equal independent of the amount of fume formed. These results correspond well to Figure 6.18 where the relative NO formation is almost horizontal at high fume concentrations.

6.7 Descriptive modelling of NO formation from a particle

It is interesting to see if the NO formation per particle can be recreated based on heat transfer from the particle itself. Using the COMSOL Multiphysics software (Comsol 2010) a heat transfer CFD model was set up using Equation 6-5 for the NO formation.

6.7.1 The model

The model simulates a particle experiencing the calculated "cloud" temperature over the time span for the fume particle growth, assuming that the particle is surrounded by air and with no velocity field present.

The heat transfer equation is given by

$$\rho \frac{\partial T}{\partial t} + \nabla \cdot (-k\nabla T) = Q \qquad \textbf{6-11}$$

Heat transfer in air is calculated as conduction only since radiation has a very limited effect on diatomic gases like O_2 and N_2. The outer boundary condition is set to 273 K and placed far away from the particle. The heat source term Q is set to zero, and instead the particle itself is given a temperature profile.

As a suited temperature profile for the particle the suggested combustion temperature profile given in *Air Pollution Control Engineering* by De Nevers, figure c) page 454 in (De Nevers 2000) is chosen. This profile assumes that the particle is rapidly heated by the chemical reactions forming it and then loses heat to the surroundings over time. The profile is shown in Figure 6.29.
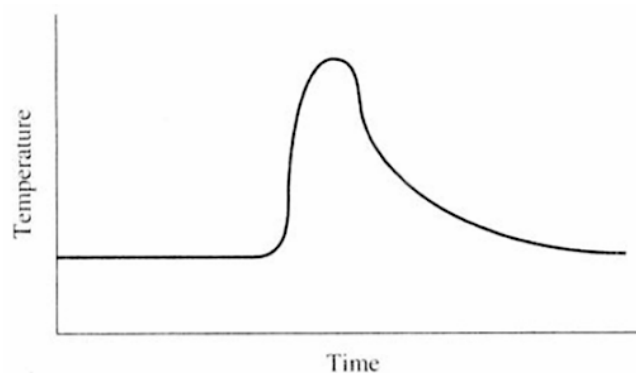
Figure 6.29: Particle temperature profile from (De Nevers 2000)

6.7.2 Modelled results

Table 6-11 shows the results from the CFD model for the particle growth times. The last row of Table 6-11 shows the CFD model result for the growth time of the NO formed in Step 2 in Figure 6.28.

Table 6-11: Results of the CFD simulations

Fume concentration	Calculated growth time [seconds]	mol NO formed
4400 mg/Nm^3	0.0283	6.343E-19
6000 mg/Nm^3	0.0207	4.829E-19
8700 mg/Nm^3	0.0143	3.308E-19
For the NO "cloud"	0.0411	9.308E-19

Figure 6.30 gives a comparison of the calculated amount of NO per fume particle in Table 6-10 with the modelled NO formed. Here the results are within the same order of magnitude.
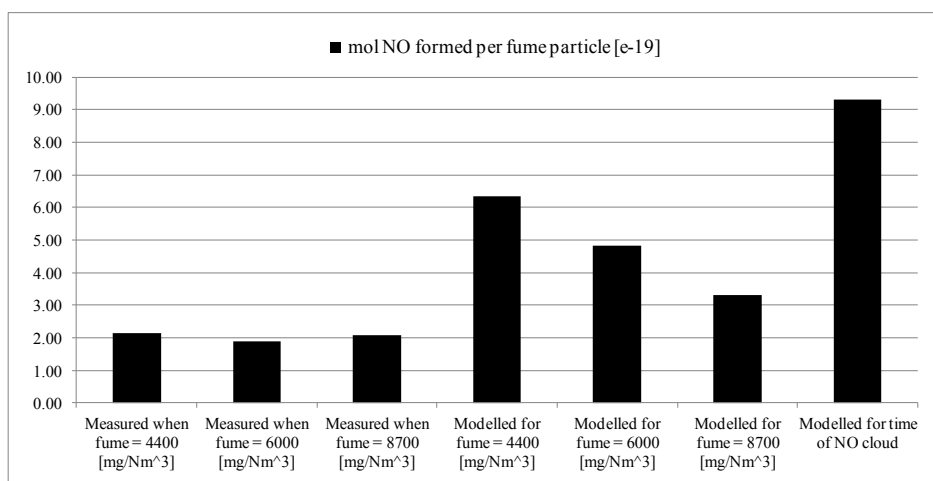
Figure 6.30: Comparison of measured and modelled NO formation per fume particle

In general the CFD model overpredicts the NO formation per particle compared to the measured results. This is probably caused by the chosen ideal conditions for the model.

6.7.2.1 Model uncertainties from O_2 and N_2 assumptions

In the rate expression for NO formation (Equation 6-6) it is assumed that the content of O_2 and N_2 is at a constant level equal to that in air during the time frame of formation. If however the content of O_2 is lower the rate of NO formed would decrease. This would affect the total amount of NO formed as well as increasing the time of the NO formation in the combustion model (Equation 6-7).

At a constant temperature of 4577 K, both the CFD model and Equation 6-6 give a rate reduction of ~ 6 % when reducing the O_2 content with 2.5 %.

Letting the concentration of O_2 and N_2 drop during the calculations means a reduced NO formation, leading to the calculated results becoming closer to the measured ones.

6.7.2.2 Model uncertainties from assuming stoichiometric combustion in a "cloud"

The assumption that the combustion of the furnace gases happens at stoichiometric conditions defines the temperature at which the particle grows (Equation 6-10), the NO formation rate (Equation 6-6) and the growth time for the NO in the "cloud" (Equation 6-7).

An alternative situation would be to dilute the combustion with more air. The consequence of dilution is an end gas mixture with higher content of O_2/N_2 and a lower "cloud" temperature.

Using HSC Sim the end temperatures when diluting the gas can be simulated. Table 12 shows the effect on growth times when the combustion occurs with an increasing surplus of air, given as surplus O_2 content.

Table 6-12 Calculations of changes in oxygen content in the combustion gas, particle density = 6000 mg/Nm^3

O_2 Content	Temperature [Kelvin]	Cloud growth time [seconds]	Fume particle growth time [seconds]
Stoichiometric	4577	0.0429	0.0207
2.5% surplus	4516	0.0498	0.0209
5% surplus	4457	0.0602	0.0210
10% surplus	4343	0.0882	0.0213

As the table shows the effect of a reduced temperature has only minor consequences for the fume particle growth time, but the formation time for the NO "cloud" is highly affected. A portion of this effect on cloud growth time is caused by the simultaneous decrease in the rate of NO formation because of the reduced temperature.

However as seen from Table 6.10 the measured amount of NO formed per fume particle is fairly equal and independent of the amount of fume formed. This suggests that each particle "experiences" somewhat equal conditions during growth. The similar results from the CFD model, based on parameters assuming stoichiometric combustion supports this.

6.7.2.3 Uncertainties in assuming heat transfer from particle as conduction only

As explained in the CFD model section the heat transfer from the particle is assumed to occur only through conduction, neglecting any radiation from the particle since its assumed that each particle only "see" diatomic gases. Imagining several particles in a cloud, interparticular radiation could sustain a higher temperature for each particle over a longer time frame, but at the same time an imagined cloud of particles would probably behave as a hot body and therefore also loose energy to the surroundings through radiation.

Maintaining a high particle temperature over a longer time frame would increase the NO formation per particle while treating the cloud of particles as a hot body losing energy would lower the NO formation, giving model results closer to the measured amounts of NO.

Another explanation combining several uncertainties could also occur, assuming that the formation happens not at stoichiometric conditions, but the interparticular radiation sustains the particle temperature to that extent that the formed NO matches the calculated results.

At last the combustion assumingly occurs in an atmosphere containing CO gas. Comparing the reaction rate for $CO+O_2 => CO_2 + O$ given by Turns to the rate for $SiO+O_2 => SiO_2 + O$ given by Jachimowski and McLain the SiO combustion at the temperature used is $3.75*10^2$ faster than the CO combustion. This means that the SiO combustion will be able to radiate some energy to the CO gas molecules. Accounting for this in the CFD model would lead to a lower temperature which again would lead to lower NO formation.

6.8 Formation differences in NO - Furnace surface vs Tapping

Comparing the measurements from the tapping area with the measurements from above the furnace surface it is clear that when using an oxygen lance the NO formation in the tapping area follows the fume formation almost instantly (see Figure 6.16), while there seems to be a time lag between the NO and fume formation when looking at the measurements above the furnace surface (see Figure 6.6).

Investigating several of the measurement series it was found this feature occurred frequently, varying in time from under a minute up until several minutes. Figure 6.31 gives the measurements of the first two stoking/charging cycles from Figure 6.6 and now the time lag in the NO formation becomes evident.
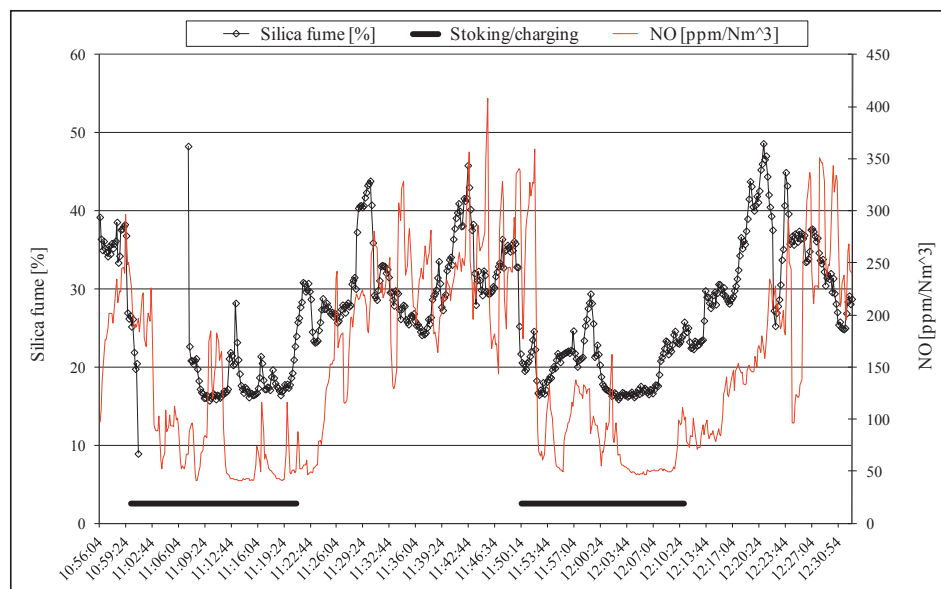
Figure 6.31: NO vs fume above the furnace surface

As discussed in Section 6.3 the combustion conditions for SiO in the tapping area are totally different from the conditions at the furnace surface. While the combustion in the tapping area mainly would be influenced by the content in air alone, the combustion at the furnace surface would implicate combustion of volatile matters (C_xH_y), evaporation of any water in the raw materials in addition to the air being sucked into the furnace.

Given this difference the combustion reactions at the furnace surface will experience a competition for oxygen and radicals while the combustion in the tapping area would be more controlled by the amounts of furnace gases since the air excess in the area is substantial.

95

The consequence of a combustion atmosphere containing species consuming or producing radicals and intermediate species influences the NO formation. Especially the effect of water on NO formation is noticeable.

Miyauchi, Mori et al. (Miyauchi, Mori et al. 1981) studied the effect on NO formation when adding steam in a methane/air combustion. They found that the NO formation was reduced even though the maximum flame temperature was kept constant. A numerical model involving 21 components and 51 reactions supported their experimental findings.

Bhargava, Colket et al. (Bhargava, Colket et al. 2000) studied the effect of humidity in the combustion air on a Humid Air Turbine. Running experiments for several levels of humidity they found that the presence of steam leads to lower O-atom concentration and a higher OH-atom concentration. Both these will lower the formation of NO. In addition they found that the moisture lowered the equilibrium temperature, giving a temperature effect on the NO formation, but even while keeping the temperature constant the added moisture suppressed the NO formation. Bhargava, Colket et al. also modelled the reactions using the GRI-Mech 2.11 reaction mechanism (Bowman, Hanson et al.), finding a good agreement between the experiments and modelled results.

Guo, Stuart Neill et al. (Guo, Stuart Neill et al. 2008) studied the effect of water addition on NO formation in counterflow CH_4/air premixed flames by a numerical simulation using the GRI-Mech 3.0 reaction mechanisms (Smith, Golden et al.). They concluded that water addition suppresses the NO formation because of a lower flame temperature and a chemical effect lowering the O concentration.

Furuhata, Kawata et al. (Furuhata, Kawata et al. 2010) experimentally investigated the effect of adding steam to a kerosene spray combustion, concluding that the steam addition lowered the flame temperature in the combustion chamber and it that way gave lower NO concentrations.

6.8.1 NO formation at the furnace surface

A more detailed description of the situation at the furnace surface right after charging/stoking could be as follows:

Primary NO formation phase:

- The rising furnace gas meets the freshly charged raw materials. According to the measurements done by Johansen, Tveit et al.(Johansen, Tveit et al. 1998) the temperature could drop from 800 ºC to as low as 400 ºC depending on how much fresh material that is added.
- The low temperature will cause most of the rising SiO gas to condensate and only minor parts reach the surface to combust.
- As the fresh materials are heated the chemical reactions involving evaporation of water and combustion of volatile matters would happen simultaneously with the combustion of SiO. The competition for oxygen in this area is assumingly high and measurements done by Arntsberg (Arntsberg 2004) show that the oxygen concentration close to the surface is as low as 2 wt%. The NO formed during this primary reaction stage is believed to be dominated by the prompt and fuel NOx formation mechanisms.
- The fume formation is slowly rising according to the raw material mixture slowly increasing in permeability.

Transient time phase:

- After some time the permeability in the raw materials will increase since some of the volatiles and water will have reacted or evaporated. This gives the rising furnace gas an opportunity to flow freely out above the charge and combust right above the surface. Fume formation will increase and so will NO formation since the combustion of SiO to solid fumes releases a lot of energy. This transient phase will continue as long as there is volatiles and water available, while the availability of oxygen increases.

Secondary NO formation phase:

- When all the volatiles and water have burned or evaporated the furnace gas can freely flow out of the charge and react. During this stage both the fume and NO formation is high and closely connected. The NO formation is believed to be dominated by the thermal NOx formation mechanism.

Figure 6.32 shows the measurements of fume and NO beginning at the end of the charging/stoking cycle and 15 minutes forward. As Figure 6.32 show the three reaction phases described seems to fit well with the measured results well.
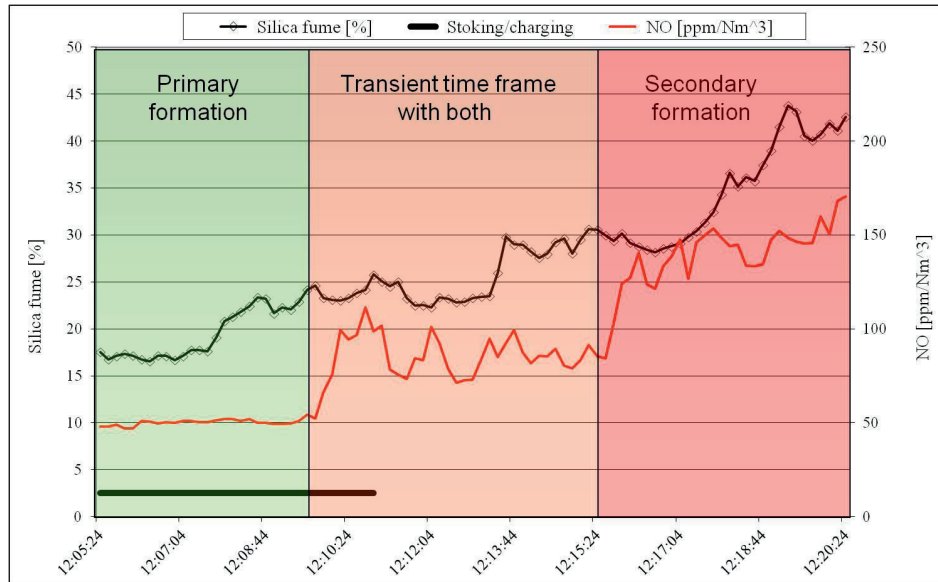
Figure 6.32: The three reaction scenarios at the furnace surface

Assuming this formation scheme for NO to be valid would mean that adding raw materials frequently suppresses the NO formation at the surface and reduces the overall emissions from the furnace. The scheme is also well in compliance with the results that Grådahl, Johansen et al. (Grådahl, Johansen et al. 2007) found when investigating the difference in NO formation as a function of adding raw materials. They found that increasing the frequency in adding raw materials removed many of the high peaks in NO, lowered the base line level of NO and in total reduced the average NO emission from 228 ppm to 105 ppm, a reduction of more than 50 %.

6.8.2 NO formation in the tapping area

The NO formation in the tapping area is assumed to be of a much simpler character since only SiO, CO and air are involved in the combustion. As discussed earlier the strong correlation between the fume formed and the level of NO suggests that the energy released from the oxidation of either metal or SiO gas triggers the thermal NO reaction chain.

6.9 Modelling combustion with GRI-Mech 3.0

Given that our combustion environment at the surface contains both water and volatile matters in addition to the SiO/CO gas a chemical reaction model that could account for all these simultaneously is needed.

GRI-Mech is an optimized detailed chemical reaction mechanism consisting of 53 species and 325 chemical reactions initially describing natural gas flames and ignition, including NO formation and reduction, in the temperature range from 1000 Kelvin to 2500 Kelvin. The mechanism is a list of elementary chemical reactions and associated rate constant expressions where most of them have been studied experimentally in a laboratory by Smith, Golden et al (Smith, Golden et al.).

Since the GRI-Mech mechanism contains the possibility to evaluate different compositions in the combustion atmosphere with respect to water and volatile matters (C_xH_y) it is suitable to describe the differences in our two environments.

Combining the GRI-Mech 3.0 reaction mechanisms with the SiO combustion mechanisms given by Jachimowski and McLain as discussed in Section 6.4, it is possible to model how the content of SiO gas, water and/or other species influence the NO formation at different temperatures. The Chemical Reaction Engineering module in COMSOL Multiphysics (Comsol 2010) is used to solve the model. This is capable of simulating a perfectly stirred reactor both with or without material flows and as a function of time.

6.9.1 Modelling combustion at furnace surface

In order to illustrate the NO formation in the different combustion environments four different cases are modelled using the complete GRI-Mech 3.0 reaction mechanism and the SiO combustion as described by Jachimowski and McLain. The four cases are:

- Combustion at the furnace surface right after charging.
- Combustion at the furnace in the intermediate phase
- Combustion at the furnace surface after all volatiles and water has been driven off
- Combustion in the tapping area

6.9.1.1 Model set up and assumptions

As the main interest is the principal differences in the level of NO produced in each case and not the exact value, the situation is simplified.

Imagining a small volume of gas situated at the furnace surface getting an inflow of water and volatiles from the charge in addition to SiO and CO gas from the furnace. Letting it have this concentration at time = zero and then flowing away from the surface

with the off gas stream a short distance it would immediately be exposed to the surrounding air and combustion would begin. Each case is calculated at a constant temperature equal to 1400 ºC, as measured just above the charge by Johansen, Tveit et al. (Johansen, Tveit et al. 1998).

The two main cases are the Primary and Secondary NO formation phases with an intermediate situation in between. The input for the amounts of SiO and CO are taken from page 169, Table 8.2 in Schei, Tuset et al. (Schei, Tuset et al. 1998) and assuming that the amounts of volatiles equals half the amount of CO from the crater. For simplification the amount of water is set to the same amount as volatiles in each case. This is clearly not accurate enough compared to a real furnace operation but would illustrate the difference in the three combustion phases well. The combustion situations are as described in "Primary NO formation phase" and "Secondary NO formation phase" in Section 6.8.1 and shown in Figure 6-33.
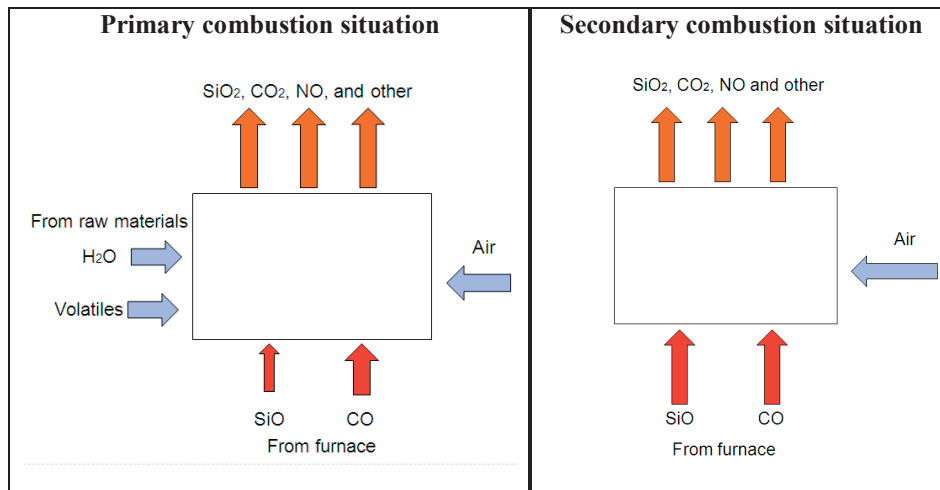
Figure 6.33: Primary and secondary combustion situations

In addition to these two an intermediate phase was modelled. The input parameters to the models are summed up in Table 6-13

Table 6-13: Initial model inputs for combustion. All numbers in [mol/m^3]

Phase	SiO	CO	C_xH_y	H_2O	O_2	N_2
Primary phase	0.073	6.55	3.28	3.28	8.31	33.28
Intermediate phase	0.73	6.55	1.64	1.64	8.31	33.28
Secondary phase	0.73	6.55	0.00	0.00	8.31	33.28

6.9.1.2 Results for combustion at the furnace surface

The three combustion phases were all calculated for two different types of hydrocarbons. Each situation was calculated letting the time elapse half a second and the results are shown in Table 6-14.

Table 6-14: Modelled results for NO formation at charge surface

Phase	Mol NO/m^3 with CH$_4$	Mol NO/m^3 with CH$_3$
Primary	1.40E-04	4.69E-04
Intermediate	6.20E-04	7.81E-04
Secondary	1.85E-03	1.84E-03

Common for both models is the total consumption of O_2 early in the run, mainly because of the high amounts of CO. This is well in accordance with Arntsberg's measurements showing that close to the surface little free O_2 exist. The calculated results also show quite a difference between the two types of hydrocarbons used to describe volatile matters. Figure 6.34 shows the plot of the numbers in Table 6-14.
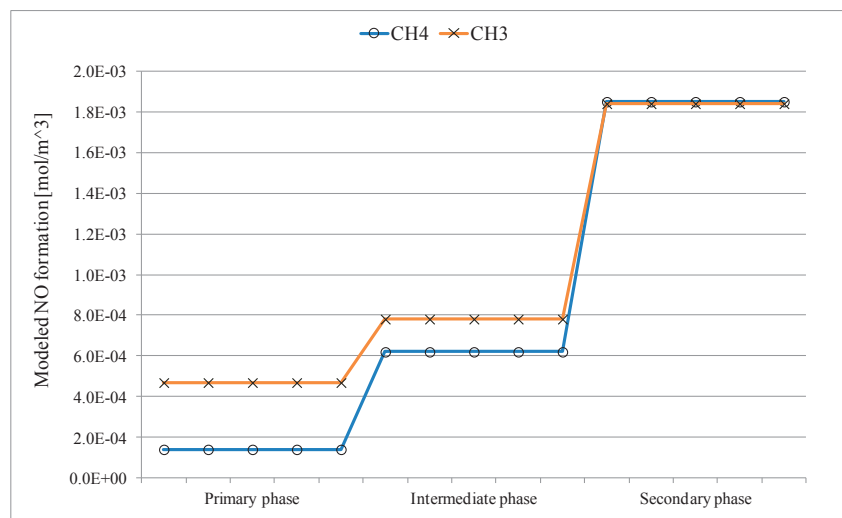
Figure 6.34: Modelled results for NO formation at surface combustion

Looking at Figure 6.32 and comparing the levels of NO formed in the primary and intermediate phases to the level formed in the secondary phase you get:

- Primary phase: NO formation in the area of 30 % of Secondary phase
- Intermediate phase: NO formation in the area 75-80 % of the Secondary phase

Looking at the numbers for CH$_3$ in Figure 6.34 they are surprisingly close to the measured results.

6.9.2 Modelling combustion in the tapping area

The situation in the tapping area is similar to the situation described in the Secondary combustion phase except the level of SiO and CO gas are equal since it is assumed they enter the area from the crater through the tap hole. This leads to a situation where the O_2 do not undergo complete consumption.

For the tapping combustion the temperature was held at a constant 1600 ºC and once again only the NO formation during the first 0.5 seconds after the gas has escaped from the furnace is modelled.

Table 6-15 show the six different levels of SiO/CO that were modelled.

Table 6-15: Initial model input to combustion in Tapping. All numbers in [mol/m³]

Case	SiO	CO	Volatiles	H₂O	O2	N2
A:	0.07	0.07	0	0.53	8.31	33.28
B:	0.15	0.15	0	0.53	8.31	33.28
C:	0.22	0.22	0	0.53	8.31	33.28
D:	0.29	0.29	0	0.53	8.31	33.28
E:	0.37	0.37	0	0.53	8.31	33.28
F	0.73	0.73	0	0.53	8.31	33.28
G	1.46	1.46	0	0.53	8.31	33.28

6.9.2.1 Results for combustion in the tapping

The results for the different tapping combustion cases are given in Table 6-16.

Table 6-16: Modelled results from the combustion in the tapping

Case	mol SiO2 formed	mol NO formed	mol NO/mol SiO2
A:	0.073	0.0132	18.02 %
B:	0.146	0.0131	8.99 %
C:	0.219	0.0131	5.98 %
D:	0.292	0.0131	4.48 %
E:	0.365	0.0131	3.57 %
F	0.731	0.0129	1.76 %
G	1.461	0.0125	0.85 %

The model gives a decreasing amount of NO formed as a function of SiO.

The reason for this could first of all be the lesser amounts of CO in the initial combustion mixture and the first reaction in the SiO combustion scheme by Jachimowski and McLain, given as $SiO + O + M \rightarrow SiO_2 + M$. Since several of the CO reactions in the GRI-Mech 3.0 mechanism release the O radical a high amount of free O radicals will exist at high CO levels, giving enough O to participate both in the

Zeldovich reactions and also in the mentioned SiO $\rightarrow$ SiO$_2$ reaction. With less CO released the competition for O radicals would be stronger, favouring the SiO combustion because of their reaction kinetic.

It is interesting to see that the relative formation of NO from the model follows the same pattern as in Figure 6.18, a curve closing in on a lower level of NO formed when the SiO$_2$ formation increases. Figure 6.35 presents the results of the different tapping situations.
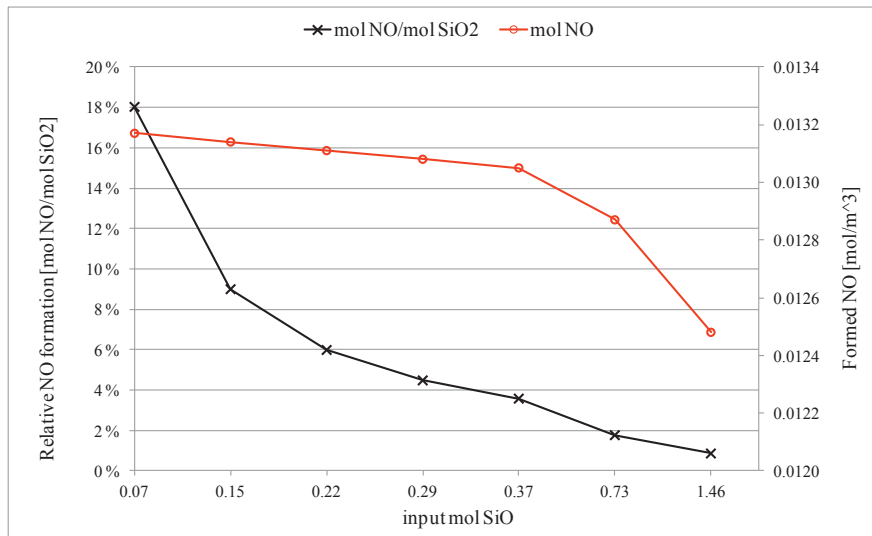
Figure 6.35: Model results from the tapping combustion

6.9.3 Consequence of modelling at constant temperature

The most significant weakness with the way the combustions are modelled is the assumption of a constant temperature. It is clear from earlier discussion in this chapter that the full reaction from SiO gas to solid fume releases a lot of energy to its surroundings. In this respect the modelled results are probably to low compared to if the complete energy situation was accounted for. Nevertheless since the constant temperature does not influence on the amount of SiO combusted it is plausible to believe that the observed differences between the cases would still be the same even though the overall temperature increases.

6.10 Concluding remarks

Emissions of NO_x in the form of NO and NO_2 are getting increasing attention because of their environmental and health related importance. Gaining more knowledge about the sources and formation mechanisms for NO in silicon production is vital for a targeted effort in reducing NO emissions since our measurements done at an industrial furnace show that NO emissions occur on a daily basis and are closely connected to process performances.

6.10.1　Combustion environments in the Silicon process

The formation of NO in the silicon process can be divided between the furnace surface and the tapping process. The combustion processes in these two places occurs under totally different conditions, in which it seems the NO formation can be influenced. While the combustion of the furnace gases at the furnace surface can be assumed to occur under the influence of volatile matters and water from the raw materials, the combustion in the tapping occurs under "cleaner" conditions since only air is mixed with the gas.

6.10.2　Measurements in the furnace off gas

Measurements of the off gas from the furnace show a similar behaviour in NO and silica fume formation. Calculations found that there is a connection between the two, but other formation mechanisms have to be operating to fully describe the NO emissions.

6.10.3　Measurements in the tapping off gas

Measurements of fumes and off gas during tapping of a silicon furnace found that there is a correlation between the levels of SiO_2 fumes generated and NO measured in the off gas. The main portion of the measured NO can be connected to work operations in draining the furnace for metal, but there are also other situations during tapping that apparently generates NO, though on a much smaller scale.

A statistical analysis of the data gives a good correlation between measured fume and measured NO up to a level of 150 ppm NO. The correlation has been used to predict NO formation based on datasets from other measurements and here the dynamics of the NO generation is captured, but the base level of NO formed is different from measurement to measurement. This is mainly believed to be caused by dilution of the off gas.

6.10.4　NO formation related to fume particle growth

Based on the measured fume concentration in the tapping off gas and the fume properties the growth time for the particles has been calculated. A stoichiometric combustion model for the furnace gases that escapes out of the tap hole has been established. Measured results for fume and NO have been calculated through this model

and the formation time of the measured NO is in the same order of magnitude as the growth time of the particles.

A Computational Fluid Dynamics (CFD) model which simulates a fume particle experiencing a combustion temperature profile has been established. Using the measured particle properties, the calculated growth time and the achieved stoichiometric temperature the CFD model show results in the NO formation in the same order of magnitude as the measurements.

Based on this it is therefore plausible that the combustion of SiO gas forming SiO_2 particles controls the formation of NO in the tapping area. This is supported by the CFD model results and the measurements which found that the amount of moles NO formed per fume particle is reasonable constant.

Based on the measurements done in the furnace and tapping off gas the relative NO formation as a function of silica fume is calculated. The results show that there are similarities in the formation behaviour supporting a universal formation mechanism connecting the two.

6.10.5 NO formation in the different combustion environments

The measurements found that the NO formation in connection to the fume formation behaves differently at the furnace surface compared to the tapping. While the formation in the tapping seems to occur instantly as the fume is formed, measurements at the furnace surface have a time difference between the fume and NO formation.

A detailed description of the conditions on the furnace surface during combustion has been established. This includes NO formation in three different steps, each characterized by having different content of SiO gas, volatiles and water. Comparing the described conditions with the measurements the time lag in NO formation could be explained.

6.10.6 Modelling of the combustion environments

Combustion of the three different furnace surface cases and several cases of SiO/CO gas mixtures in the tapping has been modelled using the GRI-Mech 3.0 chemical reaction scheme. The aim of this model was not to give the accurate level of NO in each case, but to show any differences between them and if the differences were in compliance with the assumed combustion description.

For the furnace surface environment the GRI-Mech 3.0 model has similar results to what has been measured and is assumed in our three step NO formation, while the results for the tapping combustion showed almost constant NO formation. The results for the relative NO formation as a function of fume in the tapping area is however in compliance with the results from the measurements.

Chapter 7   Pilot scale measurements of NO emissions from the silicon process

Earlier and recent industrial measurements in FeSi- and Si-metal furnaces reveal quite high NOx-emissions. The NOx is believed to be produced in the combustion zone above the furnace surface, mainly as thermal NOx.

In order to expand knowledge about NOx-formation in silicon metal production, a pilot scale experiment in a 440 kVA silicon furnace has been carried out. An experimental set-up was designed so that the formation conditions for NOx could be copied and manipulated by the control of air flowing into the combustion zone above the furnace surface.

All emissions in this experiment are measured and reported as NO, even though it after some time in nature it will react to NO_2.

7.1 The Pilot Scale Experiment

Based on the observations from the industrial measurements and the hypothesis that the NO generation is influenced by where the combusting furnace gases meet cold air a new off gas hood was built for a pilot scale silicon furnace. The hood was made with two adjustable rings containing holes, giving the possibility to control the height of the air inlet above the charge surface.

The sketch of the pilot scale furnace with the installed hood is shown in Figure 7.1.
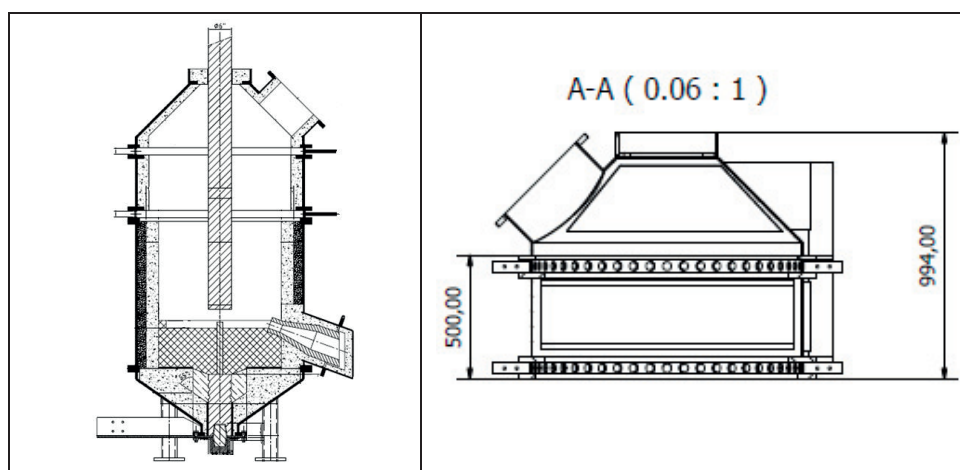
Figure 7.1: Pilot scale silicon furnace. Sketch to the right shows the hood only with the two rings for controlling the air inlet

Each ring had 50 holes with a diameter of 3.5 cm and was adjustable sideways, enabling the amount of inlet air to be reduced to a minimum if wanted. The rings were made in such that it was not possible to completely close the inlet of air, but when closing a ring the air inlet from that area was reduced to a minimum.

The following hypotheses were formulated for the pilot scale experiment:

- The supply of air (O_2/N_2) and air flow across the surface controls the amount of NO formed
- By changing the amount of air and where it is added to the combustion chamber, the amount of NO could be altered.

Figure 7.2 show a picture of the pilot scale furnace with the new hood installed. In the centre of the furnace is the electrode and to the right the off gas channel. The tap hole is located at the bottom directly below the off gas channel.

Figure 7.2: Pilot scale furnace with new hood

The placement of the lower ring is approximately 15 cm above the expected charge surface and the upper ring approximately 65 cm above the expected charge surface.

In addition, the hood is equipped with four hatches, two and two placed symmetrically on each side of the furnace for the stoking and charging of new raw materials.

7.2 Operational setup

The theory behind the silicon process is thoroughly described in Chapter 2 so it is unnecessary to go into details in this section, but only state that the furnace experiment was designed to slowly increase the silicon yield through an increased amount of Fix Carbon added to the raw material mixture.

In addition to the coke as a Fix Carbon source the charge mixture consisted of quartz and wood chips. All materials were dried for at least 48 hours at 100 ºC to minimize the amount of moisture entering the furnace.

The plan for this experiment was to operate the furnace as similarly as possible as previous pilot scale experiments (Myrhaug and Monsen 2002), only adjusted for an increased furnace diameter and a new AC power supply.

7.2.1 Electrical parameters

Since testing the new AC power supply was one of the targets, the decision was made to try to run the furnace at a high output. The aim for the experiment was 160 kW with a current of 4 kA and a voltage of 40 V. Figure 7.3 shows a plot of the furnace effect for the entire experiment.
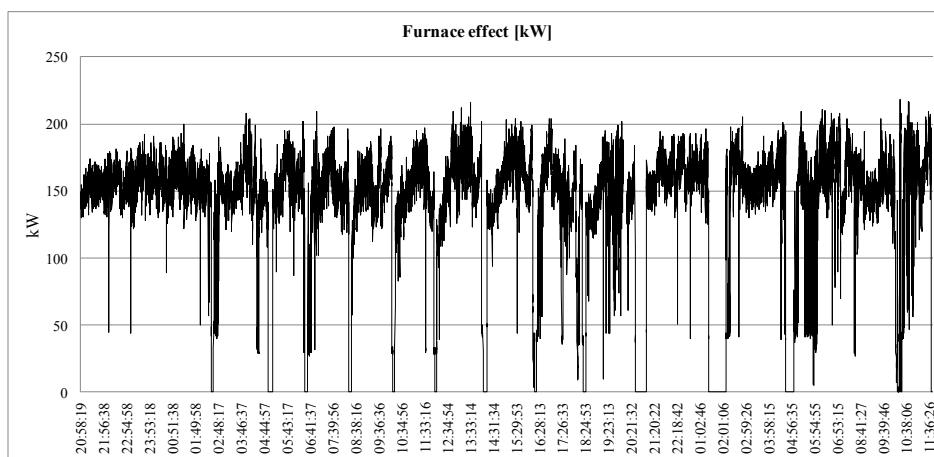
Figure 7.3: Furnace effect for the entire experiment

Each drop in furnace effect to zero is connected to a tapping of silicon metal. This was performed approximately every 250 kWh and for safety reasons the power was shut off.

7.2.2 Stoking and charging

After each tapping any build up crust in the furnace was stoked down and the power turned on again. After the power was switched on the furnace was rapidly charged with new raw material up to ¾-level then gradually refilled up to normal level (about 15-20 cm from upper pot edge). There was no stoking done during each run. If there were cases of heavy gas channelling or sinks in the raw materials some fresh charge materials were added to these areas. Figure 7.4 shows the crust that has built up inside the furnace during one run. This crust was stoked down before continuing on the next run.

Figure 7.4: Furnace after tapping

Figure 7.5 shows the furnace surface after the power was turned back on again and the initial charge materials have been added. After this the level of charge materials was slowly raised to the required level.

Figure 7.5: Furnace surface right after initial charging

7.3 Measurement setup

7.3.1 Off gas system

During the experiment the off gas temperature, flow and chemical content was measured. Figure 7.6 shows a sketch of the furnace and connecting off gas system. The measurement locations for the off gas temperature, flow measurement and chemical analysis are also shown.
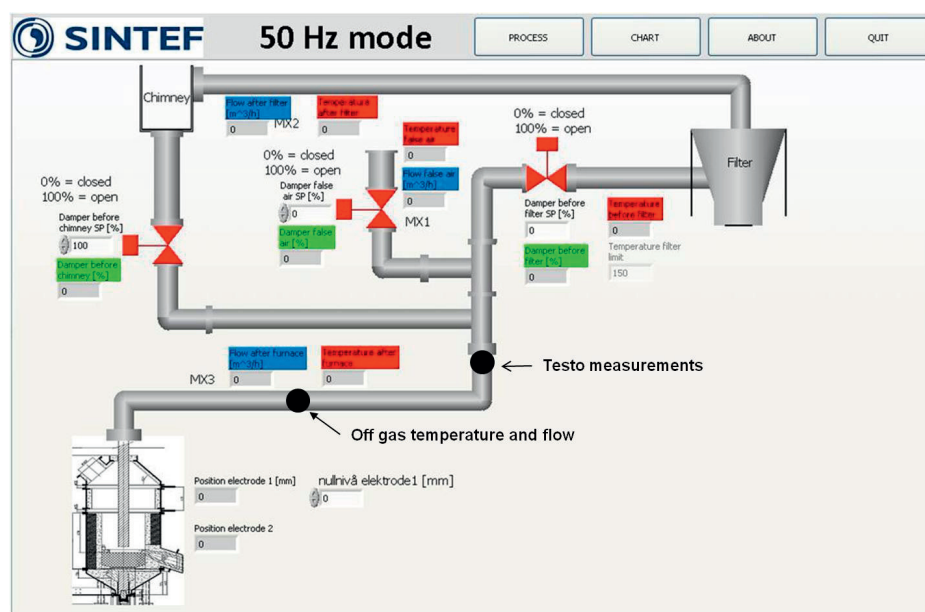
Figure 7.6: Off gas measurement setup

7.3.2 Ring set up

The main objective of the experiment was to investigate whether there is a difference in the NO formation when the air flow is added close to the surface, compared to higher up in the hood. To gain a representative data set and avoid that short time variations influenced the results too much the experimental setup was to keep the chosen ring configuration constant through each run. At the end of the experiment other ring constellations were tested, like "both closed" and "one closed - one ½ way open". These extra trials where kept for minimum 10 minutes and repeated at least four times.

In total there were six different ring set ups with data available:

- Both rings open
- Top ring open/bottom ring closed
- Top ring closed/ bottom ring ½ way open

- Both rings closed
- Top ring closed/bottom ring open
- Top ring ½ way open/bottom ring closed

7.4 Results from the experiment

7.4.1 Process results

The total operation time with charge materials was 44 hours, producing at an average silicon yield of 62 %.

The furnace was tapped 13 times, giving a total of 92 kg of silicon.

Figure 7.7 shows the development in kWh/kg silicon and tapped silicon during the experiment.
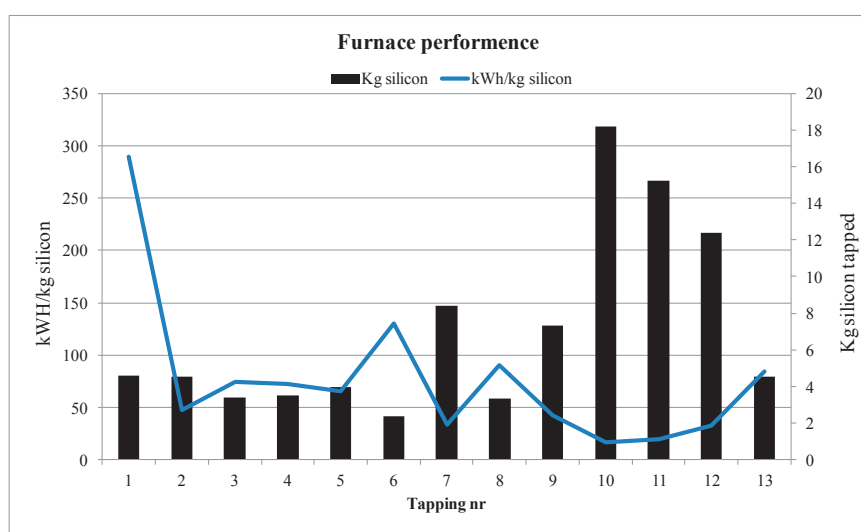
Figure 7.7: Furnace performance during experiment

7.4.2 NO measurements

To measure the NO content in the furnace off gas a TESTO 350XL (TESTO) was used. The TESTO 350XL measures both NO and NO_2 and in the data output both could be reported in addition to the sum of them. The main constituent of the two is the NO, while the measured level of NO_2 is in the area of 2.5 % of the measured NO.

Focusing on the NO measurement an electrochemical measuring cell for NO with accuracy of "*< 2 ppm*" in the range [0-39.9] ppm and "*5 % of measured value*" for measurements between 40 and 300 ppm was used.

Because of very high levels of NO in the evening of 5 May the electrochemical cell was changed to a cell with an accuracy of *"< 5 ppm*" in the area of [0-100 ppm], "*5% of measured value*" in the range [100-2000] ppm and "*10 % of measured value*" between

2001-3000 ppm. This cell with lower accuracy was only used between 00:28 and 07:28 on 6 May.

In addition to the NO/NO_2 the TESTO350XL also measures temperature and other gas components like CO and CO_2.

Figure 7.8 gives the NO measurements for the entire experiment.
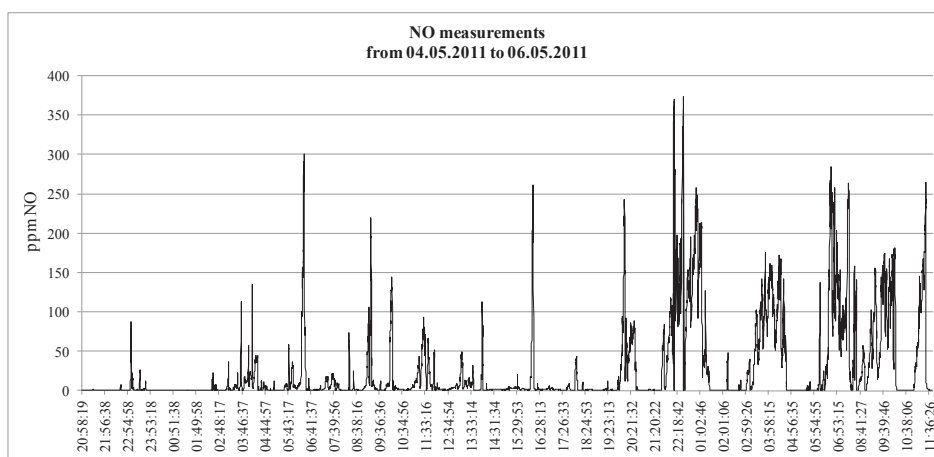
Figure 7.8: NO measurements for the entire experiment

As seen from Figure 7.8 there are several peaks in NO during the first hours of the experiment. Looking at the enhanced plots of the NO formation given in Figure 7.9 to Figure 7.11 and comparing with the tables of registered events at the furnace (see text boxes in Figure 7.9 to Figure 7.11) many of the peaks can be explained by "blows", meaning that gas channels formed in the charge lets crater gas flow to the surface and combust. In these situations a small amount of fresh raw materials was placed on top of the "blow" to physically block the gas flow.

The general low NO formation in the beginning of the trial could be explained by assuming that the chemical reactions in the furnace are still at an initial stage.

One time period is unique in that way that during this run there was no new raw materials added to the furnace. In this time period, 5 May from 21:44 to 01:01, the NO formation is very high.

As the furnace process tends to stabilize the level of NO increases and the behaviour of the NO emission cycles is similar from run to run.

 Figure 7.9 to Figure 7.11 also show the NO results with the chosen ring configuration plotted, a value of 10 meaning that the ring is open, 0 meaning half way open and -10 meaning that the ring is closed.
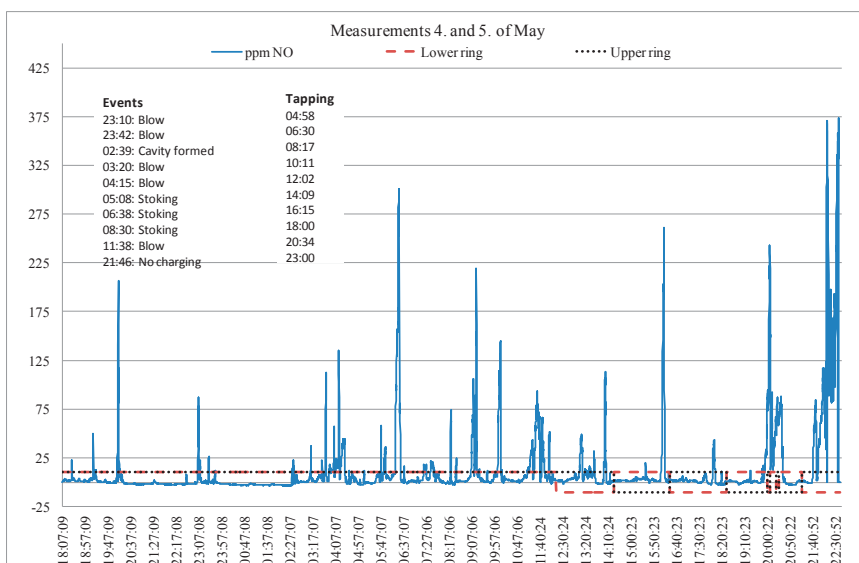
Figure 7.9: Measurements 4 and 5 May (Ring value of 10: open, 0: half open, -10: closed)
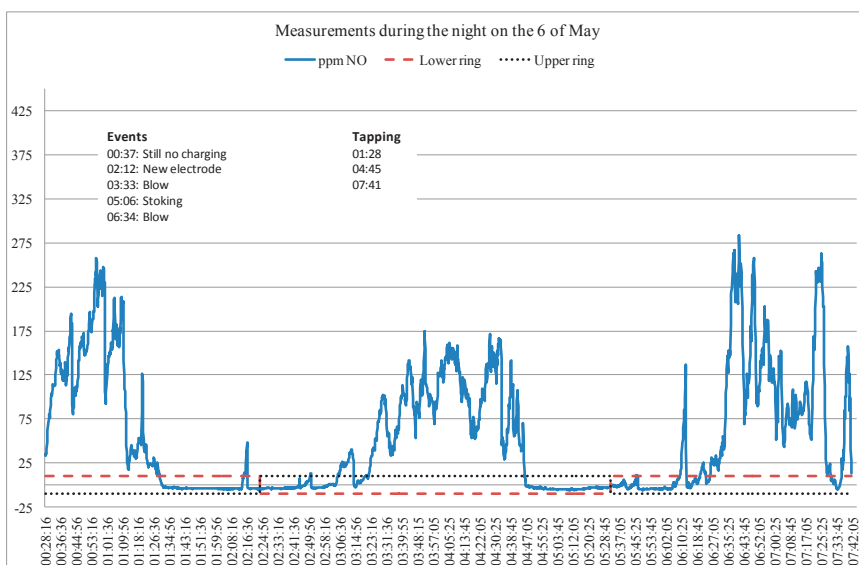
Figure 7.10: Measurements during the night of 6 May (Ring value of 10: open, 0: half open, -10: closed)

113
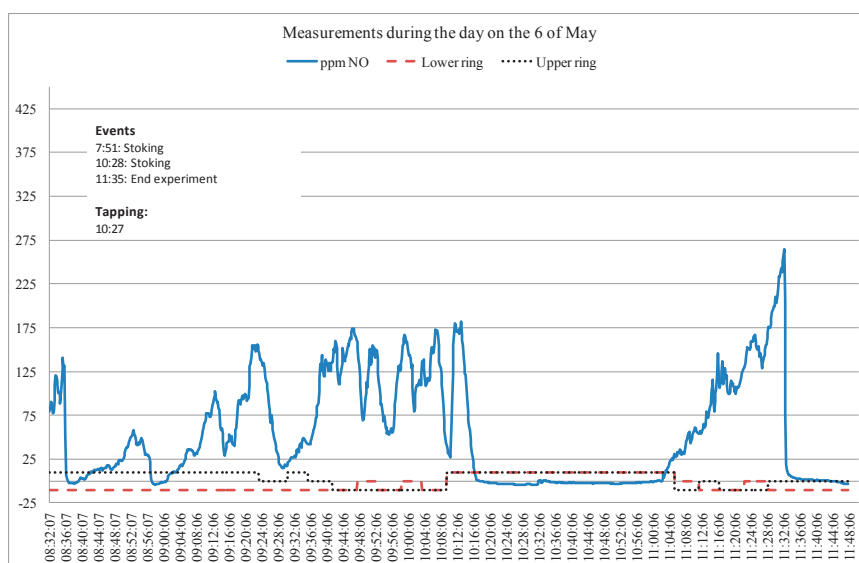
Figure 7.11: Measurements from the morning 6 May and up until end experiment (Ring value of 10: open, 0: half open, -10: closed)

When looking at the more detailed plots of the NO formation the variation on a short term basis is substantial.

7.4.3 Summarized results

In analysing the results for the different ring constellations two limitations have been done. First of all the data for the run on the evening of 5 May have been removed due to the fact that during this run no raw materials were added to the furnace. In that respect it was not representative for a normal furnace operation and should be excluded.

Second, since only data connected to running the furnace was wanted and the electric power was shut off during tapping, any data registered at electric effect below 130 kW was also removed from the final dataset.

Using the measured off gas amount and temperature the amounts of NO were recalculated from ppm to grams/hour. Table 7.1 and Figure 7.12 below show the summarized results for all six ring configurations in addition to the temperature, off gas amount, electric effect and CO concentration and in the off gas.

Unfortunately the chosen method for collecting the amount of fumes formed for each run failed so therefore the correlation between the NO and fume could not be shown for the pilot scale measurements.

Table 7-1: Measured emissions sorted on ring configuration

Ring position	Temp °C	Nm³/h	kW	Gram NO/h	Gram CO/h
Both rings open	83	3540	163	47	98
Top ring open/ bottom ring closed	91	2768	158	144	155
Top ring closed/ bottom ring open	93	2692	158	166	231
Top ring ½ way open/ bottom ring closed	97	3165	168	299	119
Top ring closed/ bottom ring ½ way open	107	2885	165	414	86
Both rings closed	107	2698	154	426	101

In Figure 7.12 the numbers from Table 1 have been arranged so that the two "pairs of similar" configurations having air coming in high or low in the hood can be compared. For both pairs the configuration that has the air flow close to the charge surface produces more NO.
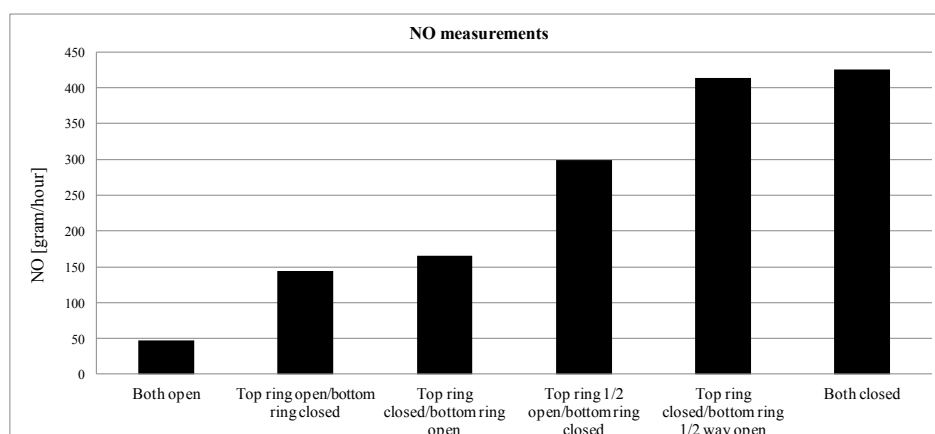
Figure 7.12: Calculated NO emissions for the different ring configurations

Both the level of NO and the difference between the ring constellations are surprisingly high. Particularly interesting are the results showing that the NO level rise with a decreasing amount of air let into the furnace. This shows the ability to form NO even with a low supply of N_2 and O_2.

One explanation to this might be that at a low inflow of air the overall velocity field through the hood is reduced, forming "hot spots" of air heated by the SiO combustion and still containing enough N_2 and O_2 to form NO. In that respect the velocity fields inside the hood will have a substantial effect on the NO formation.

After the experiment the furnace was cooled down and filled with epoxy. When the epoxy had hardened the furnace was sawed in two along the centre line, splitting the furnace in two equal parts. Figure 7.13 illustrates one of the two halves.
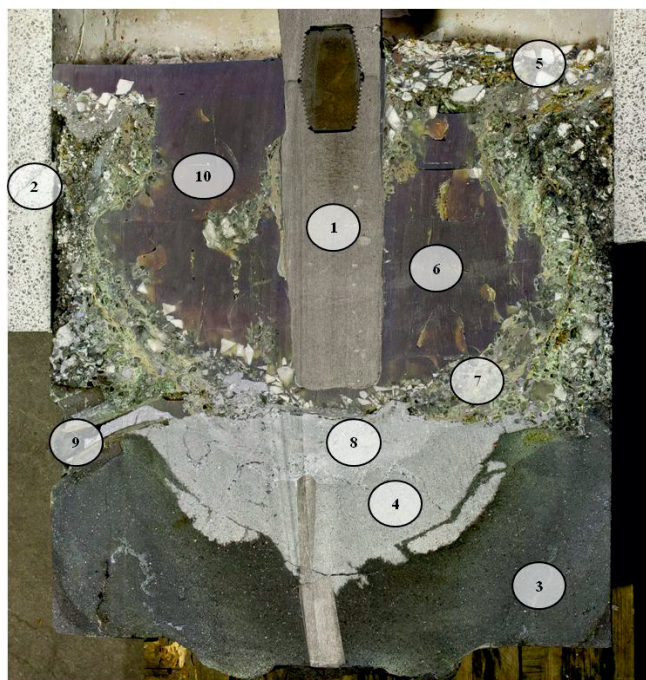
Figure 7.13: Cut plane of the pilot furnace

The different areas marked with numbers in Figure 7.13 are as follows:

Electrode

- ① Furnace lining
- ② Carbon paste bottom
- ③ Carbon paste soaked with silicon metal
- ④ Unreacted charge materials
- ⑤ Cavity
- ⑥ Half melted/reacted charge materials
- ⑦ Pool of silicon metal
- ⑧ Tap hole
- ⑨ Area where the top crust has collapsed

The picture of the furnace shows that there is a pool of metal directly underneath the electrode. If this picture describes a situation that has evolved from the start of the experiments this would mean that liquid silicon metal has been exposed to both melted

quartz and the burning arc over time. Both these situations would give an increased gas production in the form of more SiO gas. Since the furnace is very shallow it is plausible that any excess SiO would flow to the surface and combust to silica fumes, releasing energy that could lead to a higher NO production. In that respect the pool of silicon metal underneath the electrode could explain the general high level of NO during the last parts of the experiment.

7.5 CFD Simulations of the pilot scale furnace

In order to understand more of the NO results from the pilot experiment a computational fluid dynamics (CFD) model over the upper area of the furnace was made. The aim of the model was primarily to investigate the flow fields and temperature conditions inside the hoods for the two main ring configurations, "upper ring closed/lower ring open" and "upper ring open/lower ring closed".

7.5.1 The model

To begin with a 2D model of an imagined cutplane just beside the electrode was simulated, in this way the electrode itself was not a part of the model. Figure 7.14 shows the chosen CFD simulation domain. The shown boundary conditions were used on the opposite side of the furnace as well.
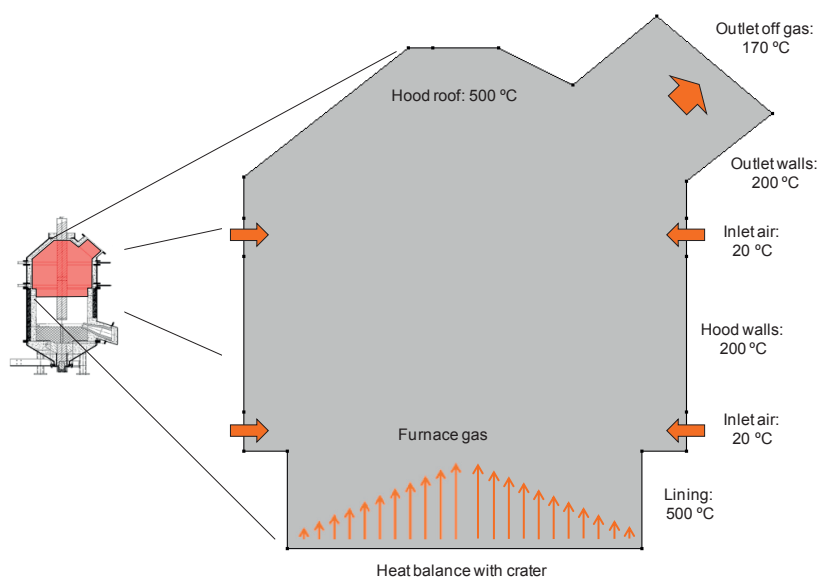
Figure 7.14: Pilot furnace simulation domain and boundary conditions

The inlet velocity for the air through the rings was measured at full off gas suction and used as a boundary condition in the model. For the outlet the chosen boundary condition was a pressure of 1 atmosphere and no viscous forces. As described earlier the set ups

with one ring closed did not mean that the air flow through that ring was totally cut off but the construction of the rings did give some leakage of air into the furnace. To account for this the other ring than the one that was open was given an inflow of air at a velocity of 1 m/s.

The temperature boundary conditions for the hood are all guessed except the charge surface temperature which was solved with an energy balance described below.

To solve the velocity and temperature fields for the chosen domain the software package COMSOL Multiphysics (Comsol 2010) with a Reynolds-averaged Navier–Stokes (RANS) based k-ε turbulence model and heat transfer in fluids was used. When solving the k-ε model streamline and crosswind diffusion as well as isotropic diffusion was used for both the Navier-Stokes equations and for the turbulence equations.

The flow was treated as compressible with a Mach number < 0.3. For the heat transfer in fluids the ingoing air was treated as an ideal gas with a density of 1.23 [kg/m^3] and a dynamic viscosity of 1.79e-5[Pa*s]. Assuming a more or less constant pressure for the entire domain a heat capacity (Cp) of 1005 [J/Kg*K] and a thermal conductivity of 0.024 [W/m*K] was used.

7.5.2 Adding SiO combustion

As in a full scale silicon furnace excess SiO from the process will flow to the surface and combust to silica fume, assumed to be the source of energy generating the NO formed inside the combustion chamber. The combustion of SiO to SiO_2 could as described in Chapter 6 consist of several steps, including both gaseous reactions and condensation of liquid particles and by evaluating the kinetics in the combustion with O_2 given by Jachimowski and McLain (Jachimowski and McLain 1983) it is clear that in addition to having a high reaction rate the combustion also includes the active radical O. Since the NO formation is much slower one might assume that the only thing influencing the NO formation would be the energy released from the SiO combustion and that the SiO combustion occurs at or right inside the charge surface.

To add the energy from the SiO combustion and to deal with the fact that estimating the charge surface temperature is difficult the situation was simplified by letting the boundary condition for the charge surface be determined by an energy balance. The Heat Transfer module in COMSOL contains a boundary condition named "Inflow Heat Flux" used for situations where one needs to add energy to a single boundary and in addition do not know the temperature at that specific boundary. Instead it was assumed that the crater temperature inside the furnace was fixed at 1400 ºC and that the temperature at the surface was determined by the energy balance between the crater and the combustion chamber, taking into account the energy fed to the surface. To calculate the amount of energy from the SiO combustion the experiments obtained silicon yield

was used, assuming that no silicon was accumulated in the system in the steady state situation.

7.5.3 Model results

Figure 7.15 gives the stationary solutions for the flow and temperature fields in the 2D models. The surface describes the temperature in centigrade while the arrows and streamlines describe the velocity field strength and directions.
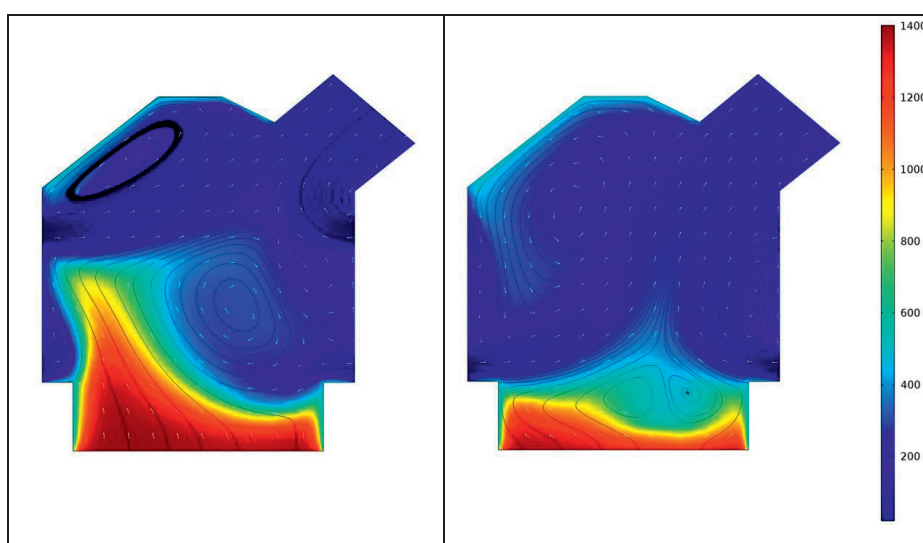
Figure 7.15: 2D model results for both ring configurations (left: lower upper open, right: lower ring open)

Looking at Figure 7.15 the flow fields are quite different but the maximum obtained temperature situation for the two cases is close to each other. Also the leakage of air seems to have a sideways effect low in the furnace in the situations with the upper rings fully open.

From a NO formation point of view the results show what was suspected when investigating the experimental results. Changing the height of the inlet air changes the flow fields inside the hood substantially and could in that way create "hot spots" of stagnant air/gas reaching very high temperatures. These hot spots will probably form NO if there is sufficient O_2 and N_2 available.

7.5.4 Expanding to 3D

Expanding the models to 3D and only looking at the flow fields from the bottom and the two rings the results are presented in Figure 7.16. To distinguish the flows of inlet air, leakage and furnaces gases each have been given a different colour. Black indicates the main inlet flow, yellow the leakage of air and red the flow of the gas rising from the furnace surface.
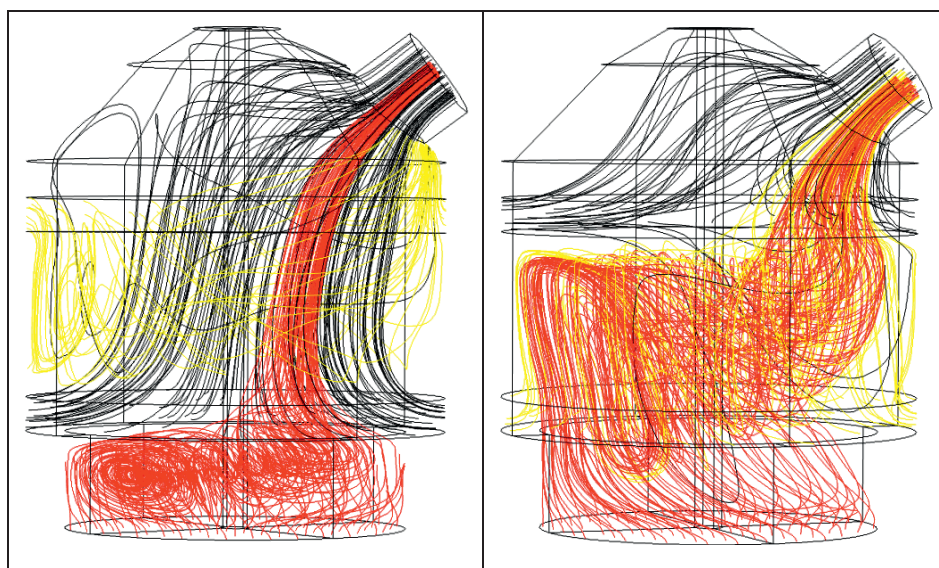
Figure 7.16: 3D model results for flow fields (left: lower ring open, right: upper ring open)

Comparing the two it is clear that the solution with the lower ring open could create an area close to the surface with accumulating hot gases and thereby give areas with high temperatures or "hot spots" forming NO.

Even though the modelled results with air leakage corresponds with what was suspected based on the pilot scale experiments, it is important to remember that a CFD model does not necessary describe the real situation but only the mathematical solution to whatever is put in as conditions and criteria. In that respect the model could be used to advise the user about what could be expected to happen if changes are made in a system. Bearing this in mind and according to the model inputs that was given it seems evident that small changes in the flow field inside the combustion chamber could have substantial consequences for NO formation.

7.6 Concluding remarks

A pilot scale experiment of the silicon process has been conducted to investigate the hypotheses that:

- The supply of air (O_2/N_2) and air flow across the surface controls the amount of NO formed
- By changing the amount of air and where it is added into the combustion chamber, the amount of NO could be altered.

To ensure satisfactory off gas collection and accurate results a new furnace hood with the possibility to control the height of the ingoing air was built. The hood was installed with two sets of rings which could be opened and closed. In this way it was possible to let the air into the combustion chamber above the charge either close to the surface or higher up.

Based on the data from this experiment the following can be concluded for the pilot scale silicon furnace experiment:

- Having the inlet of air close to the charge surface produces more NO than moving it higher towards the off gas channel.
- Decreasing the amount of air into the combustion chamber increases the amount of NO produced.
- Based on the results there is reason to believe that the velocity fields inside the hood influence NO formation significantly.

A computational fluid dynamics model of the pilot scale furnace shows that the results from the furnace trial could be caused by the velocity fields inside the hood. Both the 2D and the 3D models found areas inside the hood with possibilities in accumulating hot gases.

After the experiment was finished the furnace was cooled down and filled with epoxy. When the epoxy had hardened the furnace was sawn in two, showing the conditions around the electrode when closing down the furnace. Evaluating the two pieces a pool of liquid metal was found directly underneath the electrode. Given that this pool of metal has been there for longer time periods this could be an extra source of SiO gas. The combustion of this extra SiO to silica fumes at the furnace surface could explain the high levels of NO.

Understanding the mechanisms in NO formation connected to the silicon process is of vital importance for the work in reducing emissions. In that respect this experiment found that the NO emissions could be influenced by the air inlet design in the off gas system. A better understanding of the connection between the velocity fields above the furnace surface and the NO formation is needed to be able to enforce effective emission reducing measures.

References

K. Almås, H. K. Delbeck, T. Halland, H. Rong and H. Tveit (2002). "Improved Environmental and Energy Recovery Performance with New Furnace Hood Design at Elkem Thamshavn". Silicon for the Chemical Industry VI, Loen, Norway

A. E. Arntsberg (2004) "Transportprosesser og forbrenning av CO og sot i ovnshette og avgasskanal for Si og FeSi-ovner" SINTEF STF80 FO4011

J. A. Bakken (1993). "Metallurgiteknikk II. Compendium in Metallurgical Transfer Processes ", Institute of Metallurgy, Norwegian Institute of Technology.

P. Balram, S. Andersson and H. Midtdal (2011). "Effect of SiO Combustion on NOx Emission; Theory and Validation". 8th International Conference on CFD in Oil & Gas, Metallurgical and Process Industries, Trondheim, Norway, SINTEF/Norwegian University of Science and Technology.

A. Bhargava, M. Colket, W. Sowa, K. Casleton and D. Maloney (2000). "An Experimental and Modeling Study of Humid Air Premixed Flames." Journal of Engineering for Gas Turbines and Power Vol. 122.

P. Bireswar and D. Amitava (2008). "Burner Development for the Reduction of NOx Emissions from Coal Fired Electric Utilities." Recent Patents on Mechanical Engineering 1: 175-189.

C. T. Bowman, R. K. Hanson, D. F. Davidson, G. J. W.C, V. Lissianski, G. P. Smith, D. M. Golden, M. Frenklach and M. Goldenberg. "GRI-Mech 2.11." from http://www.me.berkeley.edu/gri_mech/.

J. A. Britten, J. Tong and C. K. Westbrook (1990). "A NUMERICAL STUDY OF SILANE COMBUSTION". Twenty-Third Symposium (International) on Combustion, The Combustion Institute.

H. K. Chagger, D. Hainsworth, P. M. Patterson, M. Pourkashanian and A. Williams (1996). "THE FORMATION OF SiO2 FROM HEXAMETHYLDISILOXANE COMBUSTION IN COUNTERFLOW METHANE-AIR FLAMES". Twenty-Sixth Symposium (International) on Combustion, The Combustion Institute.

Comsol (2010) "Comsol Multiphysics" www.comsol.com

N. De Nevers (2000). "Air pollution control engineering". Boston, McGraw-Hill. ISBN 0-07-039367-2

EEA. (2009). "NEC Directive status report 2009." from http://www.eea.europa.eu/publications/nec-directive-status-report-2009.

Elkem (2009) Personal communication with maintenance department at Elkem Salten

Endress & Hauser. (2009). "Supplier of measuring instruments and automation solutions for the industrial process engineering industry." from www.endress.com.

Energy Information Administration. (2009). "International Energy Outlook 2009." from http://www.setav.org/ups/dosya/25025.pdf.

ENOVA (2009) "Potensialstudie for utnyttelse av spillvarme fra norsk industri" Oslo, Norway

FUME (2009). "Fugitive Emissions of Materials and Energy - Application form", The Research Council of Norway, Oslo, Norway.

T. Furuhata, T. Kawata, N. Mizukoshi and M. Arai (2010). "Effect of steam addition pathways on NO reduction characteristics in a can-type spray combustor." Fuel(nr. 89): p. 3119–3126.

S. Grådahl, S. Johansen, B. Ravary, B. Andresen and H. Tveit (2007). "Reduction of emissions from ferroalloy furnaces". INFACON XI, New Dehli, India.

S. Grådahl, S. T. Johansen, G. Nubdal, B. Ravary, J. C. Laclau, T. Vassbotn and L. R. Hellevik (2000) "Miljø og ovnsprosesser. Del III" SINTEF STF24 F00600

H. Guo, W. Stuart Neill and G. J. Smallwood (2008). "A Numerical Study on the Effect of Water Addition on NO Formation in Counterflow CH4/Air Premixed Flames." Journal of Engineering for Gas Turbines and Power Vol. 130.

C. J. Jachimowski and A. G. McLain (1983) "A Chemical Kinetic Mechanism for the Ignition of Silane/Hydrogen Mixtures" NASA Technical Paper 2129

S. T. Johansen, H. Tveit, S. Grådahl, A. Valderhaug and J. Å. Byberg (1998). "Environmental aspects of Ferro-Silicon furnace operations - an investigation of waste gas dynamics". INFACON 8, Beijing, China.

H. L. Johnsen (2009). "Lung function, respiratory symptoms, and occupational exposure". Thesis for the degree of Ph.D, Faculty of Medicine, University of Oslo

M. Kadkhodabeigi (2011). "Modeling of Tapping Processes in Submerged Arc Furnaces". Thesis for the degree of Ph.D, Norwegian University of Science and Technology

M. Kadkhodabeigi, H. Tveit and K. H. Berget (2010). "SILICON PROCESS - NEW HOOD DESIGN FOR TAPPING GAS COLLECTION". INFACON XII, Helsinki, Finland.

KIMO Instruments. (2011). "KIMO AMI 300 Multifunction." from http://www.kimo.fr/produits/265/ami_300.html?lang=en.

Kjelforeningen-Norsk Energi and Institutt for energiteknikk (2002) "Potensialer for mer miljøeffektiv energibruk og produksjon i norsk prosessindustri" Oslo, Norway

KLIF. (2010). "Norske Utslipp." from www.norskeutslipp.no.

L. Kolbeinsen (1984) "Communication to Elkem A/S from the Department of Metallurgy, SINTEF" Report STF34 F84076

Minitab® (2007) "Minitab® Statistical Software." www.minitab.com

T. Miyauchi, Y. Mori and T. Yamaguchi (1981). "EFFECT OF STEAM ADDITION ON NO FORMATION". Eighteenth Symposium (International) on Combustion, The Combustion Institute.

MOLAB (2011) "Arbeidsmiljømålinger Totalstøv. Report for Elkem Salten"

K. Motzfeldt (1961) "An Evaluation of the Chemistry of the Production of Ferrosilicon with Special Aim at the Possibilities of Increasing the Silicon Recovery (in norwegian)" Report for Elkem from the Inst. of Silicate Science/Inst. of Inorganic Chemistry, Norwegian Institute of Technology, Trondheim, Norway

K. Motzfeldt and M. Steinmo (1972). "Kinetics of the reaction between carbon and refractory oxides". Third Nordic High Temperature Symposium, Atomic Energy Commission Research Establishment, Risø, Denmark, Polyteknisk Forlag.

E. H. Myrhaug (2003). "Non-fossil reduction materials in the silicon process - properties and behavior". Thesis for the degree of Dr.ing, Norwegian University of Science and Technology

E. H. Myrhaug and B. Monsen (2002) "Silisium smelteforsøk i 150 kW pilotovn høsten 2001" SINTEF STF24 F02521

NEO. (2009). "DM4 Open Path Dust Monitor." from http://www.neomonitors.com/.

NEO. (2009). "LaserDust MP and LaserGas II SP." from http://www.neomonitors.com/.

NEO (2011) Personal communication regarding measurement principles and accuracy

Norwegian Labour Inspection Authority (2009). "Veiledning om administrative normer for forurensning i arbeidsatmosfære".

M. K. Næss, G. M. Tranell, J. E. Olsen and N. E. Kamfjord (2012) "Mechanisms and Kinetics of Liquid Silicon Oxidation During Industrial Refining." Oxidation of Metals, Springer Netherlands. DOI: 10.1007/s11085-012-9303-9.

PROMILJØ, The Research Council of Norway, Oslo, Norway.

Roine, Lamberg, Björklund and Kentala (2007) "HSC 6.12" http://www.outotec.com

Roine, Lamberg, Björklund and Kentala (2011) "HSC 7.14" http://www.outotec.com

A. Roine, P. Lamberg, J. Mansikka-aho, P. Björklund, J.-P. Kentala and T. Talonen (2010) "HSC Sim" http://www.outotec.com

A. Schei and S. A. Halvorsen (1991). "A stochiometric Model of the Silicon Process". Ketil Motzfeldt Symposium, Institute of Inorganic Chemistry, The Technical University of Norway.

A. Schei, J. K. Tuset and H. Tveit (1998). "Production of High Silicon Alloys". Trondheim, Norway, Tapir Forlag. ISBN 85-519-1317-9

G. P. Smith, D. M. Golden, M. Frenklach, N. W. Moriarty, B. Eiteneer, M. Goldenberg, Thomas Bowman, R. K. Hanson, S. Song, W. C. Gardiner Jr., V. V. Lissianski and Z. Qin. "GRI-Mech 3.0." from http://www.me.berkeley.edu/gri_mech/.

E. Takasuka, E. Tokizaki, K. Terashima and S. Kimura (1997). "Emissivity of liquid silicon in visible and infrared regions." Journal of Applied Physics 81(9): 6384-6389.

M. Takla (2009) "An investigation of the opportunity to recover radiation waste heat by the means of thermoelectricity" Department of Chemistry, Norwegian University of Science and Technology

TESTO. "Testo 350XL Portable Combustion Analyzer Specifications." from www.cleanair.com.

S. R. Turns (2000). "An Introduction to Combustion: Concepts and Applications - 2nd ed.", McGraw-Hill Science Engineering. ISBN 0-07-230096-5

H. Tveit, M. Garcia, H. Delbeck, A. T. Haug, B. Saugestad and I. J. Eikeland (2008). "Water leakages in ferroalloy and silicon reduction furnaces - experience gained from a severe accident in 2006". Silicon for the Chemical and Solar Industry IX.

H. Tveit, E. H. Myrhaug and I. J. Eikeland (2008) Personal communication: Sources for diffusive emission in silicon production

G. D. Ulrich (1971). "Theory of Particle Formation and Growth in Oxide Synthesis Flames." Combustion Science and Technology 4(1): 47 — 57.

UNECE. (1999). "The 1999 Gothenburg Protocol to Abate Acidification, Eutrophication and Ground-level Ozone." from http://live.unece.org/env/lrtap/multi_h1.html.

WHO. (2003). "Health Aspects of Air Pollution with Particulate Matter, Ozone and Nitrogen Dioxide." from http://www.euro.who.int/__data/assets/pdf_file/0005/112199/E79097.pdf.

WHO. (2005). "Air quality guidelines for particulate matter, ozone, nitrogen dioxide and sulfur dioxideGlobal update 2005 Summary of risk assessment." from http://whqlibdoc.who.int/hq/2006/WHO_SDE_PHE_OEH_06.02_eng.pdf.

J. B. Zeldovich (1946). "Oxydation of Nitrogen in Combustion and Explotion." Comptes Rendus (Doklady) de L'Acadèmie des Sciences de l'URSS LI(3): 217-220.

Appendix A - Sample preparation guidance from LabNett

DET NORSKE VERITAS

Heavy metal analysis of raw materials for the ferro-alloy industry.
Guidance on submission of samples

Raw material samples should be sent from each FeSi and Si-plant to LabNett Telemark for analysis of trace elements according to the specified list.

The samples delivered must be as representativ as possible for the raw material.

Nr.	Task	Guidance
1	Raw materials	According to list
2	Analysis program	Hg, As, Cd, Cr, Cu, Pb, Zn og Ni. In addition: Ba, Be, Co, Mo, Ni, Sb, Se, Sr, Tl, V.
3	Sampling	Each sample must be representative for that specific raw material, preferably on a yearly basis.
4	Drying	Samples dried at max. 105 ° C.
5	Sample size	50 grams. LabNett will archive the remaing sample for two years.
6	Contamination	Avoid crushers/mills made from alloyed steel. Mills made with wolfram carbide are preferable if possible.
7	Size reduction/crushing	Crushed to approximately 100 μm (size not so critical).
8	Carbon materials	Prebaked electrodes, coke, coal and char coal <u>not</u> to be reduced to ash.
9	Electrode paste	Crushed if possible
10	Woodchips	Wood chips are not to be heated. Preferred size < 5 mm, cut by knife.
11	Metallic iron	Preferably as chips, like bore chips
12	Use of packaging	New, clean and tight packaging. Plastic or paper bags.
13	Sample ID	Each sample tagged with <u>Type</u>, <u>Serialnr</u>, <u>date in DDMMYY</u> and <u>plant id</u>. See list
14	Adress	LabNett, Rødmyrlia 14, N-3740 Skien, Norway. Contact: Marianne Hansen. Tlf. 98 26 75 73. Fax 35 50 56 20. E-mail: <u>marianne.hansen@labnett.com</u>
15	Order and Invoice	As defined by customer
16	Dead lines for analysis	Samples shipped within January 10. Results ready by Februar 1-10.
17	Other information	

- o0o -

Appendix B – Testo 350 XL Specification

CleanAir.

CleanAir Instrument Rental
500 W. Wood Street
Palatine, IL 60067-4975
800-553-5511
www.cleanair.com

Testo 350XL Portable Combustion Analyzer

The 350XL Includes:

* 350XL Analyzer
* 454 Control Unit
* Extra Printer Paper
* Probe and Umbilical
* Shoulder Strap
* Spare Filters
* Power Cord
* Data Cable
* Comsoft 3 Software
* Manual (CD ROM & Print)
* Instrument Rental Shipping Carton

Specifications:

* Approximate Shipping Weight: 30 lbs.
* Dimensions: 16" x 11" x 4" (actual)
* Probe: Standard size 15" length (1000°C max temp), 8mm external diameter, 5mm internal, w/90" umbilical (longer probes and umbilicals may be available)
* Detection Method: Electrochemical Sensors for O2, CO, SO2 , NO, NO2, H2S, CO2 calculated unless the infrared CO2 cell is , CxHy- pellistor
* Electrical requirements: 110-230, 90-260V, or rechargeable battery
* Battery Life: Analyzer Box is NiMH 2-3 hrs, Control Unit is 4AA batteries 8 hrs
* Operating Temperature: -20 to +115°F
* Material: ABS
* Memory: 250,000 readings
* Max. Pos. Pressure: 20" H2O
* Max. Neg. Pressure: 80" H2O
* Pump Draw: 0.8 to 1.2 LPM (results can vary depending on duct pressure)
* CO Dilution: Factors- 0, 2, 5, 10, 20, 40; Accuracy-Readings +2%; Gas- Fresh Air or N2
* Data Transfer: RS232 Interface (Optional 4-20mA available)

Rental/Application Notes:

* This unit has temperature-controlled sensors.
* A CO dilution system is available upon request
* It can be operated remotely from 150' away.
* The sample conditioner has a built in chiller.
* CO2 is a calculated value on most of our units. An infrared cell is available that can read from 0- 50 Vol. % CO2. Accuracy: +/-0.3 Vol.% + 1% of mv (0 to 25Vol.%CO2), +/-0.5 Vol.% CO2 + 1.5 Vol.% CO2 (>25 to 50 Vol.% CO2). Resolution: 0.01 Vol.% (0-25 Vol.%). Units with this option rent for more than the calculated CO2 Testo 350XL's.
* The NO low and NO cells can not be combined on the same unit. If the maximum value of 300ppm is exceeded on the NO low cell it will shut down flow to the entire unit.
* If you need a pitot with umbilical please request one when placing your order.
* The cells for this unit can be swapped/replaced for different configurations. Please call with specific cell requirements. Our standard unit comes equipped with O2, CO, NO, NO2, & SO2 cells.
* A 4-20mA output adapter can be rented for an additional price if specified.
* Equipment must be returned in its original packaging.

1/2

CleanAir.

Testo 350XL Portable Combustion Analyzer

	O_2	CO	CO-low	NO	NO-low	NO_2	SO_2	H_2S	C_xH_y
Range	0-25%vol	0-10,000 H2 comp	0-500ppm H2 comp	0-3000 ppm	0-300ppm	0-500 ppm	0-5000 ppm	0-300 ppm	0-4%
Accuracy	<0.8% of f.v	<5ppm 0-99 ppm <5% of m.v. 100-2000 ppm <10% of m.v. 2001-10000 ppm	<2 ppm 0-39.9 ppm <5% of m.v. 40-500 ppm	<5 ppm 0-99 ppm <5% of m.v. 100-2000 ppm <10% of m.v. 2001-3000 ppm	<2 ppm 0-39.9ppm <5% of m.v. 300 ppm	<5 ppm 0-99 ppm <5% of m.v. 500 ppm	<5 ppm 0-99 ppm <5% of m.v. 100-2000 ppm <10% of m.v. 2001-5000 ppm	<2 ppm 0-39.9 ppm <5% of m.v. 40-300 ppm	<0.04% vol. 0-0.4% vol. <10% of m.v. 0.41 - 4% vol.
Resolution	0.1% vol	1 ppm	0.1 ppm	1 ppm	0.1 ppm	0.1 ppm	1 ppm	0.1 ppm	0.01 vol%
Resp. Time	20s (t95)	40s (t90)	40s (t90)	30s (t90)	30s (t90)	40s (t90)	30s (t90)	35s (t90)	40s (t90)

Our Standard cell configuration is NO (0-3000ppm), NO2, CO (0-10,000ppm), O2, & SO2. Advanced notification is necessary for alternative cell requirements.

2/2

129

Appendix C – LaserDust™ MP Monitors

LaserDust™ MP, LP and XLP Monitors
- Data sheet

Key Features

- Response time down to one second
- Suitable for high gas temperatures
- Cross stack measurement up to 10 m
- High dynamic range (mg or g with one instrument)
- Scattered light detection for high sensitivity
- Non-contact measurement (no probes)

NEO Monitors LaserDust Medium Path (MP), Long Path (LP), and Extra Long Path (XLP) Monitors are compact, optical dust monitors for true continuous in-situ measurement of dust concentration or opacity. The monitors are designed for measurement across pipes, stacks, and ducts with typical path lengths of 0.5 – 10 m. LaserDust Monitors use a transmitter / receiver configuration to probe the dust concentration along the optical line-of-sight. Our true non-contact approach (no probes) is superior to point type dust meters.

State of the Art Technology

With innovative laser technology the LaserDust combines two measurement principles in one instrument. At low dust levels it operates with forward scattered light technology: The incident laser light is scattered by dust particles and collected onto a solid-state sensor for dust quantification. This highly sensible mode enables detection limits of < 0.5 mg/Nm³ and is unaffected by dust depositing on the windows. At high dust levels the LaserDust will measure transmittance or opacity: Light absorption by dust particles is captured by a 2nd sensor. The operation mode is user selectable and can be changed on site.

Installation

Transmitter and receiver are mounted opposite each other onto DN or ANSI flanges, which include purge gas connections and a tilting mechanism for easy alignment. A continuous purge flow will prevent dust and other contamination from settling on the optical windows. Once power and data lines are connected, measurements are performed in real-time.

Main Applications

The LaserDust monitors are suitable for measuring particles after baghouse filters and electrostatic precipitators even at elevated gas temperatures. Their response is unaffected by charged particles and changes in velocity, making them the choice for obtaining robust and reliable emissions data. Some of the typical applications:

- Emission monitoring in Aluminium smelters and steel works
- Emission monitoring in waste incinerators, power plants, cement kilns
- Scrubber and filter optimisation, bag house filter surveillance
- Dust explosion prevention (e.g. in silos or bins)

Technical Data LaserDust MP, LP and XLP

neomonitors.com

Instrument data

Specifications

Process temperature	Above dew point up to 700 °C
Process pressure	0.1 – 1.5 bar abs (optional windows for up to 5 bar)
Detection limit	< 0.5 mg/Nm^3 (in scattered mode)
Measurement range	min. 0 – 15 mg/Nm^3 (scattered mode)
	max. 0 – 10.000 mg/Nm^3 (transmission mode)
Resolution	0.05 mg/Nm^3
Optical path length	Medium Path: 0.5 – 3 m
	Long Path: 3 – 6 m
	Extra Long Path: 6 – 10 m
Response time	1 – 2 sec
	Pulse mode: 50 ms

Environmental conditions

Operating temperature	-20 °C to +55 °C
Storage temperature	-20 °C to +55 °C
Protection classification	IP66

Inputs / Outputs

Analogue output (3)	4 – 20 mA current loop
Digital output	RS – 232 format
	Optional 10 or 10/100 Base T Ethernet, optional fibre optic (ASCII – format)
Relay output (3)	High dust -, Warning - and Fault relays (normally closed-circuit relays)
Analogue input	Optional 4 – 20 mA process temperature and pressure reading

Ratings

Input power supply unit	100 – 240 VAC, 50/60 Hz, 0.36 – 0.26 A
Output power supply unit	24 VDC, 900 – 1000 mA
Input transmitter unit	18 – 36 VDC, max. 20 W
4 – 20 mA output	500 Ohm max. isolated
Relay output	1 A at 30 V DC/AC

Installation and Operation

Flange dimension	Medium Path: DN50/PN10
	Long Path: DN80/PN10
	Extra Long Path: DN150/PN10
	Optional ANSI or other on request
Alignment tolerances	Flanges parallel within 1.5°
Purging of windows	Dry and oil-free pressurised air or gas, or by fan
Purge flow	50 – 100 l/min (application dependent)

Maintenance

Visual inspection	Recommended every 6 – 12 months (no consumables needed)
	Remote instrument check by Ethernet connection or external modem possible
Calibration	Recommended every year (against gravimetric analysis)
Validation	Integrated zero and span check (EN 14181 compliant)

Security

Laser class	Class IIIb according to IEC 60825-1
CE	Certified, conformant with LVD 73/23/EEC, including 93/68/EEC
EMC	Conformant with directive 2004/108/EC

Explosion protection (optional)

ATEX Cat 3 (zone 2)	II 3 GD T100 °C Ex nA nC II T5
CSA	Class I, Div. 2 on request

Dimension and weight

Transmitter unit (MP, LP, XLP)	200 (plus 100 for purge unit) x 270 x 170 mm, 6.2 kg
Transmitter unit (Ex version)	200 (plus 100 for purge unit) x 270 x 310 mm, 7.9 kg
Receiver unit (MP)	300 (plus 100 for purge unit) x 120 x 120 mm, 3.9 kg
Receiver unit (LP)	380 (plus 100 for purge unit) x 120 x 120 mm, 5 kg
Receiver unit (XLP)	410 (plus 100 for purge unit) x 270 x 170 mm, 8 kg
Power supply unit	180 x 85 x 70 mm, 1.6 kg

Your local distributor:

© neo monitors as May 2010

131

Appendix D – DM4 Open Path Dust Monitor

neo monitors as

DM4 Open Path Dust Monitor
- Data sheet

The DM4 Open Path (OP) dust monitor from NEO Monitors AS combines a rugged industrial design with superior monitoring technology for long distance measurement of dust concentration. Based on well-proven diode laser technology, this online instrument has a number of unique features.

- **Up to 400 m measurement path**
- **Response time down to one second**
- **Low detection limit (< 1 mg/Nm³ for 200 m OPL)**
- **High dynamic range**
- **Selectable measurement range**
- **Low cost of ownership**

The monitor consists of a transceiver, retro-reflector, and electronics unit. These are protection classified for outdoor use. Measurement readings are provided through standard 4-20mA current loops or an optional fibre-optic output. Dust is easily measured at different path lengths by entering the selected distance.

Measuring principle
The DM4's optical measuring principle is based on the property of particles to absorb incident light. A red laser light beam is transmitted between transceiver and retro-reflector. A detector inside the transceiver unit detects the amount of direct light transmitted. The signal will depend on the number of dust particles present in the measurement path so that dust concentration can be calculated.

Installation and Operation
The DM4 OP monitor is easy to install and designed to operate in very rough industrial environments. The instrument contains no moving parts, thereby limiting preventive maintenance to visual inspection and cleaning of optical windows. Purging with instrument air prevents dust from fouling the optical windows. Upon installation calibration against an extractive reference method is important to ensure that different types of dust with different optical properties are measured correctly.

Main applications
The DM4 OP dust monitor's most important applications are within continuous emission monitoring in different industrial sectors. The following are some of the typical applications:

- **Monitoring of pot rooms for Aluminium production**
- **Emission monitoring in Silicon carbide production**
- **Dust explosion prevention**
- **Leak detection**

Technical Data DM4 Open Path Dust Monitor

Instrument data

Specifications

Optical path length (OPL)	maximum 400 m
Detection limit	1 mg/Nm3 or better (application dependent) for OPL = 200 m
Measurement range	0 – 1000 mg/Nm³ (depending on OPL)
Accuracy	+/- 1 mg/Nm³ or +/- 5% of measured value (whichever is higher)
Response time	5 sec
Averaging time	5 – 600 sec (default = 50 sec)
Zero drift	< 0.5 mg/Nm³ between maintenance intervals

Environmental conditions

Operating temperature	-20 ºC to +55 ºC
Storage temperature	-20 ºC to +55 ºC
Protection classification	Transceiver and retro-reflector: IP65
	Electronics unit: IP 55 (optional IP65 cabinet)

Inputs / Outputs

Analogue output	4 – 20 mA current loop
Digital output	RS – 232 format
	Optional fibre optic (ASCII – format)
Relay output (3)	High dust -, Warning - and Fault relays (normally closed-circuit relays)
Analogue input	Optional 4 – 20 mA temperature and pressure reading

Ratings

Input electronics unit	100 – 240 VAC, 50/60 Hz, max. 50 W
4 – 20 mA output	500 Ohm max. isolated
Relay output	0.5 A at 220 VAC

Installation and Operation

Installation	DN80/PN10 flanges, special X/Y alignment platform or tripod
Purging of windows	Dry and oil-free pressurised air or gas, or by fan
Purge flow	Application dependent

Maintenance

Interval	Recommended every 3 months (no consumables needed)
	Remote instrument check by modem possible
Calibration	Recommended every year against extractive reference method

Security

Laser class	Class IIIb according to IEC 60825-1
CE	Certified
EMC	Conformant with directives EMC 89/336/EEC and LVD 73/23/EEC

Dimension and weight

Transceiver unit	480 x 150 x 150 mm, 10 kg
Retro-reflector unit	480 x 150 x 150 mm, 3 kg
Electronics unit	300 x 400 x 200 mm, 12 kg

neo monitors as

a subsidiary of Norsk Elektro Optikk AS
Solheimveien 62A, P.O. Box 384.
N-1471 Lørenskog, Norway.
Phone: +47 67974700 Fax: +47 67974900
Web: www.neomonitors.com

Your local distributor:

133

Appendix E – LaserGas II SP

Key Features

- Response time down to one second
- No gas sampling: IN-SITU measurement
- No interference from background gases
- Stable calibration, no zero drift
- Applicable for many process conditions: High temperature, high dust, corrosive gases
- Line measurement, integral concentration over the full stack diameter
- No moving parts, no consumables
- ATEX and CSA certified
- TÜV approved technology

NEO Monitors LaserGas II Single Path (SP) Monitor is a highly reliable gas analyser for true continuous in-situ monitoring. Single Path Monitors are designed for measurements across stacks, ducts, and reactors with typical path lengths of 0.5 – 20 m. By-pass and extractive configurations are also possible. The SP Monitor utilizes a transmitter / receiver configuration to measure the average gas concentration along the optical line-of-sight.

State of the Art Technology

NEO Monitors LaserGas is using Tuneable Diode Laser Absorption Spectroscopy (TDLAS) i.e. a non-contact optical measurement method employing solid-state laser sources. Therefore, the sensor remains unaffected by contaminants and corrosives and does not require regular maintenance. The absence of extractive conditioning systems further improves availability of the measurement and eliminates errors related to sample handling.

Easy Installation

The monitor is mounted directly onto DN50 or ANSI 2" flanges, which include

purge gas connections and a tilting mechanism for easy alignment. A continuous purge flow will prevent dust and other contamination from settling on the optical windows. Once power and data lines are connected, measurements are performed in real-time.

Key Application Areas

With **market experience since 1995** and an installed base of more than 3000 LaserGas analysers, we offer our customers a long-term experience from many challenging applications:

- Chemical industry (inertisation control of reactors, Vinyl Chloride or PVC, Acrylic acid, solvent acid recovery, carbon black etc.)
- Petrochemical industry (FCC Units, tail gas treatment, flare gas monitoring, sulphur recovery, vent headers of incinerators etc.)
- Steel industry (Coke oven gas, converter coal gas, reheating furnaces)
- Power plants (boiler control, DeNOx - ammonia slip control, economiser)
- Waste incineration, cement plants, aluminium smelters (emission monitoring)

Technical Data LaserGas™ II SP

neomonitors.com

Table of Principal Gases

Gas	Detection limit [ppm]	Max temp. [°C]	Max pressure [bar abs]
NH₃	0.15	600	2
HCl	0.05	600	2
HF	0.015	400	2
H₂S	3	300	2
O₂	100	1500	20
% H₂O	50	1500	2
ppm H₂O	0.1	400	2
% CO	30	1500	2
% CO₂	30	1200	2
ppm CO	0.3	1500	2
ppm CO₂	0.2	300	2
NO	10	300	2
N₂O	1	200	2
CH₄	0.2	300	3

NOTE: Detection limits are specified as the 95% confidence interval for 1 m optical path and gas temperature / pressure = 25 °C / 1 bar abs.

Also available are HCN, NO₂, C₂H₂, C2H₄, C₃H₆, CH₃I, CH₃O, CH₃CHCl (VCM), C2H₄O (EtO), CH₂Cl₂ (DCM), HBr, and HI.

Dual Gas: NH₃+H₂O, HCl+H₂O, HF+H₂O, CO+CO₂, CO+H₂O, CO+CH₄, O₂+temp, CO+temp

Higher pressures may be available on request for certain gases. Please contact us!

Instrument data

Specifications
Optical path length	typically 0.5 – 20 m
Response time	1 – 2 sec
Averaging time	Rolling average from 2 seconds to 24 hours (exp. decay)
Repeatability	+/- Detection limit or +/- 1% of reading, whichever is greater
Linearity	< 1%

Environmental conditions
Operating temperature	-20 °C to +55 °C (special version up to +65 °C on request)
Storage temperature	-20 °C to +55 °C
Protection classification	IP66

Inputs / Outputs
Analogue output (3)	4 – 20 mA current loop
Digital output	RS – 232 format, Optional 10 or 10/100 Base T Ethernet, Optional fibre optic (ASCII – format)
Relay output (3)	High gas-, Maintenance-, Warning - and Fault relays (normally closed-circuit relays)
Analogue input	4 – 20 mA process temperature and pressure reading

Ratings
Input power supply unit	100 – 240 VAC, 50/60 Hz, 0.36 – 0.26 A
Output power supply unit	24 VDC, 900 – 1000 mA
Input transmitter unit	18 – 36 VDC, max. 20 W
4 – 20 mA output	500 Ohm max. isolated
Relay output	1 A at 30 V DC/AC

Installation and Operation
Flange dimension	DN50/PN10 or ANSI 2"/150lbs (other dimensions on request)
Alignment tolerances	Flanges parallel within 1.5°
Purging of windows	Dry and oil-free pressurised air or gas, or by fan
Purge flow	10 – 50 l/min per flange (application dependent)

Maintenance
Visual inspection	Recommended every 6 – 12 months (no consumables needed)
	Remote instrument check by Ethernet connection or external modem possible
Calibration	Check recommended every 12 months
Validation	In-situ span and zero check with optional internal cell (EN 14181 compliant)

Security
Laser class	Class 1 according to IEC 60825-1
CE	Certified, conformant with LVD 73/23/EEC, including 93/68/EEC
EMC	Conformant with directive 2004/108/EC

Explosion protection (optional)
ATEX zone 1	II 2 G Ex px op is Gb II T4, II 2 D Ex pD 21 IP 66 T64°C
ATEX zone 2	II 3 G Ex nA nC op is Gc IIC T4, II 3 D Ex td A22 IP65 T100°C
CSA	Class I, Div. 2, Groups A, B, C and D; Temp. Code T4; non-incendive

Dimension and weight
Transmitter unit	405 (plus 65 for purge unit) x 270 x 170 mm, 6.2 kg
Transmitter unit (Ex version)	405 (plus 65 for purge unit) x 270 x 310 mm, 7.9 kg
Receiver unit	355 (plus 65 for purge unit) x 125 x 125 mm, 3.9 kg
Power supply unit	180 x 85 x 70 mm, 1.6 kg

Your local distributor:

© neo monitors as. Aug 2009

Appendix F – KIMO AMI 300

■ Functions

Manometer

PRESSURE
- Automatic or manual self-calibration
- Selection of units
- Pressure integration (0 to 9)
- Point/point, automatic point/point, automatic average
- Minimum / maximum values, hold, standard deviation
- Storage

AIR VELOCITY AND AIRFLOW
- Selection of Pitot tube, Debimo blades, hotwire or factor for other sensing elements
- Selection of duct type
- Selection of units
- Point/point, automatic point/point, automatic average
- Manual or automatic temperature balancing
- Manual air pressure balancing
- K2 factor
- Minimum / maximum values, hold, standard deviation
- Storage

Thermo-hygrometer

HYGROMETER
- Selection of units
- Minimum / maximum values and hold function
- Storage

PSYCHROMETER
- Dew point, wet temperature, enthalpy, absolute temperature
- Minimum / maximum values and hold function
- Storage

WBGT index
For hygrometry probe with black ball.
- Calculation of comfort index inside / outside
- Storage

Air Quality

CLIMATIC CONDITIONS MODULE
- Selection of units
- Minimum / maximum values and hold function
- Storage

AIR QUALITY PROBES
- Audible Alarm (2 setpoints)
- CO maximum
- Selection of units
- Minimum / maximum values and hold function
- Storage

OMNIDIRECTIONAL PROBE
- Air velocity
- Temperature
- Hygrometry

Current / voltage module
- Adjustable ranges
- Minimum / maximum values and hold function
- Storage

Thermometer

Thermocouple module, Pt100 and thermocouple temperature probes
- Dynamic delta T
- Selection of units
- Minimum / maximum values and hold function
- Alarme (upper and lower setpoints)
- Storage
- Calculation of U-value

■ Datalogger-10
- Multi-parameters recording
- Manual and automatic storage
- Memory : up to 12,000 measurement points or 50 datasets
- User-friendly with printing of customized report
- Management of instruments pool, follow-up of calibration periods
- Intervention planning
- Wired or wireless interface

■ Technical features

Sensing elements
Pressure module Piezoresistive sensor
    Overpressure allowed ±500 Pa : 250 mbar
    Overpressure allowed ±2500 Pa : 500 mbar
    Overpressure allowed ±10,000 Pa : 1,200 mbar
    Overpressure allowed ±500 mbar : 2 bar
    Overpressure allowed ±2,000 mbar : 6 bar
Hotwire : Thermistance with a negative temperature coefficient.
Ambient temperature : Pt100 1/3 Din.
Ø 70 and 100 mm vane probes : Hall effect sensor
Ambient temperature : Pt100 class A.
Ø 14 mm vane probe : Proximity sensor
Ambient temperature : Pt100 class A.
Hygrometry/Temp. Probe : capacitive sensor, Pt100 1/3 DIN
Thermocouple probes : type K, J and T class 1
Pt100 probes Smart-plus : Pt100 class 1/3 Din
Climatic conditions module
    Hygrometry : capacitive sensor
    Temperature : semiconductor sensor
    Air pressure : piezoresistive sensor
Air quality probes
    CO_2 : NDIR sensor
    CO : electrochemical sensor
    Temperature : Pt100 class A
    Hygrometry : capacitive sensor
Climatic conditions module
    Hygrometry : capacitive sensor
    Temperature : semiconductive sensor
    Air pressure : piezoresistive sensor
Multifunction probe
    Air velocity : Thermistance with a negative temperature coefficient.
    Hygrometry/Temp.: capacitive sensor, Pt100 1/3 DIN
Omnidirectional probe
    Air velocity : Thermistance with a negative temperature coefficient
    Hygrometry/Temps.: capacitive sensor, Pt100 1/3 DIN
Tachometry probe
    Optical : optical sensor
    Contact : optical probe with ETC adaptor
Instrument connections............On the top :
    2 secured mini-DIN connectors for SMART-Plus probes
    Left side :
    1 USB port for KIMO cable only
    1 power supply plug
Module connections...................Thermocouple
    4 inputs for compensated miniature
    plug of thermocouple type K, J or T Class 1
    (as per IEC 584-3norm)
    Pressure
    2 pressure connectors Ø 6,2 mm made of nickelled brass.
    2 threaded pressure connectors Ø 4,6 mm made of nickelled brass
    + 1 thermocouple temperature input for miniature connectors
    Current / voltage module
    2 stereo jacks
Display... Graphic display 320x240 pixels
    Dim. 70 x 52 mm, color display
    Display of 6 measurements (including 4 simultaneously)
Housing   IP54, ABS shock-proof
Keypad... Metal-coated, 5 keys, 1 joystick
Conformity................................... Electromagnetical compatibility
    (NF EN 61326-1 norm)
Power supply...............................4 alcaline batteries 1,5V LR6
Operating environment............. Neutral gas
Operating temperature..............from 0 to 50°C
Storage temperature.................from -20 to +80°C
Auto shut-off...............................adjustable from 0 to 120 min
Weight...380g
Languages................................... French, English, Dutch, German, Italian, Spanish, Portuguese, Swedish, Norwegian, Finn, Danish

■ **Specifications**	**Measuring units**	**Measuring range**	**Accuracy***	**Resolutions**
PRESSURE				
	Pa, mmH$_2$O, In WG, mbar, hPa, mmHg, DaPa, kPa	from 0 to ±500 Pa	± 100 Pa : ±0.2% reading ±0.8Pa, beyond ±0.2% reading ±1,5Pa,	0.1 Pa from -100 to +100 Ps, 1 Pa beyond
		from 0 to ±2500 Pa	±0.2% of reading ±2Pa	1Pa
		from 0 to ±10,000 Pa	±0.2% of reading ±10Pa	1Pa
	mmH$_2$O, In WG, mbar, hPa, mmHg, DaPa, kPa, PSI	from 0 to ±500 mBar	±0.2% of reading ±0,5mBar	0,1mBar
	bar, In WG, mbar, hPa, mmHg, kPa, PSI	from 0 to ±2000 mBar	±0.2% of reading ±2mBar	1mBar
CURRENT/VOLTAGE				
	V, mA	from 0 to 2,5 V	±2mV	0.001 V
		from 0 to 10 V	±10mV	0.01 V
		from 0 to 4/20 mA	±0.01mA	0.01 mA
THERMOCOUPLE				
	°C, °F	K : from -200 to +1,300°C	±1.1°C or ±0.4% of reading**	0.1 °C
		J : from -100 to +750°C	±0.8°C or ±0.4% of reading**	0.1 °C
		T : from -200 to +400°C	±0.5°C or ±0.4% of reading**	0.1 °C
CLIMATIC CONDITIONS				
Hygro.	%RH	from 5 to 95%RH	See datasheet	0.1 %RH
Temp.	°C, °F	from -20 to +80°C	interchangeable	0.1 °C
Air pressure	hPa	from 800 to 1100 hPa	measurement modules	1 hPa
HOTWIRE - Standard and telescopic -				
Air velocity	m/s, fpm, Km/h	from 0.15 to 3 m/s	±3% of reading ±0.03 m/s	0.01 m/s
		from 3.1 to 30 m/s	±3% of reading ±0.1 m/s	0.1 m/s
Temperature	°C, °F	from -20 to +80°C	±0.3% of reading ±0.25°C	0.1 °C
Airflow	m³/h, cfm, l/s, m³/s	from 0 to 99,999 m³/h	±3% of reading ±0.03*area(cm²)	1 m³/h
Ø 100 mm VANE PROBE				
Air velocity	m/s, fpm, Km/h	from 0,25 to 3 m/s	±3% of reading ±0,1m/s	0.01 m/s
		from 3,1 to 35 m/s	±1% of reading ±0,3m/s	0.1 m/s
Temperature	°C, °F	from -20 to +80°C	±0.4% of reading ±0.3°C	0.1 °C
Airflow	m³/h, cfm, l/s, m³/s	from 0 to 99,999 m³/h	±3% of reading ±0.03*area (cm²)	1 m³/h
Ø 70 mm VANE PROBE				
Air velocity	m/s, fpm, Km/h	from 0,to à 3 m/s	±3% of reading ±0,1m/s	0.1 m/s
		from 3,1 to 35 m/s	±1% of reading ±0,3m/s	
Temperature	°C, °F	from -20 to +80°C	±0.4% of reading ±0.3°C	0.1 °C
Airflow	m³/h, cfm, l/s, m³/s	from 0 to 99,999 m³/h	±3% of reading ±0.03*area (cm²)	1 m³/h
Ø 14 mm VANE PROBE				
Air velocity	m/s, fpm, Km/h	from 0,8 to 3 m/s	±3% of reading ±0,1m/s	0.1 m/s
		from 3,1 to 25 m/s	±1% of reading ±0,3m/s	
Airflow	m³/h, cfm, l/s, m³/s	from 0 to 99,999 m³/h	±3% of reading ±0.03*area (cm²)	1 m³/h
Temperature	°C, °F	from -20 to +80°C	±0.4% of reading ±0.3°C	0.1 °C
PITOT TUBE				
Air velocity	m/s, fpm, Km/h, mph	from 2 to 5 m/s	±0.3 m/s	0.1 m/s
		from 5.1 to 100 m/s	±0.5% of reading ±0.2m/s	
Airflow	m³/h, cfm, l/s, m³/s	from 0 to 99,999m³/h	±0.2% of reading ±1% PE	1 m³/h
DEBIMO blades				
Air velocity	m/s, fpm, Km/h, mph	from 4 to 20 m/s	±0.3 m/s	0.1 m/s
		from 21 to 100 m/s	±1% of reading ±0.1m/s	0.1 m/s
Airflow	m³/h, cfm, l/s, m³/s	from 0 to 99,999m³/h	±0.2% of reading ±1% PE	1 m³/h
Air quality probes : CO / CO$_2$ / temperature / Hygrometry				
Temperature	°C, °F	from -20 to +80°C	See related datasheet	0.1 °C
CO$_2$	ppm	from 0 to 5000 ppm	"Portable probes"	1 ppm
CO	ppm	from 0 to 500 ppm		0,1 ppm
Relative humidity	%RH	from 5 to 95%RH		0.1 %RH
STANDARD HYGROMETRY probe				
Relative humidity	%RH	from 3 to 98 %RH	See related datasheet	0.1 %RH
Absolute humidity / enthalpy	g/Kg / Kj/Kg	According to temperature and hygrometry measuring ranges	"Portable probes"	0.1 g/Kg
Dew point	°C$_{td}$, °F$_{td}$	from -50 to +80°C$_{td}$	±0.6% of reading ±0.5°C$_{td}$	0.1 °C$_{td}$
Ambient temperature	°C, °F	from -20 to	±0.3% of reading ±0.25°C	0.1 °C
HIGH TEMPERATURE HYGROMETRY probe				
Relative humidity	%RH	from 3 to 98 %RH	See related datasheet	0.1 %RH
Absolute humidity / enthalpy	g/Kg / Kj/Kg	According to temperature and hygrometry measuring ranges	"Portable probes"	0.1 g/Kg
Dew point	°C$_{td}$, °F$_{td}$	from -50 to +80°C$_{td}$	±0.6% of reading ±0.5°C$_{td}$	0.1 °C$_{td}$
Ambient temperature	°C, °F	from -40 to +180°C	±0.3% of reading ±0.25°C	0.1 °C
TACHOMETRY probe (See datasheet "Portable probes")				
MULTIFUNCTION probes (See datasheet "Portable probes")		OMNIDIRECTIONAL PROBE See datasheet "Portable probes"		
Pt100 Smart-Plus probes (See related datasheet)				

*All accuracies indicated in this document were stated in laboratory conditions and can be guaranteed for measurements carried out in the same conditions, or carried out with required compensation.
**The accuracy is expressed either by a deviation in °C, or by a percentage of the value concerned. Only the bigger value is considered.

■ **Supplied with ...** ● Supplied with ○ Option

DESCRIPTION	AMI 300	AMI 300 CLA	AMI 300 STD	AMI 300 PRO	AMI 300 CRF	AMI 300 SRF	AMI 300 PRF
Pressure module from 0 to ±500 Pa	○	○	○	●	○	○	●
Pressure module from 0 to ±2500 Pa	○	○	○	○	○	○	○
Pressure module from 0 to ±10000 Pa	○	○	●	○	○	●	○
Pressure module from 0 to ±500 mBar	○	○	○	○	○	○	○
Pressure module from 0 to ±2000 mBar	○	○	○	○	○	○	○
Current / voltage module	●	●	●	●	●	●	●
Thermocouple module	○	○	○	○	○	○	○
Climatic conditions module	○	○	○	○	○	○	○
2x1 m silicone tube Ø 4 x 7 mm	○	○	●	●	○	●	●
Stainless steel tips Ø 6 x 100 mm	○	○	●	●	○	●	●
Pitot tube Ø 6mm, lg. 300 mm	○	○	●	○	○	●	○
Pitot tube Ø 6mm, lg. 300 mm T	○	○	○	○	○	○	●
Pitot tube Ø 6mm, lg. 300 mm S	○	○	○	○	○	○	○
Optical tachometry probe	○	○	○	○	○	○	○
ETC adaptor	○	○	○	○	○	○	○
Reflective tape	○	○	○	○	○	○	○
Standard hotwire	○	●	●	○	●	●	○
Straight extension for hotwire	○	●	●	○	○	●	○
Telescopic gooseneck-shaped hotwire	○	○	○	●	○	○	●
SMART-Plus Ø 14 mm vane probe	○	○	○	○	○	○	○
Telescopic SMART-Plus Ø 14 mm vane probe	○	○	○	○	○	○	○
SMART-Plus Ø 70 mm vane probe	○	●	○	○	○	○	○
Wireless Ø 70 mm vane probe	○	○	○	○	●	○	○
SMART-Plus Ø 100 mm vane probe	○	○	●	●	○	○	○
Wireless Ø 100 mm vane probe	○	○	○	○	○	●	○
SMART-Plus standard hygrometry probe	○	●	●	○	○	○	○
Wireless standard hygrometry probe	○	○	○	○	●	●	○
SMART-Plus high temperature hygrometry probe	○	○	○	●	○	○	○
Wireless high temperature hygrometry probe	○	○	○	○	○	○	●
SMART-Plus Pt100 temperature probe	○	○	○	○	○	○	○
Wirelesss Pt100 temperature probe	○	○	○	○	○	○	○
Thermocouple K, J and T probe	○	○	○	○	○	○	○
CO_2 / temperature probe	○	○	○	○	○	○	○
CO / temperature probe	○	○	○	○	○	○	○
CO_2 / temperature / Hygrometry probe	○	○	○	○	○	○	○
Omnidirectional probe (air velocity/temperature/hygrometry)	○	○	○	○	○	○	○
Air velocity/ Temperature / Hygrometry probe	○	○	○	○	○	○	○
8 rechargeable batteries with charger	●	●	●	●	●	●	●
Calibration certificate	●	●	●	●	●	●	●
Transport case	●	●	●	●	●	●	●

■ **Accessories** (See related datasheet)

Datalogger-10	KPIJ 20 – 50 – 100 – 200 - 600	RTS	BNF	K 25 - 35 - 75 - 85 - 120 - 150
Datalogger-10 PC software for data recording and processing. Wired (LPCF) wireless (LPCR) interface.	Ammeter clamp with PVC cable lg. 2m and jack connector.	Telescopic extension, length 1 m, bent at 90° for measuring probe.	Hotwire cleaning spray	Airflow cones (See related datasheet)
CE 300	**GST**	**ADS**	**See related datasheet**	**See related datasheet**
Hands-free protective cover	Silicone heat conductive grease for temperature probes	Adaptor for power supply 230 Vac	Silicone tube and crystal flexible tube	Debimo airflow blades of different sizes
BN	**RD 300**	**JAC**	**CHA**	
Black ball Ø 150mm with junction for temperature probe Ø 4,5mm. Further dimensions available.	Straight extension for hotwire Ø 10 mm. lg. 300 mm	Set of 4 LR6 batteries	4 batteries charger	

■ **Warranty period**

Instruments have 1-year guarantee for any manufacturing defect (return to our After-Sales Service required for appraisal).

www.kimo.fr Distributed by :

EXPORT DEPARTMENT
Tel : + 33. 1. 60. 06. 69. 25 - Fax : + 33. 1. 60. 06. 69. 29
e-mail : export@kimo.fr

FTang – AMI300 – 15/03/10 – RCS (24) Périgueux 349 282 095 Non-contractual document – We reserve the right to modify the characteristics of our products without prior notice.

139